

**MODIS Level 1A Earth Location:  
Algorithm Theoretical Basis Document  
Version 3.0**



SDST-092

August 26,1997



**MODIS Level 1A Earth Location:  
Algorithm Theoretical Basis Document  
Version 3.0**

**By the MODIS Science Data Support Team:**

Mash Nishihama, Robert Wolfe, David Solomon  
*Hughes STX*

Frederick Patt, Jeffrey Blanchette  
*General Science Corporation*

Albert Fleig  
*University of Maryland and NASA/Goddard Spaceflight Center*

Edward Masuoka  
*NASA/Goddard Spaceflight Center*



**MODIS Level 1A Earth Location:  
Algorithm Theoretical Basis Document  
Version 3.0**

**Prepared By:**

---

Mash Nishihama, Hughes STX MODIS Geolocation Scientist	Date
---	------

**Reviewed By:**

---

Jeffery Blanchette, SAIC/General Sciences Corporation SDST Geolocation Lead	Date
--	------

---

Dr. Al Fleig, University of Maryland Data System Scientist	Date
---	------

---

Michael Freeze, SAIC/General Sciences Corporation SDST R&QA Manager	Date
--	------

---

Fred Patt, SAIC/General Sciences Corporation SDST Task Manager	Date
---	------

---

Robert Wolfe, Hughes STX MODIS Land Team Member	Date
--	------

**Approved By:**

---

Edward Masuoka, GSFC/Code 922 MODIS SDST Manager	Date
---	------







## Prologue

This is the third version of the MODIS Level 1A Earth Location Algorithm Theoretical Basis Document. The first version was published as Appendix A of the MODIS Level 1 Geolocation, Characterization and Calibration Algorithm Theoretical Basis Document, Version 1 (MODIS Technical Report Series, Volume 2, NASA Technical Memorandum 104594, Vol. 2, Goddard Space Flight Center, May 1994). A number of people reviewed Version 2 and many of their comments and contributions were received and factored into it.

Improved understanding of the instrument and more details on the algorithm in certain areas have made this version of the document about sixty percent larger compared to its predecessor. Four new sections were added and several sections were rearranged and enhanced for clarity. The four additional sections are for the solar diffuser and for the parameter error analysis: dealing with the land and island control point matching, residual measurements, and parameter estimation mainly concerned with parameters related to the satellite position/velocity and attitude. Other significant changes include:

1. Clarification of focal plane rotation in the telescope coordinate system;
2. Elimination of SOM map projection from the DEM preprocessing in the terrain correction algorithm;
3. Introduction of biquadratic equations for sub-pixel approximate ground location model while removing the original first order approximation approach;
4. Addition of appendices containing an alternative approach on the terrain correction, more details on input data validation based on some prototyping experience, and an inverse mapping algorithm.

On the whole, Version 2 of the document was fairly complete and provided a good frame-work so that Version 3 primarily contains additional detail and algorithms for ground control point matching and error analysis. As development continues, several areas will be clarified and detail will be added. More feedback from the prototyping and software builds will be factored in as will preflight and in-flight tests of the instrument/spacecraft. This will be a living document and will reflect the current understanding of the Earth location algorithm and its implementation.

After the initial Version 3 ATBD (draft version) was completed, the copies were sent to other reviewers and many valuable comments were provided. Many of their comments have been factored into this document, but we could not answer to all of their questions and include many of their suggestions. In any event we are very thankful to all those people who participated in improving this document. We thank Bert Guindon of CCRS, Hugh Kiefer of USGS, Chuck Wivell of EDC, Veljko Jovanovic of JPL, Jim Storey of EDC, Alan Strahler of Boston U, and Peter Noerdlinger of EOSDIS for many useful suggestions including small typo-graphical errors, inadequate explanations of notations and algorithms, and so on. We also thank Harry Montgomery and Nianzeng Che of MCST for their valuable comments on the focal plane/telescope coordinate systems and other information on their needs.



**MODIS Level 1A Earth Location:  
Algorithm Theoretical Basis Document  
Version 3.0**

**Table of Contents**

<b>1. INTRODUCTION .....</b>	<b>1-1</b>
1.1 Applicable Documentation.....	1-1
<b>2. OVERVIEW AND BACKGROUND INFORMATION.....</b>	<b>2-1</b>
2.1 Requirements for Earth Location .....	2-3
2.2 Historical Perspective.....	2-3
2.3 Instrument Characteristics.....	2-4
2.3.1 Detector Geometry and Detector Response.....	2-4
2.3.1.1 Triangular Weighting Function.....	2-4
2.3.1.2 Registration of 1000 and 500 m pixels .....	2-7
2.3.1.3 Combining Different Sized Pixels .....	2-10
2.3.1.4 Using Multiple Resolution Data.....	2-10
2.3.1.5 Location of Spatial Element.....	2-10
2.3.2 Scan Geometry .....	2-11
2.4 Ancillary Input Data .....	2-13
<b>3. ALGORITHM DESCRIPTION .....</b>	<b>3-1</b>
3.1 Theoretical Description .....	3-1
3.1.1 MODIS Viewing Geometry Overview.....	3-1
3.1.2 Coordinate Systems.....	3-2
3.1.2.1 Focal Plane Coordinate System.....	3-3
3.1.2.2 Telescope Coordinate System .....	3-3
3.1.2.3 Scan Mirror Assembly Coordinate System.....	3-4
3.1.2.4 Solar Diffuser Coordinate System .....	3-5
3.1.2.5 Instrument Coordinate System.....	3-6
3.1.2.6 Spacecraft Coordinate System.....	3-7
3.1.2.7 Orbital Coordinate System .....	3-7
3.1.2.8 Earth Centered Inertial Coordinate System.....	3-8
3.1.2.9 Earth Centered Rotating Coordinate System .....	3-8
3.1.2.10 Geodetic Coordinate System.....	3-8
3.1.3 Coordinate Transformations .....	3-9
3.1.3.1 Focal Plane to Telescope .....	3-10
3.1.3.2 Telescope to Instrument.....	3-11

- 3.1.3.3 Scan Mirror Assembly to Instrument ..... 3-11
- 3.1.3.4 Solar Diffuser to Instrument..... 3-12
- 3.1.3.5 Instrument to Spacecraft ..... 3-12
- 3.1.3.6 Spacecraft to Orbital..... 3-12
- 3.1.3.7 Orbital to ECI..... 3-13
- 3.1.3.8 ECI to ECR..... 3-13
- 3.1.3.9 ECR to Geodetic..... 3-14
- 3.1.4 Mathematical Description of Algorithm..... 3-14
  - 3.1.4.1 Instrument Model Algorithm ..... 3-15
  - 3.1.4.2 Earth Location Algorithm ..... 3-30
  - 3.1.4.3 Sub-pixel Approximate Ground Location Model..... 3-40
- 3.1.5 Variance or Uncertainty Estimates..... 3-45
- 3.2 Practical Considerations..... 3-51
  - 3.2.1 Numerical Computation Considerations ..... 3-51
  - 3.2.2 Programming/Procedural Considerations ..... 3-52
  - 3.2.3 Algorithm Verification ..... 3-52
    - 3.2.3.1 Verification Standard ..... 3-53
    - 3.2.3.2 Preflight Verification ..... 3-53
    - 3.2.3.3 In-flight Verification..... 3-54
    - 3.2.3.4 Verification of Inputs..... 3-55
  - 3.2.4 Product Validation ..... 3-58
  - 3.2.5 Quality Control and Diagnostics..... 3-59
  - 3.2.6 Exception Handling ..... 3-59
- 3.3 Error Analysis Algorithms..... 3-60
  - 3.3.1 Land Control Point Matching and Correlation Algorithm..... 3-60
  - 3.3.2 Island Control Point Matching Algorithm..... 3-61
  - 3.3.3 Error Analysis and Parameter Estimation Algorithm..... 3-61
- 4. CONSTRAINTS, LIMITATIONS, AND ASSUMPTIONS..... 4-1**
- APPENDIX A: ACRONYMS AND ABBREVIATIONS ..... A-1**
- APPENDIX B: ALTERNATIVE APPROACH FOR TERRAIN CORRECTION ...A-3**
- APPENDIX C: DATA VALIDATION..... A-4**
- APPENDIX D: INVERSE MAPPING ALGORITHM ..... A-6**

## List of Figures

Figure 2-1.	MODIS Instrument and Support Overview	2-2
Figure 2-2.	Coordinate Systems Overview and Coordinate Transformations	2-2
Figure 2-3.	Rectangular Response Weighting Function	2-5
Figure 2-4.	Triangular Response Function from the Effective Time Weighting	2-6
Figure 2-5.	Series of Triangular Weighted Pixels	2-6
Figure 2-6.	75 % of Signal is Collected from the Nominal Pixel	2-7
Figure 2-7.	Registration of 500 m and 1 km Pixels	2-7
Figure 2-8.	Higher Resolution Pixels Needed to Generate 1 km Pixels	2-8
Figure 2-9.	Equivalent 500 m Weighting Functions*	2-9
Figure 2-10.	Equivalent 250 m Weighting Function*	2-9
Figure 2-11.	MODIS Spatial Element Location	2-11
Figure 2-12.	Panoramic Bow Tie Effect	2-12
Figure 2-13.	Pixel Size Growth and Overlap within a Scan	2-12
Figure 3-1.	Growth of Spatial Element Ground Field of View	3-2
Figure 3-2.	Focal Plane Coordinate System	3-3
Figure 3-3.	Instrument, Telescope and Scan Mirror Assembly Coordinate Systems' Relative Orientation	3-4
Figure 3-4.	Nadir View, Scan Mirror Angle, Focal Plane Tilt in Instrument Coordinate System	3-5
Figure 3-5.	Solar Diffuser and Solar Vector Configuration	3-6
Figure 3-6.	Orbital Coordinate System	3-7
Figure 3-7.	ECI Coordinate System	3-8
Figure 3-8.	ECR Coordinate System	3-9

Figure 3-9.	Focal Plane Rotation to Compensate for Spacecraft Along-Track Motion	3-10
Figure 3-10.	Physical Layout of the Focal Planes	3-16
Figure 3-11.	Offset of Each Band Relative to the Reference Optical Axis	3-18
Figure 3-12.	Measurements of Detector Locations on Focal Plane	3-19
Figure 3-13.	Integration Area for Different Sampling Rates and Ground Resolution	3-20
Figure 3-14.	Time of Start of Earth View Sector	3-21
Figure 3-15.	Frame Start Timing for Earth View Sector Around $t_0$	3-21
Figure 3-16.	Mirror Wedge Angles and Axis Errors Definitions	3-24
Figure 3-17.	Scan Mirror Normal Vectors	3-26
Figure 3-18.	Encoder Time Sample Interpolation	3-28
Figure 3-19.	Ellipsoidal Viewing Vector Intersection	3-31
Figure 3-20.	Terrain Intersection Search Geometry	3-35
Figure 3-21.	Ideal Band Projection on the Ground	3-40
Figure 3-22.	Biquadratic Interpolation 3 x 3 Grid	3-40
Figure 3-23.	Earth Location Error (meters)	3-49
Figure 3-24.	Earth Location Error (1 km pixel fraction)	3-50
Figure 3-25.	Earth Location Error (in 1 km pixel fraction) Resulting from Various Terrain Height Errors as a Function of Scan Angle	3-51
Figure 3-26.	Three Satellite Locations	3-62
Figure 3-27.	Connecting Parts of 3 Scans	3-63
Figure 3-28.	The $\alpha$ - $\beta$ Coordinate System Reference Planes	3-66
Figure 3-29.	Thematic Mapper Pixel	3-67
Figure 3-30.	Triangular Weighting Function	3-68
Figure 3-31.	Triplet Islands Matching	3-75

Figure 3-32. Satellite Position and Ground Control Point	3-78
Figure 3-33. Look Vector Angles	3-80
Figure 3-34. Cross Track Geometry	3-81
Figure 3-35. Along Track Geometry	3-83
Figure 3-36. Linear Estimate of $dx$ as a Function of $dt$ Generated from Control Points	3-85

### List of Tables

Table 3-1. Focal Lengths for Each Focal Plane	3-15
Table 3-2. Detector Specifications	3-16
Table 3-3. Nominal Band Layout with Respect to the Optical Axis	3-17
Table 3-4. Detector Sampling	3-19
Table 3-5. Scan Mirror Assembly Geometric Specifications	3-24
Table 3-6. Scan Mirror Encoder Geometric Constants	3-26
Table 3-7. Scan Mirror Encoder Geometric Derived Values	3-27
Table 3-8. Unique Center Locations in One Spatial Element	3-39
Table 3-9. Geolocation Impact of 2 Sigma Spacecraft Position Errors	3-46
Table 3-10. Geolocation Impact of 2 Sigma EOS AM Platform Attitude Knowledge Error Components	3-47
Table 3-11. Geolocation Impact of 2 Sigma Instrument Pointing Knowledge Error Components	3-47

Table 3-12. Total Combined 2 Sigma RSS Geolocation Error 3-48

Table 3-13. In-flight Algorithm Verification Activities 3-54

## 1. INTRODUCTION

This Algorithm Theoretical Basis Document (ATBD) describes the Moderate-Resolution Imaging Spectroradiometer (MODIS) Level 1A Earth location algorithm. This algorithm will be implemented as part of the MODIS Level 1A processing software in order to include Earth location and related spatial information in the Level 1A MODIS data products. The Earth location algorithm uses Earth ellipsoid and terrain surface information in conjunction with spacecraft ephemeris and attitude data, and knowledge of the MODIS instrument and Earth Observing System (EOS) satellite geometry to compute the geodetic position (latitude, longitude, and height), ground to satellite direction and range, and sun direction for each MODIS spatial element (1 km nadir ground field of view). The heart of the algorithm is a mathematical procedure that intersects the MODIS instrument's line of sight with the Earth's terrain surface.

The term "spatial element" is used throughout this document to refer to the ground field of view of a single detector sample from one of the 1 km nadir resolution MODIS bands. A single spatial element is associated with one detector sample from each of the 1 km bands, four samples from the 500 m bands, and sixteen samples from the 250 m bands. The Earth location information generated for each MODIS spatial element is stored in eight data fields added to the MODIS scan data during Level 1A processing. These fields are:

1. geodetic latitude;
2. geodetic longitude;
3. height above the Earth ellipsoid;
4. satellite zenith angle;
5. satellite azimuth;
6. range to the satellite;
7. solar zenith angle; and
8. solar azimuth.

This document describes the algorithm used to generate these eight Earth location related fields and briefly discusses the supporting data preparation and validation processes.

### 1.1 Applicable Documents

Documents applicable to this ATBD include:

1. MODIS Technical Description Document (Preliminary), prepared for National Aeronautics and Space Administration (NASA) Goddard Space Flight Center (GSFC) by Hughes Santa Barbara Research Center (SBRC), document number DM VJ50-0073, September 1992.

2. An Analysis of MODIS Earth Location Error, Version 2.0, by Albert J. Fleig, Paul A. Hubanks, James C. Storey and Lloyd Carpenter, MODIS Science Data Support Team (SDST), September 1993.
3. MODIS Level 1A Software Requirements, SDST-032, 9/1/96 prepared by the MODIS SDST.
4. Unique Instrument Interface Document (UIID), MODIS Instrument, Revision A, EOS AM Project, GSFC, November 6, 1992.
5. EOS General Instrument Interface Specification (GIIS) for the EOS Observatory, Revision A, prepared for NASA GSFC by General Electric Company Astro Space Division, document number GSFC 420-03-02, December 1, 1992.
6. DMA TR 8350.2-A, Defense Mapping Agency (DMA) Technical Report (TR), Supplement to Department of Defense World Geodetic System 1984 (WGS84) Technical Report, prepared by the DMA WGS84 Development Committee, December 1, 1987.
7. Map Projections - A Working Manual, by John P. Snyder, United States Geological Survey (USGS) Professional Paper 1395, U. S. Government Printing Office, Washington, 1987.
8. Topographic Data Requirements for EOS Global Change Research (Draft), prepared by the USGS Earth Resources Observation System (EROS) Data Center, April 30, 1993.
9. Engineering Telemetry Description, MODIS Program, prepared for NASA GSFC by Hughes SBRC, document number DM VJ50-0062/001, April 1994.
10. Ambient Calibration and Testing (AC) Support Software, Requirements for, Hughes SBRC, document number 151868, November 18, 1993.
11. Scan Mirror Assembly, MODIS, Specification for, Hughes SBRC, document number 151766, February 15, 1994.
12. Ambient Calibration and Testing(AC) Support Software, Requirements For No. 151864 (CALTEST November 1993), SRBC.
13. MODIS Command, Telemetry, Science and Engineering Description, No. 151840, May 1996(Formerly CDRL 303 Commands & CDRL 305 Telemetry), SBRC.
14. Patt, F. S., W. W. Gregg and R. H. Woodward,"Automated Navigation Assessment for Earth Survey Sensors Using Island Targets", IJRS, accepted for publication, 1996.
15. Landsat 7 Image Assessment System Geometric Algorithm Theoretical Basis Document, Version 2, USGS EROS Data Center, January 15, 1997.

16. Rosborough, G.W., D.G. Baldwin and W.J. Emery, "Precise AVHRR Image Navigation", IEEE Transaction on Geoscience and Remote Sensing, Vol 32, No. 3, May 1994.
17. Pratt, W.K., "Digital Image Processing", Second Edition, John Wiley & Sons, Inc, 1991.
18. Theoretical Basis of the SDP Toolkit Geolocation Package for the ECS Project, Technical Paper, 445-TP-002-002, May 1995.
19. EOS-AM1 Detailed Mission Requirements, Draft, GSFC, November 1993.
20. Wertz, J.R. (ed.), Spacecraft Attitude Determination and Control, D. Reidel Publishing Co., Vol. 73, 1985, pp447-455.

(This page intentionally left blank.)

## 2. OVERVIEW AND BACKGROUND INFORMATION

The MODIS Earth location algorithm will operate as part of the Level 1 processing system for MODIS data from the EOS AM and PM satellites. Level 1 processing is divided into two phases termed Level 1A and Level 1B. Level 1A processing involves unpacking and verifying Level 0 MODIS data received from the EOS Data and Operations System (EDOS), organizing these data into MODIS scan oriented data structures, generating the Earth location data, adding associated ancillary information (metadata) required to describe the data set, and producing a data product in an EOS standard format. Level 1B processing applies radiometric calibration to the raw detector output contained in the Level 1A data product. This calibrated data is used in subsequent Level 2 science algorithm processing. MODIS science data is in the original un-resampled space throughout the Level 1 and Level 2 processing. In this context, the Earth location data fields are treated as additional attributes of the spatial elements that contain the MODIS science data, thus describing explicitly each spatial element's ground location.

The MODIS instrument contains thirty-six spectral bands at three different spatial resolutions with nominal ground fields of view of 250 m, 500 m, and 1 km. Bands 13 and 14 have two sets of channels: one for high gain and the other for low gain. The detectors from the different bands are nominally aligned to form spatial elements each with 81 data channels (one from each of the twenty-nine 1 km resolution bands, four from each of the five 500 m resolution bands, and sixteen from each of the two 250 m resolution bands). The Level 1A Earth location algorithm provides a single set of Earth location fields for each spatial element. This spatial element is modeled as a detector in an "ideal" band(0) placed near the optical axis of the instrument. The exact position of this ideal band will be chosen to best represent the locations of all of the bands(see Figure 3-11). As explained in Reference 13, an Earth scan begins at band 30 and ends at band 32. All bands are aligned to band 30 on the ground by adjusting the sampling time of each band. The imaginary band 0 is put in the middle of band 30 and 32, and used as a reference band. The use of the ideal band is explained in Section 3.1.4.3 Sub-pixel Approximate Ground Location Model.

A set of parametric equations and a table of sub-pixel corrections for each detector in each band will be included in the data product to capture the effects of band-to-band and detector to detector offsets and to permit calculation of the locations of the 500m and 250m bands. These are explained in Section 3.1.4.1 Instrument Model Algorithm/Focal Plane Assembly Model, where the telescope focal length is expressed in mm and detector locations and dimensions are expressed in  $\mu\text{m}$ . However actual computation is done in meters using ground point coordinates.

An overview of the various sections in this document is presented in Figure 2-1. Also an overview of the various coordinate systems and their relationships are illustrated in Figure 2-2.

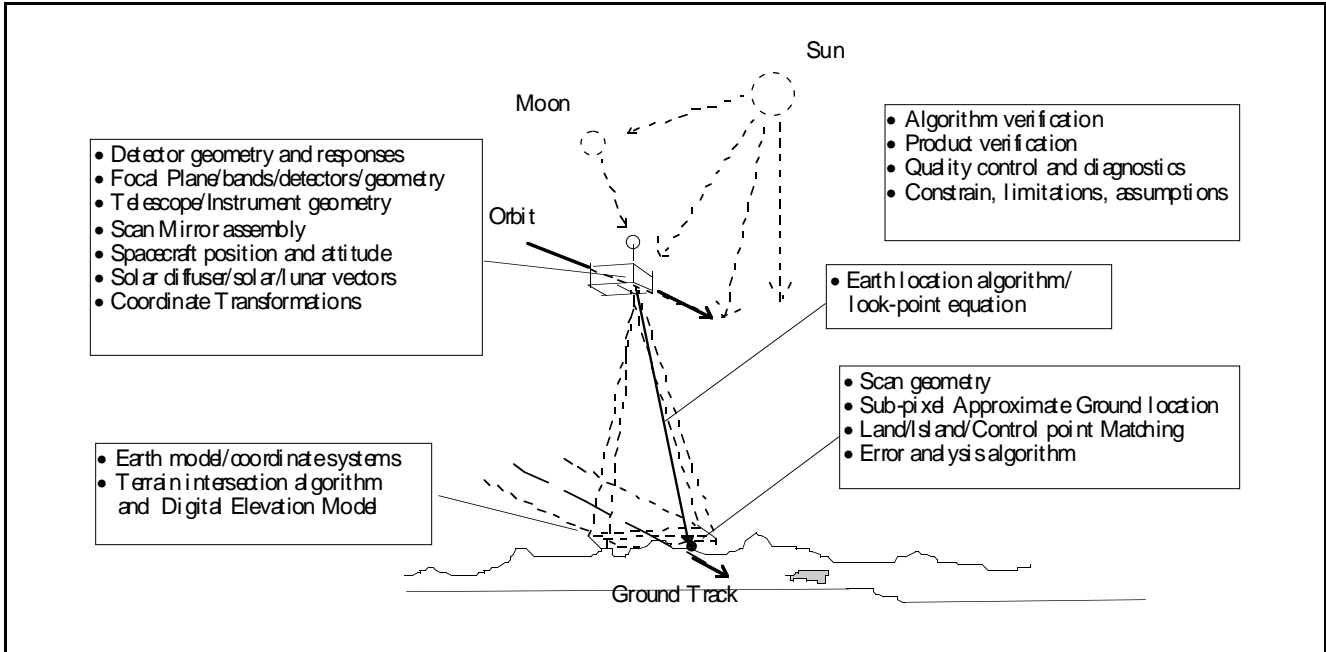


Figure 2-1. MODIS Instrument and Support Overview

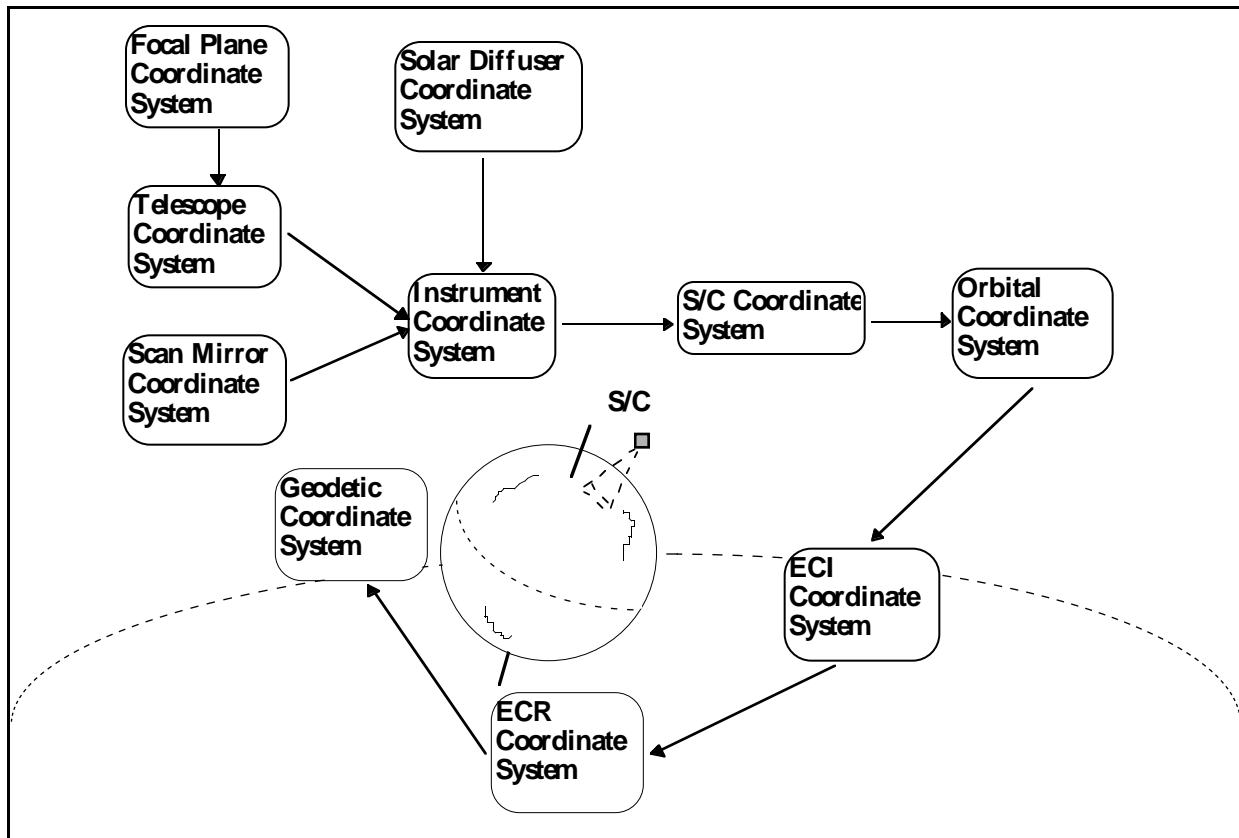


Figure 2-2. Coordinate Systems Overview and Coordinate Transformations

## 2.1 Requirements for Earth Location

The eight Earth location data fields include geodetic latitude and longitude, height above the Earth ellipsoid, satellite zenith angle, satellite azimuth, range to the satellite, solar zenith angle, and solar azimuth. These data will be used in Level 1B, Level 2, and in Level 3 processing where spatial resampling is carried out, as well as by the end users of all product levels. The MODIS Land Team requires the Earth location knowledge be accurate to 0.1 pixels ( $2\sigma$  for the 1 km bands) to support image registration for change detection. This accuracy requirement guides the design of the Earth location algorithm.

The Earth location latitude and longitude reference is needed to relate the MODIS science data to other spatially referenced data sets, including other MODIS data, and to provide a uniform, worldwide spatial reference system for all data products. Earth locations are provided at each spatial element in order to capture the terrain relief parallax, the high spatial frequency variations in the locations of off-nadir spatial elements caused by the Earth's terrain. If effects of the parallax were not included, samples in two data sets acquired with different viewing geometry would be incorrectly located relative to each other by tens of kilometers in areas of high relief. Earth location refinement for higher resolution bands and/or to incorporate sub-pixel band/detector misalignment is accomplished by interpolating between spatial element Earth locations using parametric equations (see Section 3.1.4.3).

The solar angles, satellite angles, satellite range and height are for use in MODIS Level 2 processing, such as atmospheric correction. The ground point height and zenith angles are measured with respect to the local ellipsoid normal. The azimuth angles are relative to local geodetic north.

## 2.2 Historical Perspective

Similar Earth location algorithms are widely used in modeling and geometrically correcting satellite image data from the Land Remote Sensing Satellite (Landsat) Multi-spectral Scanner (MSS), Landsat Thematic Mapper (TM), System pour l'Observation de la Terre (SPOT), and Advanced Very High Resolution Radiometer (AVHRR) missions. In each case, the fundamental problem is in computing the point at which the sensor line of sight intersects the Earth ellipsoid and/or terrain surface, leading to much commonality among these algorithms. Experience with SPOT and AVHRR data in particular has demonstrated the importance of compensating for the effects of terrain relief when Earth locating off-nadir satellite imagery.

In the MODIS Level 1A processing system, the Earth location algorithm is used to tag each spatial element with its locational "attributes." This information contributes to the subsequent Level 1B and Level 2 processing prior to being used to perform spatial resampling during Level 3 processing. In most Landsat and SPOT applications, the Earth location data are used immediately, prior to data analysis, to resample the instrument detector output to an Earth referenced grid. This difference in philosophy leads to data processing and data storage considerations that are somewhat unusual

for the MODIS Earth location algorithm. Two places where this is particularly relevant are the density at which Earth locations must be stored to capture the high spatial frequency variations due to terrain relief (see Section 3.1.4.2), and the need to defer band and detector alignment resampling until Level 3 processing (see Section 3.1.4.3).

## **2.3 Instrument Characteristics**

Although the basic outline of the Earth location algorithm has much in common with other instruments, there are particular characteristics of the MODIS instrument and science data stream that have special relevance to Earth location. There are two specific geometric characteristics of the instrument: detector and scan.

### ***2.3.1 Detector Geometry and Detector Response***

Of particular significance is the geometry of the multiple detectors (ten each for the 1 km bands, twenty each for the 500m bands, and forty each for the 250 m bands) from the multiple bands (36), which are themselves distributed over four focal planes. These bands and detectors are nominally aligned into coincident spatial elements. All bands are nominally aligned to 1 km band 30 IFOV and make up a dataset called "frame". Misalignments will be measured preflight at the Santa Barbara Research Center (SBRC), monitored in-flight by the MODIS Spectroradiometric Calibration Assembly (SRCA) and through image data analysis, and adjusted in-flight (focal plane-to-focal plane) through adjustments of sampling times. The best estimates of the sub-pixel offsets from nominal locations for each detector in each band will be included with the Level 1A data products for use in subsequent processing (e.g., Level 3 resampling).

In developing algorithms for the MODIS instrument, it is important to understand exactly what the sensor measurements represent. What follows is a basic description of the actual MODIS sensor pattern. It describes the response of the instrument on a single pixel basis and shows how individual pixels actually overlap in the along-scan direction. It also discusses how the 1000, 500, and 250 m pixels are registered.

#### ***2.3.1.1 Triangular Weighting Function***

The MODIS instrument has detectors that are square or rectangular in shape and receive a signal at any particular instant of time from an area of the Earth's surface that is 1000, 500, or 250m on a side (all dimensions are for nadir pixels). There is a temptation to think that the detector dwells over a single location until a sample is taken and then steps to the next pixel. This would produce a rectangular response weighting function as shown in Figure 2-3.

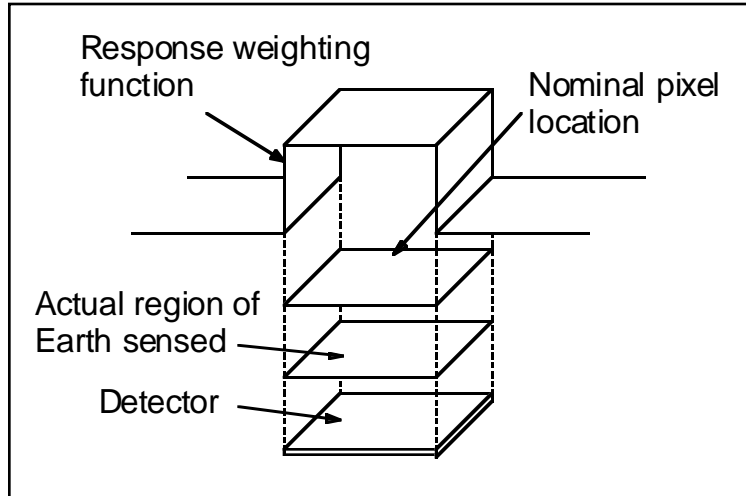


**Figure 2-3. Rectangular Response Weighting Function**

However, this is not the case; instead, MODIS senses the Earth using a scan mirror that rotates at a constant speed. A single sample consists of the integrated signal received at the detector during the entire sampling interval. This sampling interval is typically the amount of time it takes the projected image of the detector on the ground to move sideways (along-scan) one sample, 333.333  $\mu\text{sec}$  (dwell time) for the 1 km bands. The small amount of time (10  $\mu\text{sec}$ ) at the beginning of the sampling interval needed to read out the integrated information from the detector and reset the detector is ignored in this discussion (see Section 3.1.4 Mathematical Description of Algorithm, Time of Individual Samples in Each Band).

Although what actually happens is that the ground image travels across the detector, it is common to speak as if the pixel moves across the surface of the Earth, which is portrayed in this description. So, for a detector with a perfect rectangular response, the area actually sensed is twice as long as the nominal detector pattern, and the effective time weighted response is triangular as shown in Figure 2-4.

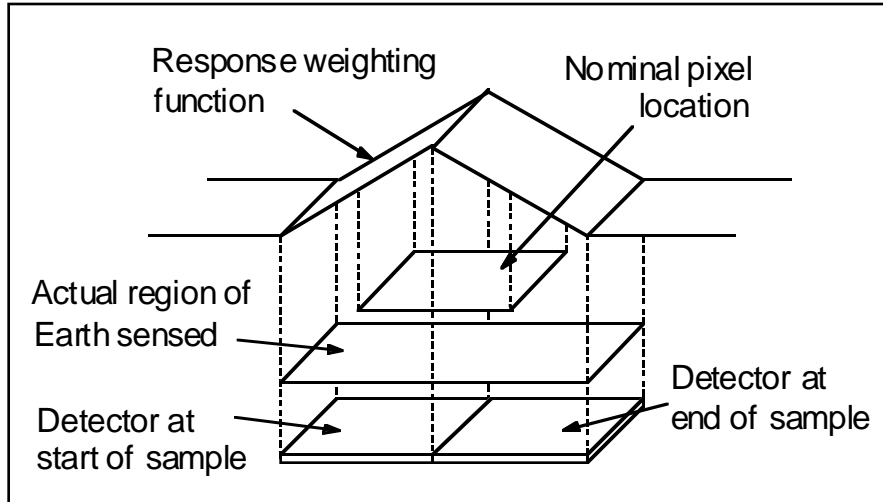


**Figure 2-4. Triangular Response Function from the Effective Time Weighting**

Of course, there is not just one sample along a scan line. As soon as the time for one sample ends a new sample is begun. The result is a series of triangular weighted pixels as shown in Figures 2-5 and 2-6. (For simplicity the remaining figures are done in two dimensions.)

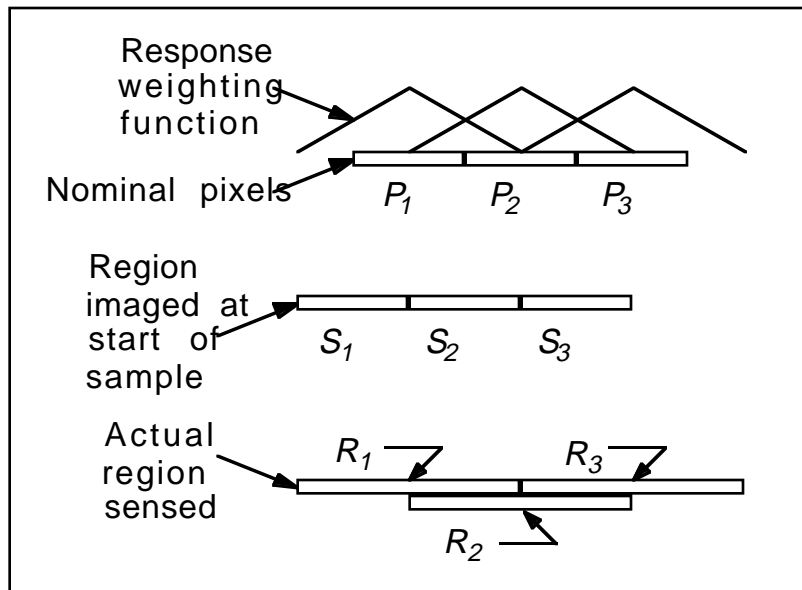


**Figure 2-5. Series of Triangular Weighted Pixels**

Figure 2-5 shows that nominal pixel  $P_2$  actually obtains signal from the right hand side of nominal pixel  $P_1$  and from the left hand side of nominal pixel  $P_3$ . It also shows that a small hot spot in the exact center of region  $P_1$  would have all of its response in  $P_1$ , but the same hot spot, such as a fire, located at the right hand edge of  $P_1$  would have half of its response shown in  $P_1$  and half in  $P_2$ . Although we speak of nominal 1 km pixels, the signal is obtained from a strip that is 2 km along-scan and 1 km along-track at nadir.

In fact, as shown in Figure 2-6, for a uniform scene of constant brightness, 12.5% of the signal is collected from each side and 75% of the signal is collected from the nominal pixel itself.

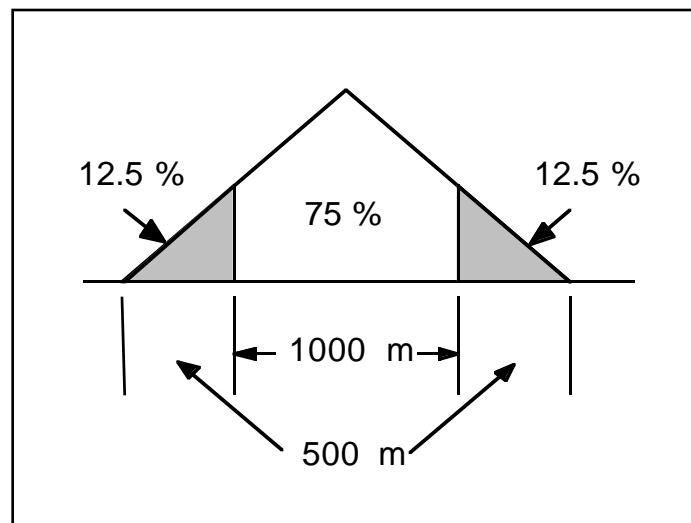


**Figure 2-6. 75 % of Signal is Collected from the Nominal Pixel**

### 2.3.1.2 Registration of 1000 and 500 m pixels

The same thing happens for the 500 m pixels. MODIS is built so that the start of the weighting function for the 500 m pixel is the same as the start of the weighting function for the 1 km pixel. This means that four 500 m pixels are not contained within a 1 km pixel. This is shown in Figure 2-7.

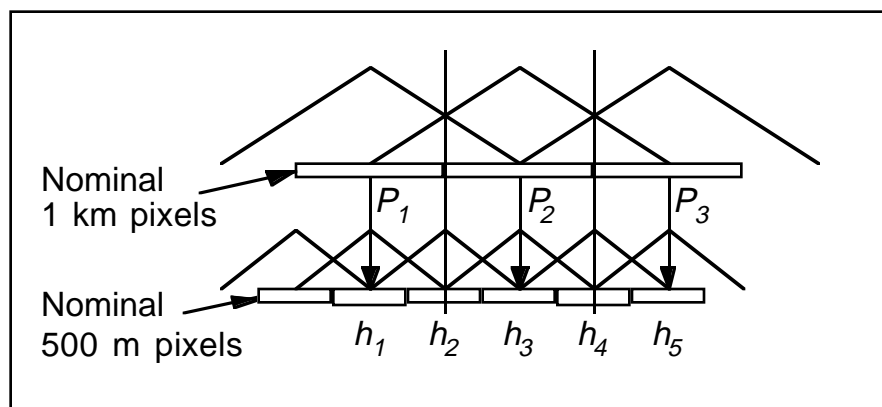


**Figure 2-7. Registration of 500 m and 1 km Pixels**

The same relationship exists between the 250 m and 500 m pixels. Just as the along-scan 500 m nominal pixel edges are 250 m from either side of a 1 km pixel, the 250 m nominal pixel edges are 125 m from the edges of the 500 m pixels, thus 375 m from the edge of the 1 km pixels.

With this sample timing, nominal 1 km pixel  $P_2$  covers the same region as the right hand half of nominal 500 m pixel  $h_2$  and all of  $h_3$ , plus the left hand half of  $h_4$  and three similar 500 m pixels in the next row. This means four complete 500 m nominal pixels, or sixteen 250 m nominal pixels, do not cover a single 1 km nominal pixel. Instead, as seen in Figure 2-8, which shows the situation when looking down at the nominal pixels, a 1 km pixel is overlaid by two complete 500 m pixels and 1/2 of each of four more 500 m pixels. Similarly, a single 1 km nominal pixel is overlaid by twelve complete, and eight half, 250 m pixels as shown in Figure 2-8. However, to see the same total time weighted signal as with the 1 km pixel, it is necessary to combine the signal from all six 500 m pixels, or twenty-eight 250 m pixels, including eight 250 m pixels that are outside the nominal 1 km pixel! This somewhat counterintuitive result is shown in Figures 2-9 and 2-10 and discussed below.

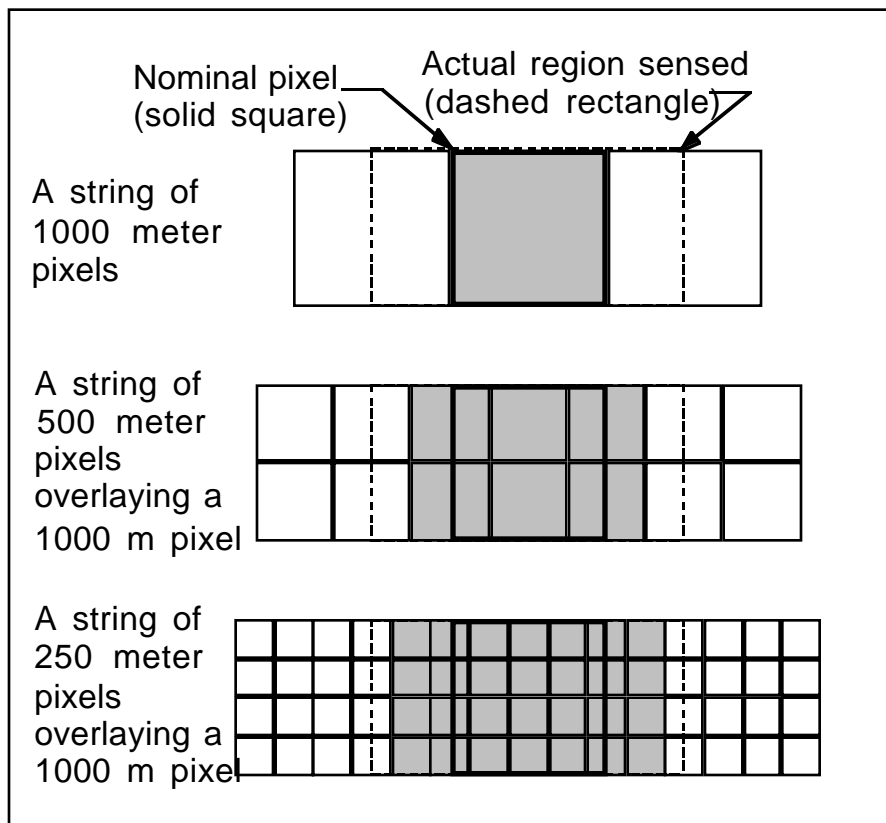


**Figure 2-8. Higher Resolution Pixels Needed to Generate 1 km Pixels**

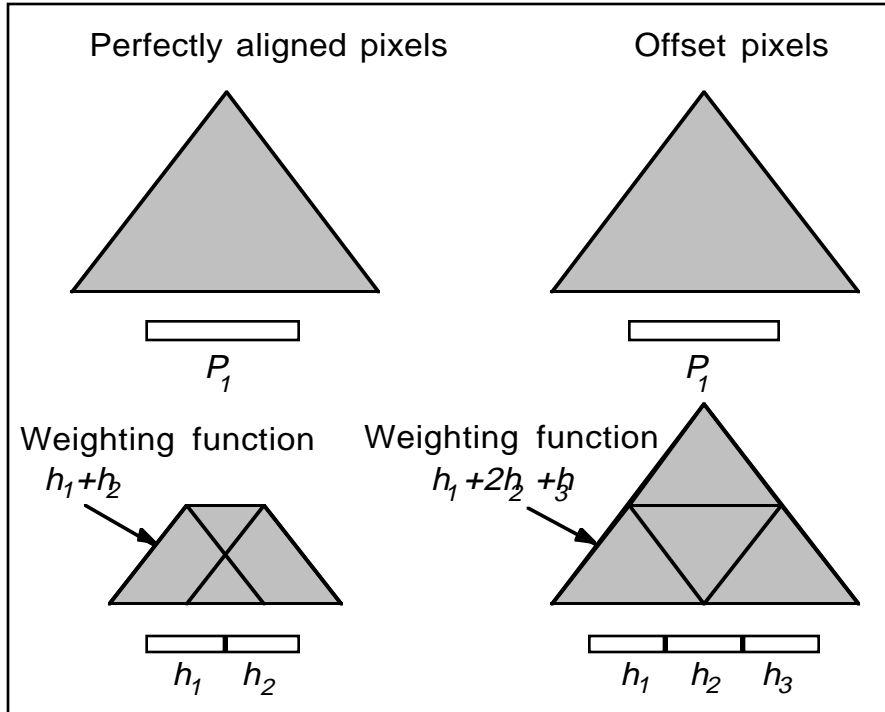


Figure 2-9. Equivalent 500 m Weighting Functions \*

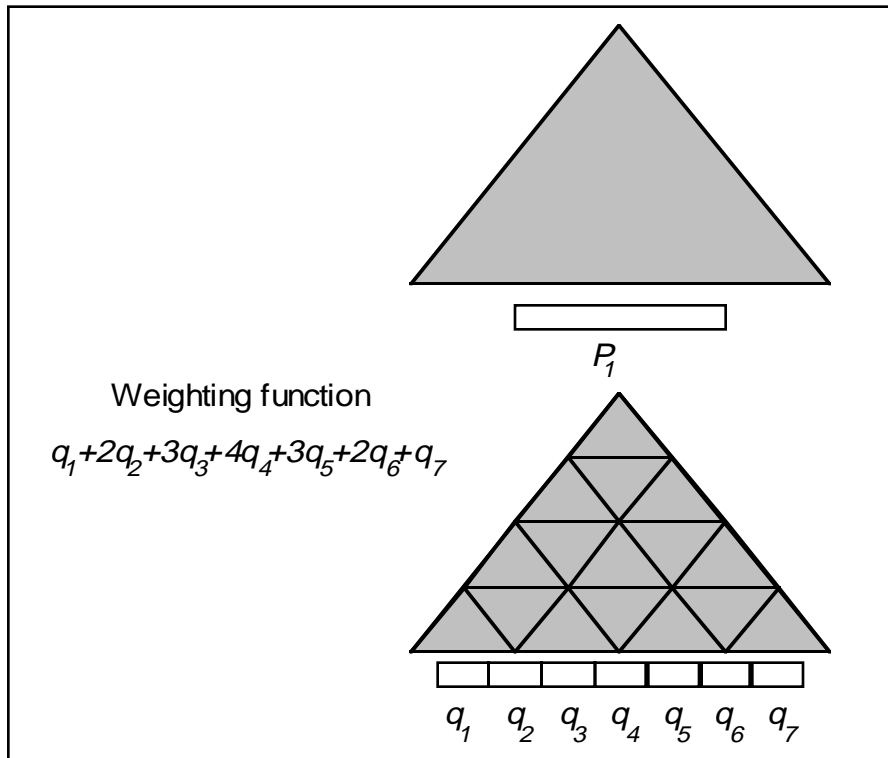


Figure 2-10. Equivalent 250 m Weighting Function \*

### 2.3.1.3 Combining Different Sized Pixels

The equations for combining samples from different sized pixels are shown in Figures 2-9 and 2-10. If the 500 m and 1 km pixels were perfectly aligned, the sum of the two 500 m pixels would sense a smaller region with a different weighting function than the 1 km pixel. There is no simple way to combine two (actually four counting the two in the other row) 500 m pixels to get the same field of view as a single 1 km pixel. However, with the pixels offset by adjusting sampling time, there is a simple linear combination of three (actually six) 500 m pixels with the same weighting function as the overlapped 1 km pixel. Similarly, it is possible to find a linear combination of 250 m pixels that have the same weighting function as a single 500 m pixel or as a single 1 km pixel.

Figures 2-9 and 2-10 (and the listed weighting functions) only show the first row of 500m or 250 m pixels. It is necessary to include the contribution of both rows of 500m pixels, or all four rows of 250m pixels as shown in Figure 2-8.

### 2.3.1.4 Using Multiple Resolution Data

Several things should be considered when using multiple resolution data in this pixel arrangement:

- 1) Even for a perfect detector, nominal pixels are rectangular with some overlap, not square and independent.
- 2) It is possible to calculate a linear sum of high resolution pixels that have the same effective weighting function as a lower resolution pixel.
- 3) The response to sub-pixel sized bright targets depends on what part of the pixel contains the anomalous area.
- 4) This is a simplified discussion of a complex situation. Many things were omitted such as the instrument point spread function, atmospheric smearing, cross talk, bright target recovery, registration error, and more. Also, the scenes that will be observed will not be uniform targets.

### 2.3.1.5 Location of Spatial Element

Figure 2-11 shows the correspondence between the location of a spatial element and the actual samples included in single frame of MODIS data. Each frame of MODIS data contains all of the samples from all of the bands corresponding to ten 1 km ground locations along-track ignoring the triangular response function from the effective time weighting. For the two frames of data shown in the figure below, the location of the spatial element for frame A corresponds to the center of the only sample in the 1 km bands, the center of the second sample in the 500 m bands, and the center of the fourth sample for the 250 m bands.

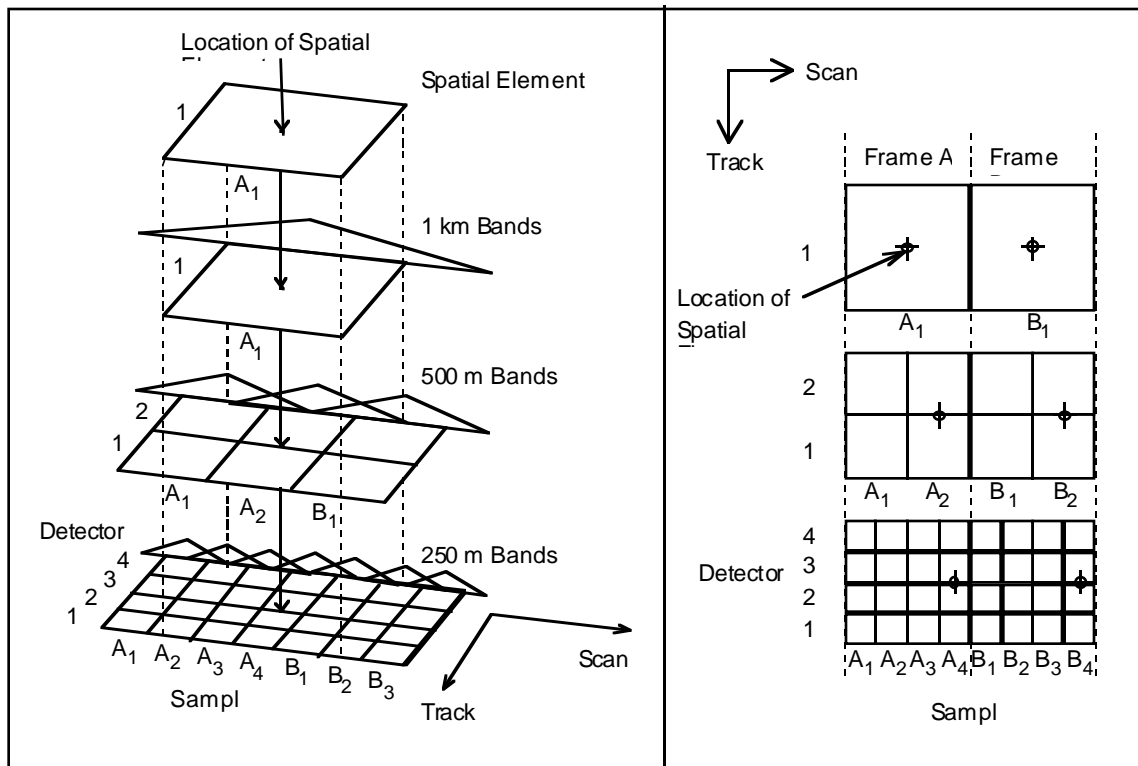


**Figure 2-11. MODIS Spatial Element Location**

### 2.3.2 Scan Geometry

The second characteristic of the MODIS instrument of particular importance for Earth location is the behavior of the cross-track scanning mirror. The double-sided scan mirror sweeps out a 110 deg Earth field of view in each scan, effectively moving the instrument's ten spatial elements over a swath of the Earth 10 km wide at nadir. This scan width increases to 20 km at scan angles of +/- 55 deg due to the panoramic "bow tie" effect (Figure 2-12). This effect leads to scan-to-scan overlap at scan angles greater than 25 deg (Figure 2-13) (actually, the 500m and 250m bands overlap at smaller scan angles, around 17 deg for the 250 m bands). On the other hand, the scan gap at nadir is nominally zero. The scanning mirror motion is measured and down-linked in the instrument data stream. These mirror measurements will be used by the Earth location algorithm to determine the instrument pointing (rather than assuming mirror motion linearity. See Section 3.1.4.1 Instrument Model Algorithm Scan Mirror Encoder Assembly).

A copy of the spacecraft ancillary data message containing spacecraft ephemeris and attitude information is included in the MODIS instrument data stream. This data will be included in the Level 0 data set used as input to the Level 1A process. Under normal operating conditions the ephemeris and attitude information contained in the Level 0 data will be used to provide the spacecraft knowledge required by the Earth location algorithm. A description of this data message and additional information on spacecraft characteristics can be found in References 4 and 9.

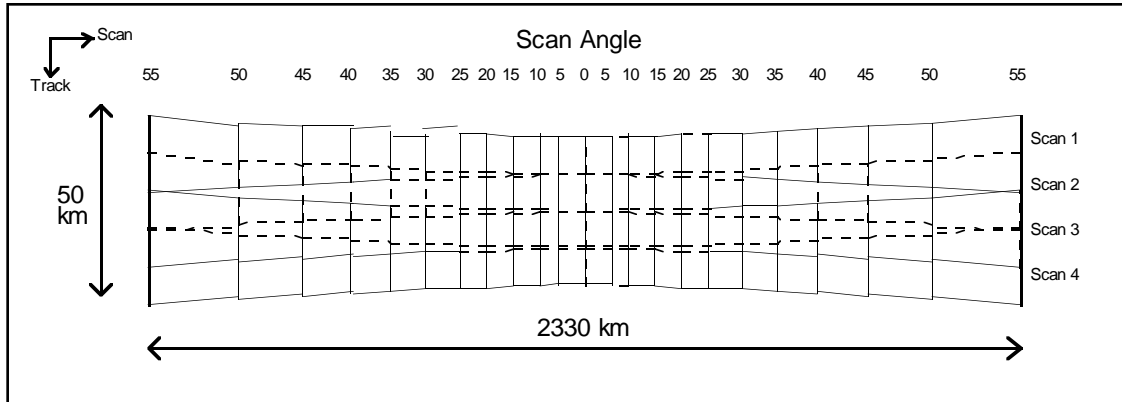


Figure 2-12. Panoramic Bow Tie Effect

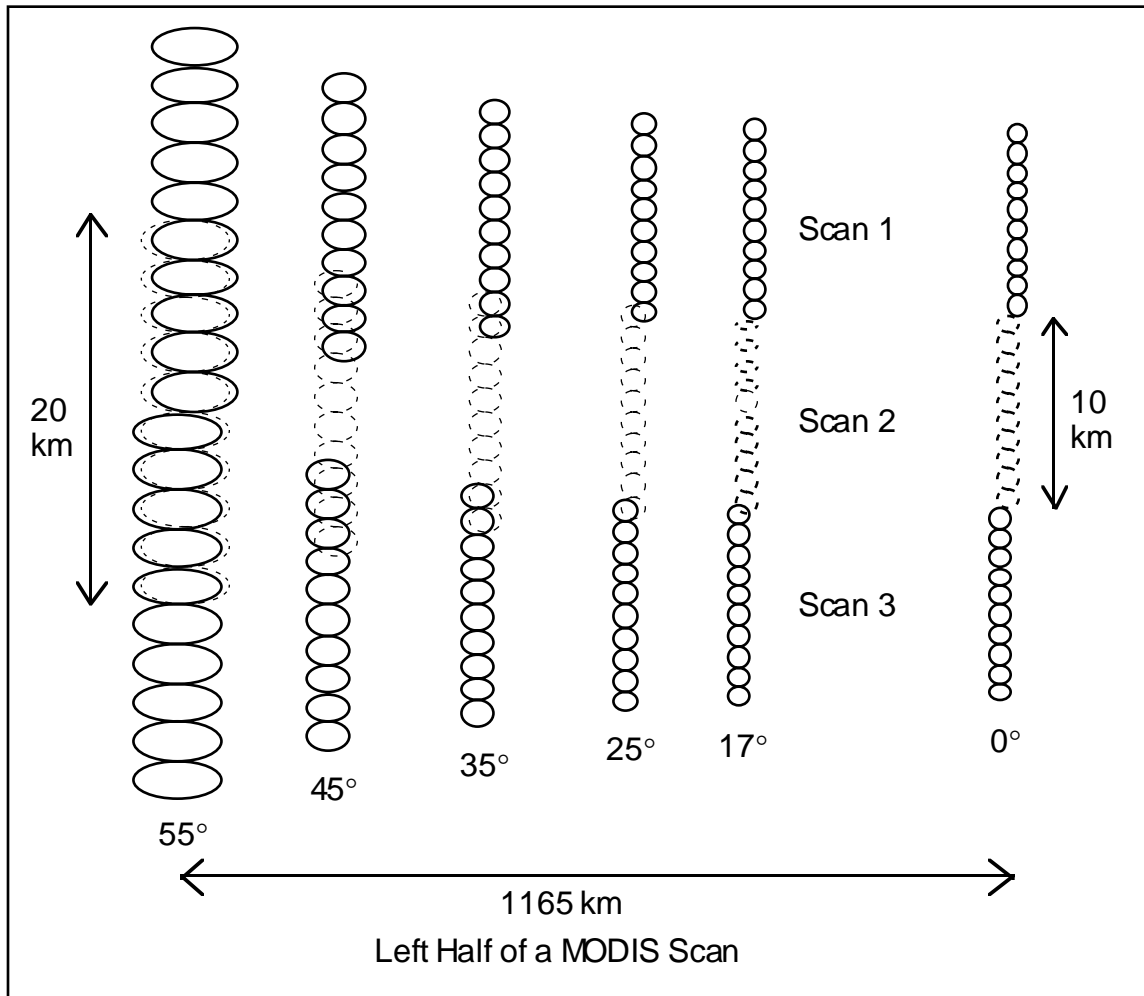


Figure 2-13. Pixel Size Growth and Overlap within a Scan

## 2.4 Ancillary Input Data

Several important ancillary input data sets are used by the MODIS Earth location algorithm. These include digital elevation data used to describe the Earth's terrain surface, instrument constants used to describe the internal geometry of the MODIS instrument, and ground control points used to validate the accuracy of the Earth location data.

The digital elevation model (DEM) used by the MODIS Earth location algorithm will be derived from the best available global database of terrain information provided by the EOS Project. The EOS-wide requirements for terrain data are described in Reference 8. The relationship between the accuracy of this ancillary data set and the resulting accuracy of the MODIS Earth location data is discussed in Reference 2.

Three types of instrument constants are required for MODIS Earth location processing. Although the term "constants" is used here it is understood that the values of these parameters may be intentionally adjusted, change with time, or may be updated as better knowledge of their true values becomes available. They are constants when generating a particular data product.

The first type of instrument constants include the focal plane, band, and detector locations. These constants will be stored in the MODIS data product as a table of locations to generate corrections applicable to each detector (channel) in a spatial element. The second type may be classified as optics parameters. They include the focal lengths of the aft optics, the relationship between the optical axis and instrument alignment axes, angles that describe the scan mirror surfaces, the relationship between the scan mirror assembly and the instrument alignment axis, and the scan angle as a function of mirror encoder number. The aft focal lengths are needed to generate a viewing vector from a location on the focal plane. The other optics parameters are needed to determine the orientation of the normal to the scan mirror surface at a given sample time. Once this is known, the viewing vector is reflected off the scan mirror to produce an object space viewing vector. The third type of instrument constant required is the instrument-to-spacecraft alignment matrix. This matrix describes the spatial relationship between the MODIS instrument alignment axes and the EOS spacecraft. This relationship may have a time varying component that can be detected and modeled over time, but will be assumed to be static at launch.

The spacecraft's orbital ephemeris and attitude can be retrieved from either the spacecraft ancillary data packets included in the MODIS instrument telemetry or from archived ephemeris through ECS Science Data Processing Toolkit routines. Attitude information in the spacecraft ancillary data packets is unreliable during AM-1 Platform maneuvers when the vehicle is commanded away from Earth-centered pointing. The archived attitude data, however, will be extracted from valid spacecraft housekeeping data. Accurate attitude data is required for MODIS calibration during the spacecraft calibration maneuvers. The preferred source of ephemeris and attitude data is the ECS-supplied data available through the Toolkit routines.

The ground control points (land and islands) used to validate the MODIS Earth location algorithm's performance are image windows containing well defined features with known ground locations. These control points will be collected from a number of sources, including, Landsat TM data and World Vector Shoreline Data. The current MODIS operational concept includes the use of control with a subset of MODIS Level 1A products only. This is based on the idea that it will be more effective to concentrate the acquisition of high quality ground control along a few orbits so that one product in ten, for example, has abundant control rather than all having minimal control. Concentrating high quality control throughout a few orbits allows both short-term and long-term variations in parameter biases to be found. Additional ground control will be used throughout the rest of the world to verify the accuracy of the Earth location parameters globally.

### **3. ALGORITHM DESCRIPTION**

## Table of Contents

<b>1. INTRODUCTION .....</b>	<b>1-1</b>
<b>2. OVERVIEW AND BACKGROUND INFORMATION .....</b>	<b>2-1</b>
<b>3. ALGORITHM DESCRIPTION.....</b>	<b>3-1</b>
3.1 Theoretical Description .....	3-1
3.1.1 MODIS Viewing Geometry Overview .....	3-1
3.1.2 Coordinate Systems.....	3-2
3.1.2.1 Focal Plane Coordinate System .....	3-3
3.1.2.2 Telescope Coordinate System.....	3-3
3.1.2.3 Scan Mirror Assembly Coordinate System .....	3-4
3.1.2.4 Solar Diffuser Coordinate System.....	3-5
3.1.2.5 Instrument Coordinate System .....	3-6
3.1.2.6 Spacecraft Coordinate System .....	3-7
3.1.2.7 Orbital Coordinate System.....	3-7
3.1.2.8 Earth Centered Inertial Coordinate System.....	3-7
3.1.2.9 Earth Centered Rotating Coordinate System.....	3-8
3.1.2.10 Geodetic Coordinate System .....	3-9
3.1.3 Coordinate Transformations.....	3-9
3.1.3.1 Focal Plane to Telescope.....	3-10
3.1.3.2 Telescope to Instrument .....	3-11
3.1.3.3 Scan Mirror Assembly to Instrument.....	3-11
3.1.3.4 Solar Diffuser to Instrument .....	3-12
3.1.3.5 Instrument to Spacecraft .....	3-12
3.1.3.6 Spacecraft to Orbital .....	3-12
3.1.3.7 Orbital to ECI .....	3-13
3.1.3.8 ECI to ECR .....	3-13
3.1.3.9 ECR to Geodetic .....	3-14
3.1.4 Mathematical Description of Algorithm.....	3-14
3.1.4.1 Instrument Model Algorithm .....	3-15

Figure 3-1. Growth of Spatial Element Ground Field of View .....	3-2
Figure 3-2. Focal Plane Coordinate System .....	3-3
Figure 3-3. Instrument, Telescope and Scan Mirror Assembly Coordinate Systems' Relative Orientation .....	3-4
Figure 3-4. Nadir View, Scan Mirror Angle, Focal Plane Tilt in Instrument Coordinate System.....	3-5
Figure 3-5. Solar Diffuser and Solar Vector Configuration .....	3-6
Figure 3-6. Orbital Coordinate System .....	3-7
Figure 3-7. ECI Coordinate System.....	3-8
Figure 3-8. ECR Coordinate System .....	3-9
Figure 3-9. Focal Plane Rotation to Compensate for Spacecraft Along-Track Motion	3-10
Figure 3-10. Physical Layout of the Focal Planes.....	3-16
Figure 3-11. Offset of Each Band Relative to the Reference Optical Axis.....	3-18
Figure 3-12. Measurements of Detector Locations on Focal Plane.....	3-20
Figure 3-13. Integration Area for Different Sampling Rates and Ground Resolution.	3-21
Figure 3-14. Time of Start of Earth View Sector .....	3-22
Figure 3-15. Frame Start Timing for Earth View Sector Around $t_0$ .....	3-22
Figure 3-16. Mirror Wedge Angles and Axis Errors Definitions .....	3-26
Figure 3-17. Scan Mirror Normal Vectors .....	3-28
Figure 3-18. Encoder Time Sample Interpolation .....	3-30
Table 3-1. Focal Lengths for Each Focal Plane.....	3-15
Table 3-2. Detector Specifications .....	3-17
Table 3-3. Nominal Band Layout with Respect to the Optical Axis.....	3-18
Table 3-4. Detector Sampling .....	3-20
Table 3-5. Scan Mirror Assembly Geometric Specifications.....	3-25
Table 3-6. Scan Mirror Encoder Geometric Constants.....	3-28
Table 3-7. Scan Mirror Encoder Geometric Derived Values.....	3-28

## **1. INTRODUCTION**

## **2. OVERVIEW AND BACKGROUND INFORMATION**

### 3. ALGORITHM DESCRIPTION

This section presents the underlying theory and mathematical development of the MODIS Earth location algorithm in Section 3.1. It addresses implementation and operational considerations in Section 3.2.

#### 3.1 Theoretical Description

The supporting theoretical concepts and mathematics of the MODIS Earth location algorithm are presented in the following subsections. Section 3.1.1 presents a review of the MODIS viewing geometry to put the subsequent discussion in context. Sections 3.1.2 and 3.1.3 address the coordinate systems used by the algorithm and the relationships between them, citing references where appropriate. Section 3.1.4 is the heart of this document, presenting the mathematical development of, and solution procedure for, the Earth location algorithm. Section 3.1.5 briefly discusses estimates of uncertainty and product accuracy issues. This last topic is treated in more detail in Reference 2.

##### 3.1.1 MODIS Viewing Geometry Overview

The MODIS instrument detectors are aligned in parallel rows on four separate focal planes. Each focal plane has its own aft optics assembly that illuminates the detectors on that focal plane. The detector placement geometry and aft optics focal length define the internal geometry of each focal plane relative to the instrument optical axis. The rows of detectors from each band are separated on the focal plane in the along-scan (cross-track) direction. The different bands are aligned into corresponding spatial elements on-board by delaying the samples from each band to account for the slight along-scan motion needed to view the same target point. These delays are fixed within each focal plane, but the relative delays between focal planes can be adjusted in-flight.

The instrument's 110 deg field of view is swept over the four focal planes by the double-sided rotating scan mirror. The preflight optical alignment tests of the MODIS instrument should document any differences in the scanning geometry of the two mirror sides. The scan mirror rotates at a rate of  $20.3092 \pm 0.1\%$  revolutions per minute. With each mirror rotation capturing two scans (one for each mirror side), the scan period is 1.477 sec. Of this time, approximately 0.451 sec is devoted to the Earth view portion of the scan with detector samples being taken every 333.333  $\mu$ sec (for the 1 km resolution bands). Significant spacecraft motion and Earth rotation take place during this scan period. More detailed information on the MODIS instrument's construction, operation, and preflight testing is provided in Reference 1.

The 110 deg-wide instrument field of view sweeps out a ground swath approximately 2330 km long during the 0.451 seconds Earth view period. This swath is sampled 1354 times by the MODIS spatial elements. Since ten spatial elements are sampled in each data frame, the nominal scan width is 10 km at nadir. The wide ground swath made

possible by the +/- 55 deg viewing angles exhibits significant Earth curvature effects. The apparent Earth zenith angle of a line of sight at a 55 deg scan angle is increased to approximately 65 deg by Earth curvature. This effect, along with the increasing target range, also contributes to the growth of the projected ground spatial element as a function of scan angle. Figure 3-1 is a graph depicting the growth of the spatial element ground field of view with scan angle. A 1 km (nadir) resolution spatial element at a 55 deg scan angle has ground dimensions of approximately 4800 m along-scan by 2 km along-track. The center of the spatial element (nominal detector) will be used when computing spatial element lines of sight. It should be noted that there is a very small distance between the spatial element center and the centroid of the ground projected field of view for off-nadir pixels. This distance is less than 2 m near the edges of the scan.

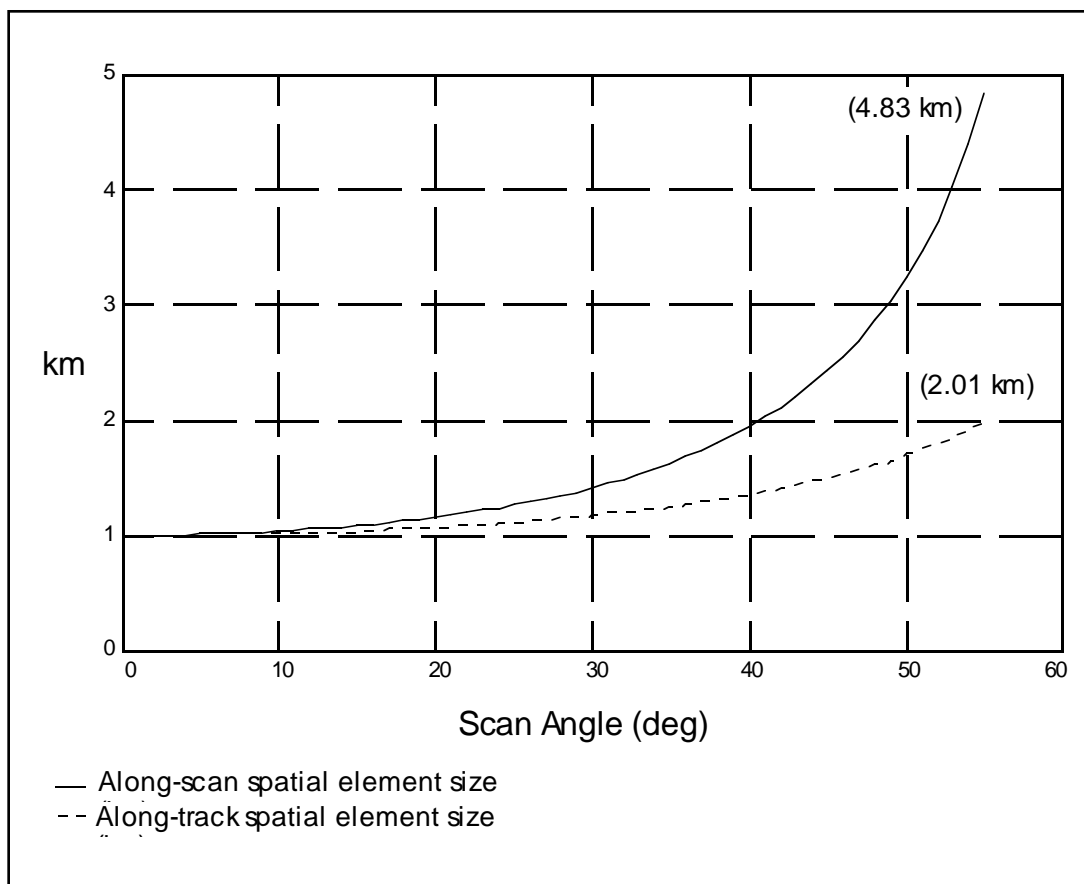


**Figure 3-1. Growth of Spatial Element Ground Field of View**

### 3.1.2 Coordinate Systems

There are nine basic coordinate systems used by the MODIS Earth location algorithm. These coordinate systems are defined here and referred to frequently in the remainder of this document. They are presented in the logical order in which a viewing vector and sample time would be transformed into a geodetic position. The orientation of the focal plane, telescope, scan mirror assembly, Solar Diffuser (SD), and instrument coordinate

system's axes chosen for this model are somewhat arbitrary, therefore SBRC may be using a different set of axes. It should be noted that the origin of the instrument coordinate system does not coincide with the origin of the spacecraft (about six meters off). This offset will be ignored in the rest of the document.

*3.1.2.1 Focal Plane Coordinate System*

The axis of the focal plane coordinate system coincides with the telescope z-axis. Because of a small rotation of the focal plane in the telescope coordinate system, the focal plane coordinate system is needed. The X-axis of the focal plane almost corresponds to the scan direction. The Y-axis corresponds to the negative direction of the ground track. The origin of each focal plane is marked in Figure 3-2 using NIR focal plane. A detailed layout of each band and its detectors are shown later in Figure 3-10. For example, X-coordinates of the detectors in Band 17 are all positive, while all detectors in band 19 have negative X-coordinates. Detectors are numbered so that detector 1 will see the south of where detector 2 sees on the ground during the descending path.

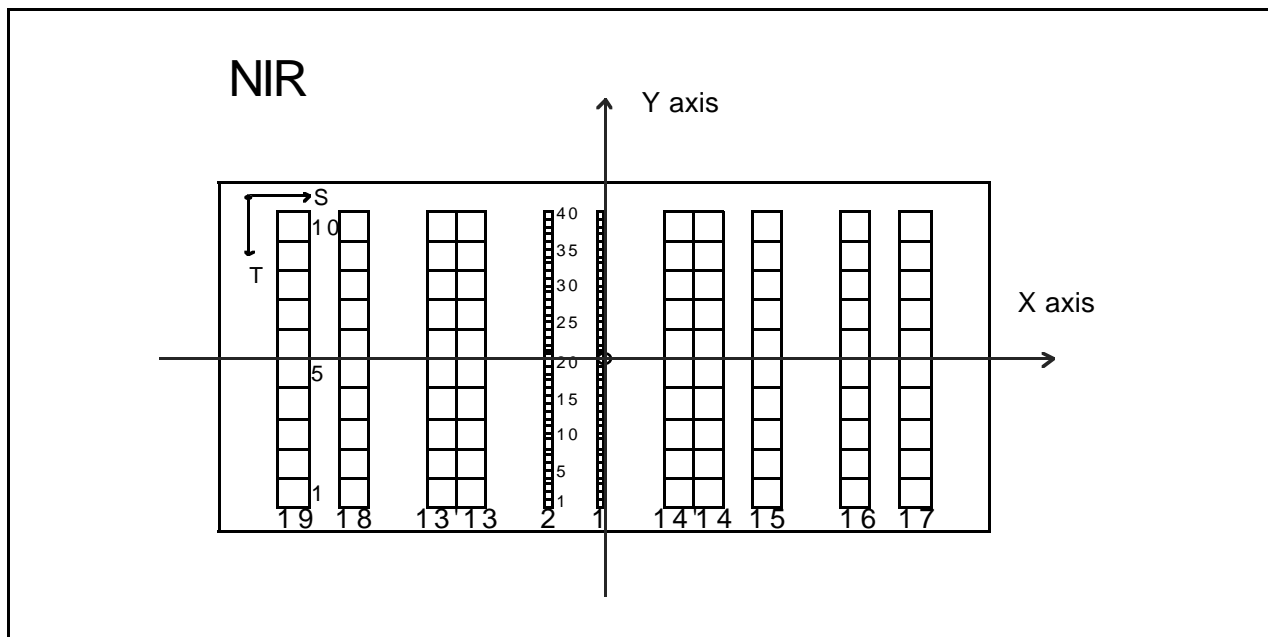


**Figure 3-2. Focal Plane Coordinate System**

*3.1.2.2 Telescope Coordinate System*

The telescope coordinate system is the place where the image space viewing vector is generated for either individual detector samples or for the ideal spatial elements. The origin is where an ideal optical axis intersects the focal planes (Figure 3-3 where the focal plane rotation is shown). The Z axis is both pointed at and is approximately

perpendicular to the center of the scan mirror axis of rotation. However, it is not perpendicular to the scan mirror Z axis, which is not visible in Figure 3-3. The X axis is perpendicular to the scan mirror's axis of rotation (unless there is some axis error as shown in Figure 3-16 and 3-17) and is in the along-scan direction after a reflection off the scan mirror. The positive direction is toward the band on the leading edge of the focal plane( band 30 in LWIR focal plane). The Y axis is in the focal plane's negative along-track direction after a reflection off the scan mirror with the positive direction toward the highest detector number.

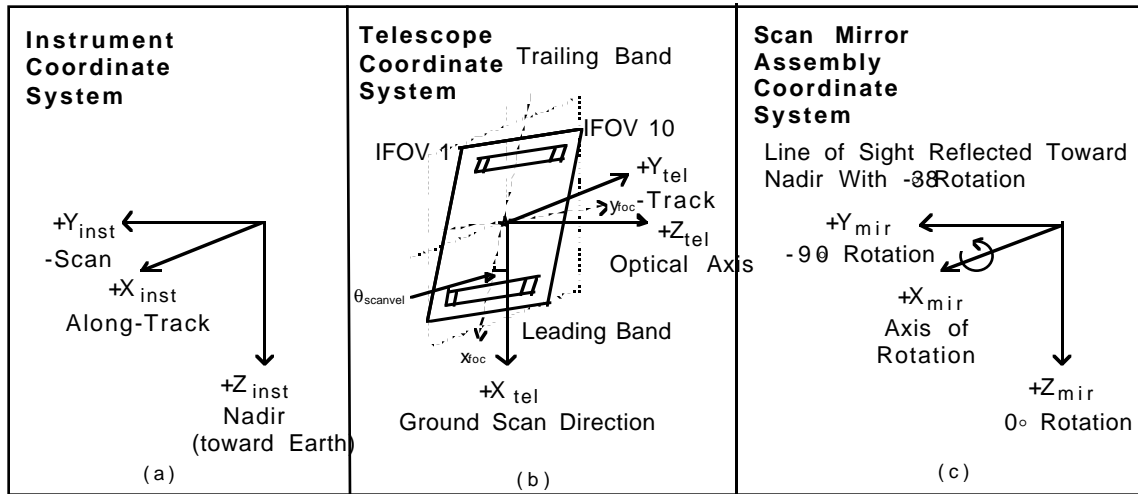


**Figure 3-3. Instrument, Telescope and Scan Mirror Assembly Coordinate Systems' Relative Orientation**

*3.1.2.3 Scan Mirror Assembly Coordinate System*

The scan mirror model is defined in the scan mirror assembly coordinate system. It is nominally aligned with the instrument coordinate system. This coordinate system is defined (Figure 3-3) so that the X axis is along the axis of rotation of the scan mirror, which is parallel to the along-track direction, and the Z axis is in the nadir direction (downward toward the Earth). The Y axis completes the right handed coordinate system.

When the normal of scan mirror side 1 is parallel to the Z axis, the mirror is defined to have a zero rotation angle (ignoring the small mirror wedge angles and axis error). When the mirror is rotated to either -38 or +142 deg, the line of sight along the telescope's optical axis is reflected by the mirror straight down toward nadir. In order to make the nadir view vector reaches back to telescope z-axis at scan mirror angle -38° or 142°, the telescope coordinate system must be rotated -14° around  $Y_{tel}$  axis. A view of the scan mirror, telescope, and instrument coordinate systems from the positive  $X_{inst}$  is illustrated in Figure 3-4 to show their relationship.

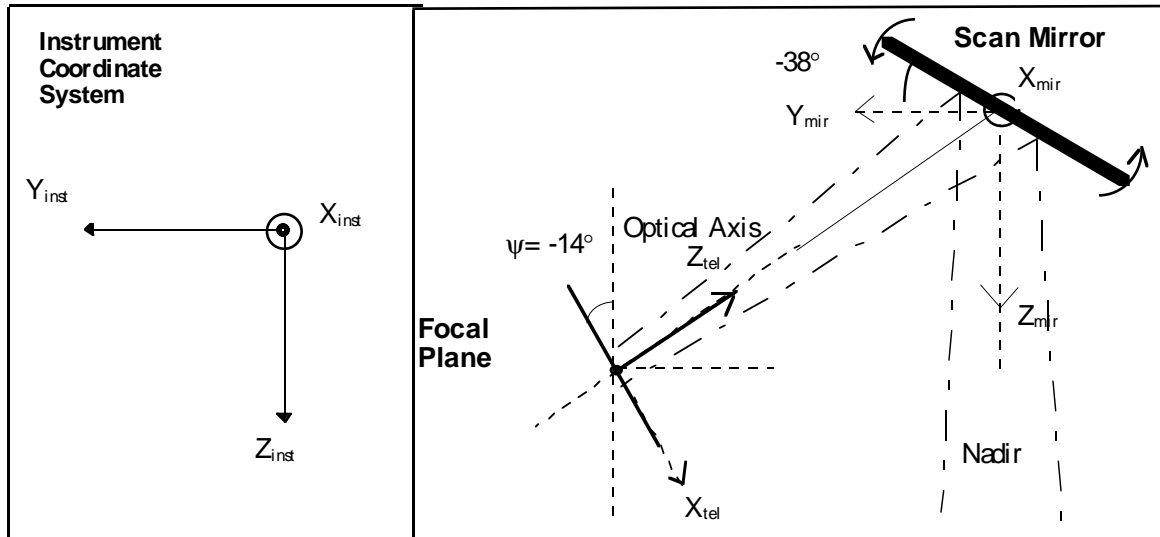


**Figure 3-4. Nadir View , Scan Mirror Angle, Focal Plane Tilt in Instrument Coordinate System**

The matrix expression for the coordinate transformation is given in Section 3.1.3.2.

It should be noted that the actual locations of the four focal planes vary. Two of them are mounted vertically and one horizontally. However, all the focal planes can be symbolized and placed at one location as depicted in Figure 3-4. The actual light leaving the scan mirror will be reflected by the other mirrors and pass through lenses and filters to reach a final focal plane.

#### 3.1.2.4 Solar Diffuser Coordinate System

At the time of calibration, the SD is illuminated by the sun for a short time at each orbit when the spacecraft is near the North Pole and when the subsatellite point is not sunlit. Before the sunlight reaches SD, an attenuation screen is deployed in order to permit calibration of the 9 bands which would saturate if sampling the SD in full sun. It will admit about 8.5 % of the sunlight. When the satellite is above sunlit parts of the earth, the SD is not illuminated. This provides accurate calibration and reduces stray light mixing into either the calibration signal or into the earth measurement. Figure 3-5 illustrates the SD surface and how the light, represented by this solar vector from the sun, reflects on the lambertian surface and scatter all directions.

Approximate ranges and values for the angles in Figure 3-5 are:

$$\theta_i = 54 - 63 \text{ degrees,}$$

$$\theta_M = 20.49 \text{ degrees,}$$

$$\phi_i = 14 - 21 \text{ degrees.}$$

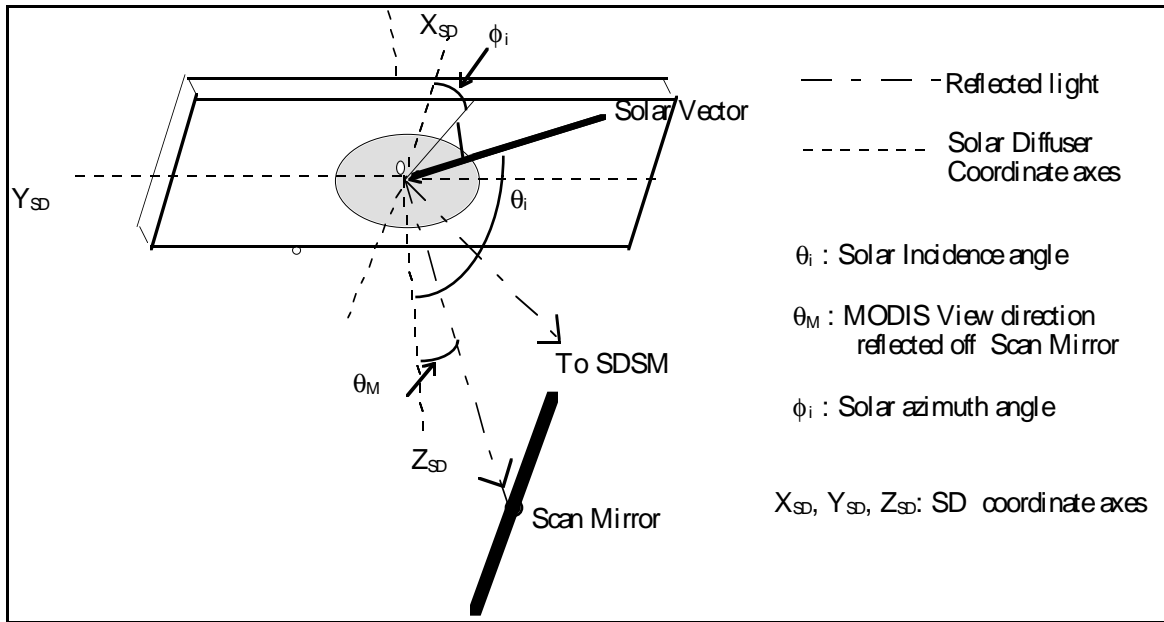


**Figure 3-5. Solar Diffuser and Solar Vector Configuration**

Two of the light vectors from the SD reach the Scan Mirror and the SD stability monitor (SDSM). The light from the SD is monitored during the 50 frames of the sampling beginning at a scan angle of -180 degrees which approximately corresponds to the scan mirror angle of -128 degrees. Section 3.1.3.4 describes the coordinate transformation from the SD coordinate system to the instrument coordinate system is described.

A vector to the sun from the spacecraft will be expressed in both the instrument and the SD coordinate systems in the Section 3.1.4.2.

### 3.1.2.5 Instrument Coordinate System

The instrument coordinate system (Figure 3-3) is the coordinate system in which an image space vector emanating from the center of a detector or spatial element number (1 through 10) and mirror angle is converted to an object space viewing vector. It is based on the MODIS reference axes defined by the MODIS alignment cube. During preflight testing, the actual alignment of the scan mirror assembly, telescope, and the spacecraft coordinate system to the instrument coordinate system will be measured. This relationship will be monitored in-flight by analyzing pointing errors as functions of scan angles.

This coordinate system is based on preflight measurements of the orientation of the instrument alignment cube. The sides of this cube could be slightly non-orthogonal because of manufacturing limits but an orthogonal transformation is used to convert to and from this coordinate system.

### 3.1.2.6 Spacecraft Coordinate System

The spacecraft coordinate system is fixed to the EOS spacecraft with its origin at the spacecraft center of mass. The coordinate axes are defined by the spacecraft attitude control system. It is the orientation of this coordinate system relative to the orbital coordinate system that is captured in the spacecraft attitude data.

### 3.1.2.7 Orbital Coordinate System

The orbital coordinate system is centered on the satellite and its orientation is based on the spacecraft position in inertial space (Figure 3-6). The origin is the spacecraft center of mass with the Z axis pointing from the spacecraft center of mass to the Earth center of mass. The Y axis is the normalized cross product of the Z axis and the instantaneous (inertial) velocity vector. It corresponds to the direction of the negative of the instantaneous angular momentum vector direction. The X axis is the cross product of the Y and Z axes. This coordinate system is defined in the MODIS Unique Instrument Interface Document (UIID) (Reference 4).

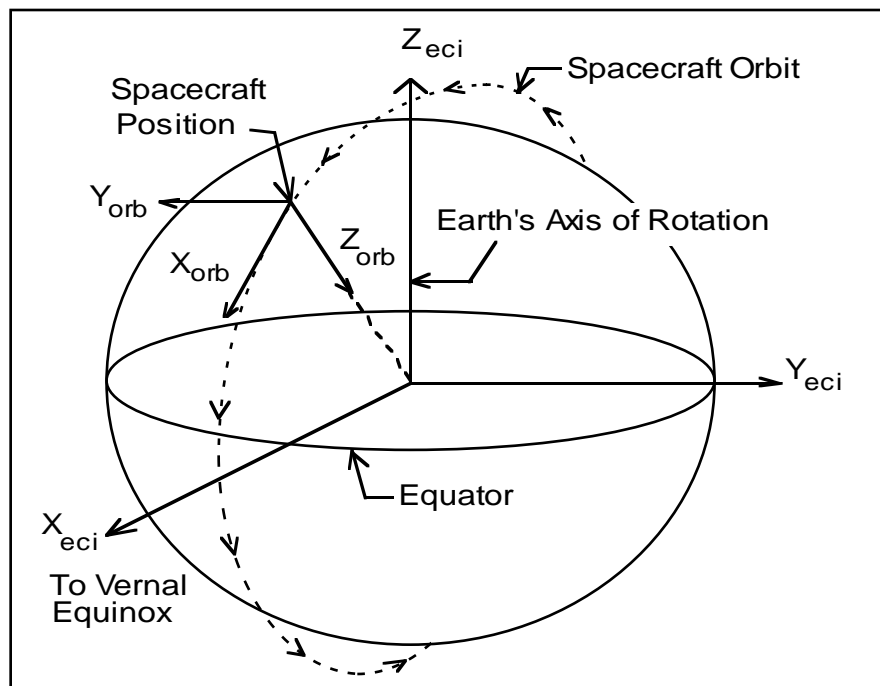


**Figure 3-6. Orbital Coordinate System**

### 3.1.2.8 Earth Centered Inertial Coordinate System

The Earth Centered Inertial (ECI) coordinate system is space fixed with its origin at the Earth's center of mass (Figure 3-7). The Z axis corresponds to the mean north celestial

pole of epoch J2000.0. The X axis is based on the mean vernal equinox of epoch J2000.0. The Y axis is the cross product of the Z and X axes. This coordinate system is described in detail in Reference 6. Data in the ECI coordinate system will be present in the MODIS Level 1A product in the form of ephemeris data contained in the spacecraft ancillary data message.

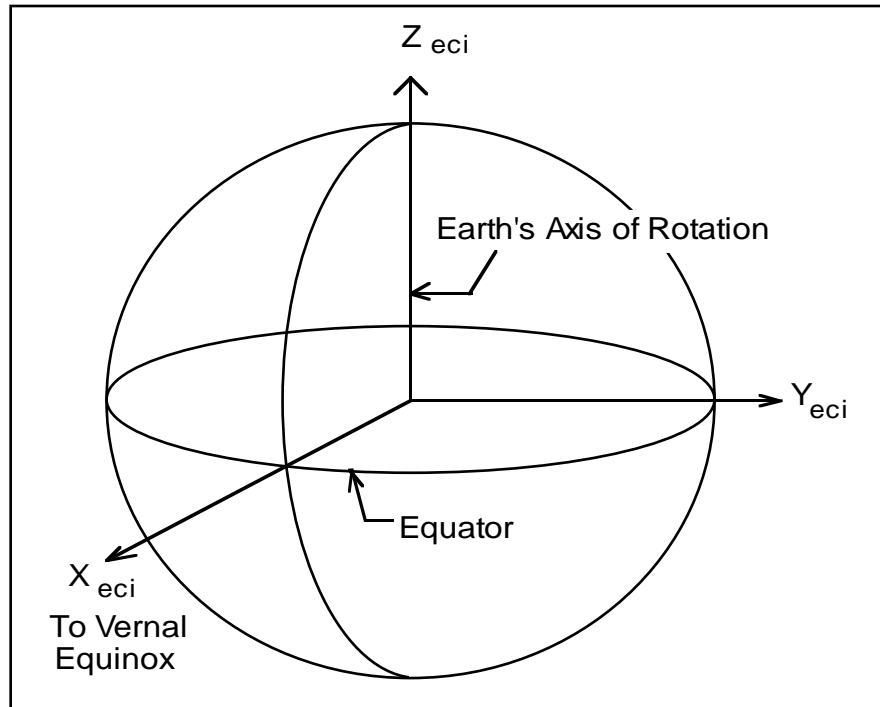


**Figure 3-7. ECI Coordinate System**

### 3.1.2.9 Earth Centered Rotating Coordinate System

The Earth Centered Rotating (ECR) coordinate system is Earth fixed with its origin at the center of mass of the Earth (Figure 3-8). It corresponds to the Conventional Terrestrial System (CTS) defined by the International Earth Rotation Service (IERS), which is the same as the U. S. Department of Defense World Geodetic System 1984 (WGS84) geocentric reference system. This coordinate system is described thoroughly in Reference 6.

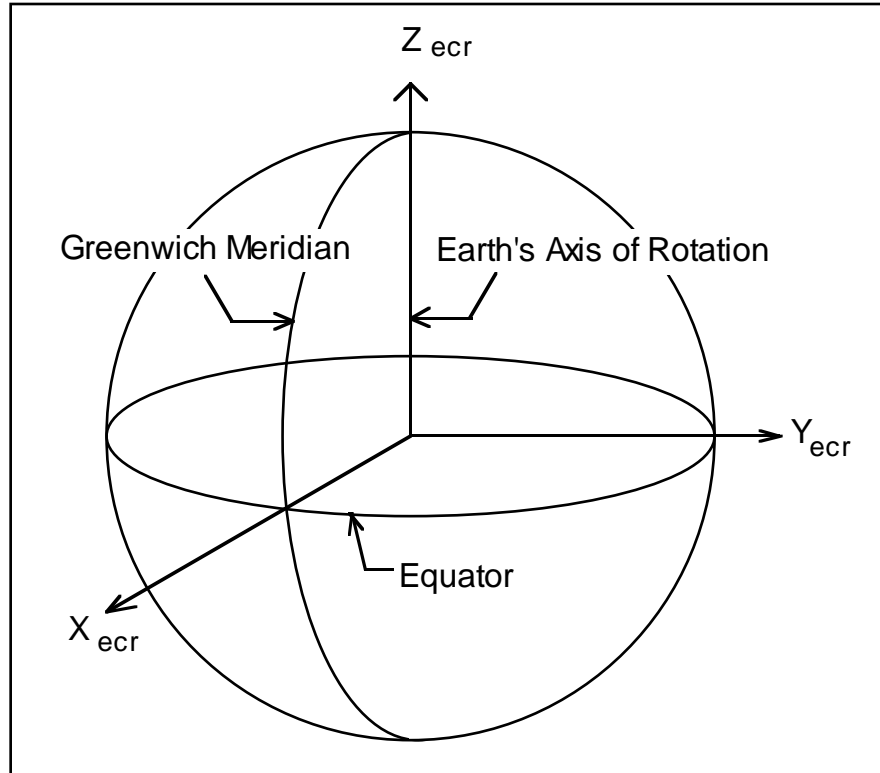


**Figure 3-8. ECR Coordinate System**

#### *3.1.2.10 Geodetic Coordinate System*

The geodetic coordinate system is based on the WGS84 reference frame with coordinates expressed in latitude, longitude, and height above the reference Earth ellipsoid. No ellipsoid is required by the definition of the ECR coordinate system but the geodetic coordinate system depends on the selection of an Earth ellipsoid. Latitude and longitude are defined as the angle between the ellipsoid normal and its projection onto the equator and the angle between the local meridian and the Greenwich meridian, respectively. The Earth location data fields in the MODIS Level 1A product will be expressed in the geodetic coordinate system.

#### **3.1.3 Coordinate Transformations**

There are nine transformations between the ten basic coordinate systems used by the MODIS Earth location algorithm. These transformations are referred to frequently in the remainder of this document and are defined here. They are presented in the logical order in which a spatial element number and mirror angle would be transformed into a geodetic position. An overview of the ten coordinate systems and their relationship is illustrated in Figure 2-2.

### 3.1.3.1 Focal Plane to Telescope

Because of the along-track satellite motion during the scan the focal planes are rotated by a small angle  $\theta_{scanvel}$  of -0.129 deg. The instantaneous projection of a rotated focal plane to the ground is illustrated in Figure 3-9, where the outer box is aligned to the telescope coordinate system. This rotation is necessary to compensate for the along-track spacecraft sub-satellite point movement of about 65.2 m during the 9.67 msec between the times the bands at the leading and trailing edges see the same area on the ground. The motion along the spacecraft ground track velocity varies a small amount because of the velocity of the Earth relative to the satellite and the orbit's and Earth's eccentricity. The actual rotation will be measured preflight and be included in the transformation from the focal to the telescope coordinate system. If there is a slight difference in rotation between the focal planes one value will be used and the residual rotation will be absorbed in the detector focal plane locations. The transformation matrix for this rotation is given by:

$$T_{tel\ foc} = \begin{bmatrix} \cos(\theta_{scanvel}) & -\sin(\theta_{scanvel}) & 0 \\ \sin(\theta_{scanvel}) & \cos(\theta_{scanvel}) & 0 \\ 0 & 0 & 1 \end{bmatrix}$$

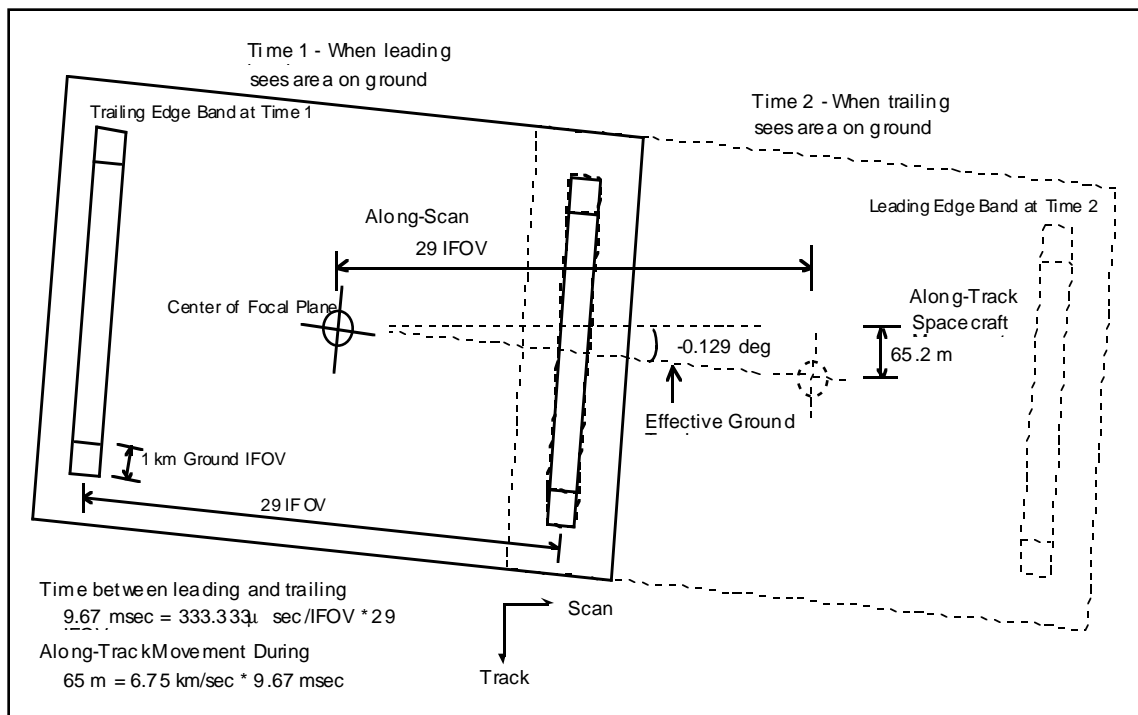


**Figure 3-9. Focal Plane Rotation to Compensate for Spacecraft Along-Track Motion**

### 3.1.3.2 Telescope to Instrument

The relationship between the telescope and instrument coordinate systems is described by the telescope alignment matrix. This relationship will be measured preflight. The transformation  $\mathbf{T}_{inst/telescope}$  from the telescope to the instrument coordinate system is a three dimensional transformation implemented as a matrix multiplication. The transformation matrix is expected to be constant in-flight. Considering the mirror angle  $-38^\circ$  or  $142^\circ$  to make view vector  $(0,0,f)$  should be nadir vector from the scan mirror pointing to the ground, telescope coordinate system is rotated around  $\mathbf{Y}_{tel}$  axis by  $\psi = -14^\circ$ . In the matrix notation, this is given by:

$$\begin{bmatrix} \cos(\psi) & 0 & \sin(\psi) \\ 0 & 1 & 0 \\ -\sin(\psi) & 0 & \cos(\psi) \end{bmatrix}$$

See Figure 3-4 to understand how the telescope coordinate system is tilted with respect to the instrument coordinate system.

Relationship between instrument and telescope coordinate systems before rotation around Y-axis can be expressed by:

$$\begin{bmatrix} 0 & -1 & 0 \\ 0 & 0 & -1 \\ 1 & 0 & 0 \end{bmatrix}$$

Combining these two transformations,  $\mathbf{T}_{inst/telescope}$  can be expressed by:

$$\mathbf{T}_{inst/telescope} = \begin{bmatrix} 0 & -1 & 0 \\ \sin(\psi) & 0 & -\cos(\psi) \\ \cos(\psi) & 0 & \sin(\psi) \end{bmatrix}$$

### 3.1.3.3 Scan Mirror Assembly to Instrument

The relationship between the scan mirror assembly and instrument coordinate systems is described by the mirror alignment matrix. This relationship will be measured preflight. The transformation  $\mathbf{T}_{inst/mir}$  from scan mirror to the instrument coordinate system is a three dimensional affine transformation implemented as a matrix multiplication. The transformation matrix is expected to be constant in-flight.

The nominal rotation matrix is:

$$\mathbf{T}_{inst/mir} = \begin{bmatrix} 1 & 0 & 0 \\ 0 & 1 & 0 \\ 0 & 0 & 1 \end{bmatrix}$$

### 3.1.3.4 Solar Diffuser to Instrument

The relationship between the SD assembly and instrument coordinate systems is described by the transformation matrix  $\mathbf{T}_{instSD}$ .

The rotation matrix is:

$$\mathbf{T}_{instSD} = \begin{bmatrix} \cos(\theta) & 0 & \sin(\theta) \\ 0 & 1 & 0 \\ -\sin(\theta) & 0 & \cos(\theta) \end{bmatrix}$$

where  $\theta = 20.232$  degrees.

### 3.1.3.5 Instrument to Spacecraft

The relationship between the instrument and spacecraft coordinate systems is described by the instrument alignment matrix. This relationship will be measured preflight and refined in-flight as described in Section 3.2.3. The transformation from instrument coordinates to spacecraft coordinates  $\mathbf{T}_{sc/inst}$  is a three dimensional affine transformation implemented as a matrix multiplication. The transformation matrix will initially be defined to be fixed. Subsequent analysis may detect repeatable variations with time that can be effectively modeled making this a (slowly) time varying transformation.

The terminator flexure effect, non-uniform thermal expansion/contraction when going from the night to day or vice versa, is one of the dynamic error sources that may be included in this time varying transformation. Typically, the settle time for this phenomenon is several minutes and may have very high frequency components (thermal snap). Based on current analysis (Reference 2), this error source is expected to be relatively small and below the measurement threshold. Still, analysis will follow (see Section 3.2.3) to determine if a repeatable pattern can be found.

The nominal rotation matrix is the identity matrix:

$$\mathbf{T}_{sc/inst} = \begin{bmatrix} 1 & 0 & 0 \\ 0 & 1 & 0 \\ 0 & 0 & 1 \end{bmatrix}$$

### 3.1.3.6 Spacecraft to Orbital

The relationship between the spacecraft and orbital coordinate systems is defined by the spacecraft attitude. This transformation is a three dimensional rotation matrix with the components of the rotation matrix being functions of the spacecraft roll, pitch, and yaw attitude angles. The nature of the functions of roll  $\xi_r$ , pitch  $\xi_p$ , and yaw  $\xi_y$  depends

on the exact definition of these angles (i.e. how they are generated by the attitude control system). Reference 19 requires the proper order to perform the rotation to be yaw, roll, and pitch. Since the spacecraft attitude is constantly changing, this transformation is time varying. The transformation matrix is:

$$\mathbf{T}_{orb/sc} = \begin{bmatrix} \cos\xi_y & -\sin\xi_y & 0 \\ \sin\xi_y & \cos\xi_y & 0 \\ 0 & 0 & 1 \end{bmatrix} \begin{bmatrix} 1 & 0 & 0 \\ 0 & \cos\xi_r & -\sin\xi_r \\ 0 & \sin\xi_r & \cos\xi_r \end{bmatrix} \begin{bmatrix} \cos\xi_p & 0 & \sin\xi_p \\ 0 & 1 & 0 \\ -\sin\xi_p & 0 & \cos\xi_p \end{bmatrix}$$

$$\mathbf{T}_{orb/sc} = \begin{bmatrix} \cos\xi_y \cos\xi_p - \sin\xi_y \sin\xi_r \sin\xi_p & -\sin\xi_y \cos\xi_r & \cos\xi_y \sin\xi_p + \sin\xi_y \sin\xi_r \cos\xi_p \\ \sin\xi_y \cos\xi_p + \cos\xi_y \sin\xi_r \sin\xi_p & \cos\xi_y \cos\xi_r & \sin\xi_y \sin\xi_p - \cos\xi_y \sin\xi_r \cos\xi_p \\ -\cos\xi_r \sin\xi_p & \sin\xi_r & \cos\xi_r \cos\xi_p \end{bmatrix}$$

### 3.1.3.7 Orbital to ECI

The relationship between the orbital and ECI coordinate systems is based on the spacecraft's instantaneous ECI position and velocity vectors. The rotation matrix to convert from orbital to ECI can be constructed by forming the orbital coordinate system axes in ECI coordinates:

$\mathbf{p}$  - spacecraft position vector in ECI

$\mathbf{v}$  - spacecraft velocity vector in ECI

$\mathbf{T}_{eciorb}$  - rotation matrix from orbital to ECI

$\hat{\mathbf{b}}_3 = -\mathbf{p}/|\mathbf{p}|$  (nadir vector direction)

$\hat{\mathbf{b}}_2 = \hat{\mathbf{b}}_3 \times \mathbf{v} / |\hat{\mathbf{b}}_3 \times \mathbf{v}|$  (negative of angular momentum vector direction)

$\hat{\mathbf{b}}_1 = \hat{\mathbf{b}}_2 \times \hat{\mathbf{b}}_3$  (circular velocity vector direction)

$$\mathbf{T}_{eciorb} = \begin{bmatrix} \hat{\mathbf{b}}_1 & \hat{\mathbf{b}}_2 & \hat{\mathbf{b}}_3 \end{bmatrix}$$

### 3.1.3.8 ECI to ECR

The transformation from ECI to ECR coordinates is a time varying rotation due primarily to Earth rotation but also containing more slowly varying terms for precession, astronomic nutation, and polar wander. The ECI to ECR rotation matrix can be expressed as a composite of these transformations:

$$\mathbf{T}_{ec/eci} = \mathbf{A} \mathbf{B} \mathbf{C} \mathbf{D}$$

**A** - Polar Motion

**B** - Sidereal Time

**C** - Astronomic Nutation

**D** - Precession

Each of these transformation terms is described in detail in Reference 6. The actual transformation from ECI to ECR coordinates is done by calling a routine of the SDP Toolkit (see Reference 18).

### 3.1.3.9 ECR to Geodetic

The relationship between ECR and geodetic coordinates can be expressed simply in its direct form (Reference 6):

$$x = (N + h) \cos(la) \cos(lon)$$

$$y = (N + h) \cos(la) \sin(lon)$$

$$z = (N(1 - e^2) + h) \sin(la)$$

$$N = a / (1 - e^2 \sin^2(la))^{1/2}$$

$$e^2 = 1 - \frac{b^2}{a^2}$$

where:

$(x, y, z)$	-	ECR coordinates
$(la, lon, h)$	-	Geodetic coordinates
$N$	-	Ellipsoid radius of curvature in the prime vertical
$e$	-	Ellipsoid eccentricity
$a, b$	-	Ellipsoid semi-major and semi-minor axes

Unfortunately, there is no closed form solution for the inverse problem (which is the problem of interest here). Latitude and height must be solved iteratively for points that do not lie on the ellipsoid surface.

### 3.1.4 Mathematical Description of Algorithm

The MODIS Earth location algorithm is separated into three parts. The first part describes the algorithm that generates a viewing vector in object space corresponding to either the center of a spatial element or a detector. The second part describes the algorithm that calculates the Earth location of the viewing vector. The third part describes an algorithm for calculating approximate sub-pixel locations. It should be noted that this sub-pixel algorithm is not performed during the MODIS geolocation processing.

### 3.1.4.1 Instrument Model Algorithm

A model of the instrument is used to generate an object space viewing vector in instrument coordinates for a spatial element or detector. The instrument model is composed of three elements: the telescope; the focal plane assembly; and the scan mirror assembly. After discussing each model in depth, a summary of the algorithm for the generation of the viewing vector is given.

Instrument models are described in the following order:

- Telescope Model,
- Focal Plane Assembly Model,
- Detector Readout and Formatting,
- Time of the Start of the Earth View Sector,
- Time of individual Samples in Each Band
- Scan Mirror Assembly Model,
- Scan Mirror Encoder Assembly,
- Generation of the Object Viewing Vector.

#### **Telescope Model**

The telescope is modeled as a simple optical system. There are four independent focal planes each with several independent elements in optical path. In Table 3-1 are the nominal focal lengths for each of the telescopes for the four focal planes: Long Wave Infrared (LWIR); Short and Medium Wave Infrared (SWIR/MWIR); Near Infrared (NIR); and Visible (VIS).

**Table 3-1. Focal Lengths for Each Focal Plane**

<b>Focal Planes</b>	<b>Focal Length (<math>f</math>)</b>
LWIR	282.118 mm
SWIR/MWIR, NIR and VIS	380.859 mm

The optical distortion of the lenses for each optical path was modeled before the focal planes were built and the layout of the detectors on the focal plane was adjusted for this distortion. These adjustments to the detector locations are not included in the focal plane coordinates used in the instrument model; thus a simple optical model can be used. Given focal plane coordinates  $(x, y)$  and focal length  $f$ , the corresponding image space viewing vector  $\mathbf{u}_{foc}$  in the telescope coordinate system is:

$$\mathbf{u}_{foc} = \begin{bmatrix} x \\ y \\ f \end{bmatrix}$$

When doing this calculation for the ideal band, a focal length of exactly 380.859 mm will be used with  $10\ 540\ \mu\text{m} \times 540\ \mu\text{m}$  detectors .

**Focal Plane Assembly Model**

The layout of the 36 MODIS spectral bands on the four focal planes is illustrated in Figure 3-10. The focal planes have the same relative scale so that the detectors for the LWIR focal plane are smaller because of the shorter focal length. The relationship between the focal plane coordinate system given in Figure 3-10 and the telescope coordinate system is described in the beginning of Section 3.1.3.1. All four focal planes are rotated around the optical axis.

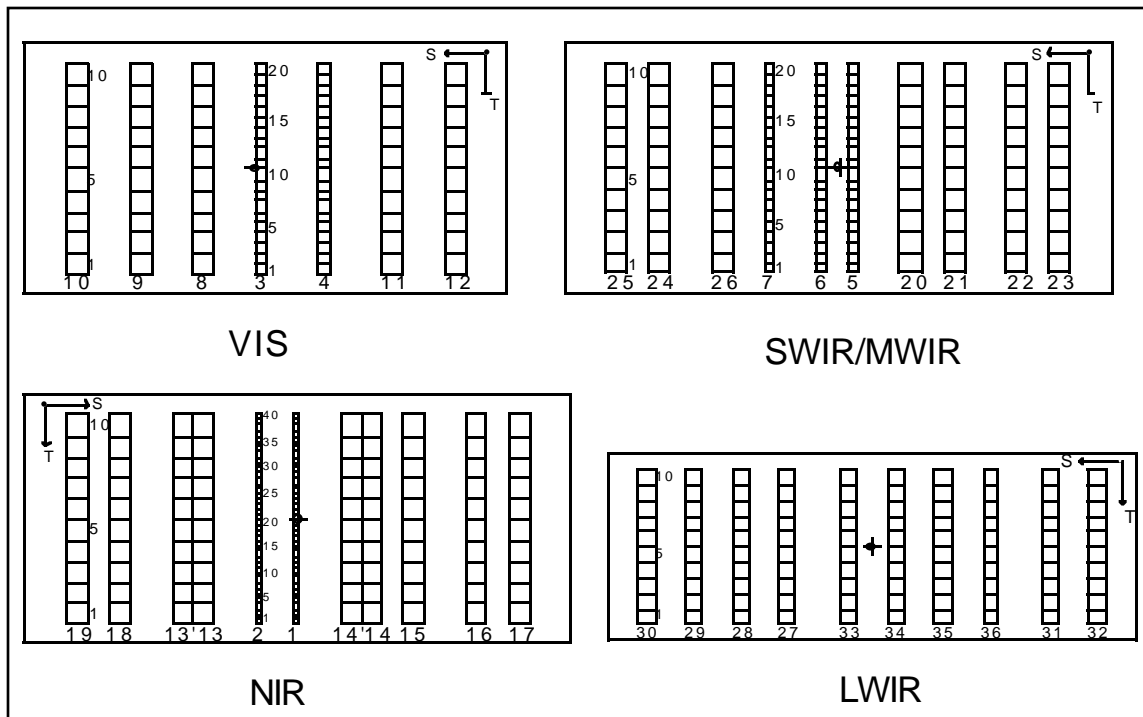


**Figure 3-10. Physical Layout of the Focal Planes**

The detector sizes, ground resolutions, and number of detectors for each of the bands is given in Table 3-2.

**Table 3-2. Detector Specifications**

<b>Bands</b>	<b>Ground Projection</b>	<b>Detector Size</b>	<b>Number of Detectors</b>
1, 2	250 m	135 $\mu\text{m}$	40
3 to 7	500 m	270 $\mu\text{m}$	20
8 to 26	1 km	540 $\mu\text{m}$	10
27 to 30	1 km	400 $\mu\text{m}$	10
31 to 36 (LWIR)	1 km	400 (track) by 380 (scan) $\mu\text{m}$	10

The detectors are laid out on the focal plane so that when they are sampled there are an integral number of frames between the 1 km bands as illustrated in Figure 3-11. The relative location in units of 1 km Instantaneous Field of View (IFOV) in the along-scan direction of the trailing edge of all bands, with respect to the optical axis, is given in Table 3-3 and illustrated in Figure 3-11.

Bands 13 and 14 are Time Delayed Integration (TDI) bands which were designed for detecting low signals when MODIS is viewing the ocean. In order to meet specifications for maximum SNR, each band contains two physical detector arrays electronically phased as shown in Figure 3-10 NIR, so that the sampling area on the Earth coincides. The signals from 13, 13', 14 and 14' are logically equivalent to four bands, 13L, 13H, 14L, and 14H. The two channels 13L and 13H provide the same measurement at the mid-location between detectors 13 and 13', except 13L(low gain) is for measuring bright scenes and 13H(high gain) is for measuring dark scenes. The two channels 14L and 14H function in a similar way. See Figure 3-11 for their locations.

**Table 3-3. Nominal Band Layout with Respect to the Optical Axis  
(1 km IFOV Units)**

Band	Ref. Optic Axis
Ideal Band	0
1	0.25
2	2
3	0.5
4	3.5
5	1
6	-0.5
7	-3
8	-2
9	-5
10	-8
11	7
12	10
13H	5.5
13L	5.5
14H	-2.5
14L	-2.5
15	-5
16	-8
17	-10

Band	Ref. Optic Axis
18	9
19	11
20	4
21	6
22	9
23	11
24	-8
25	-10
26	-5
27	-5
28	-8
29	-11
30	-14
31	12
32	15
33	-1
34	2
35	5
36	8

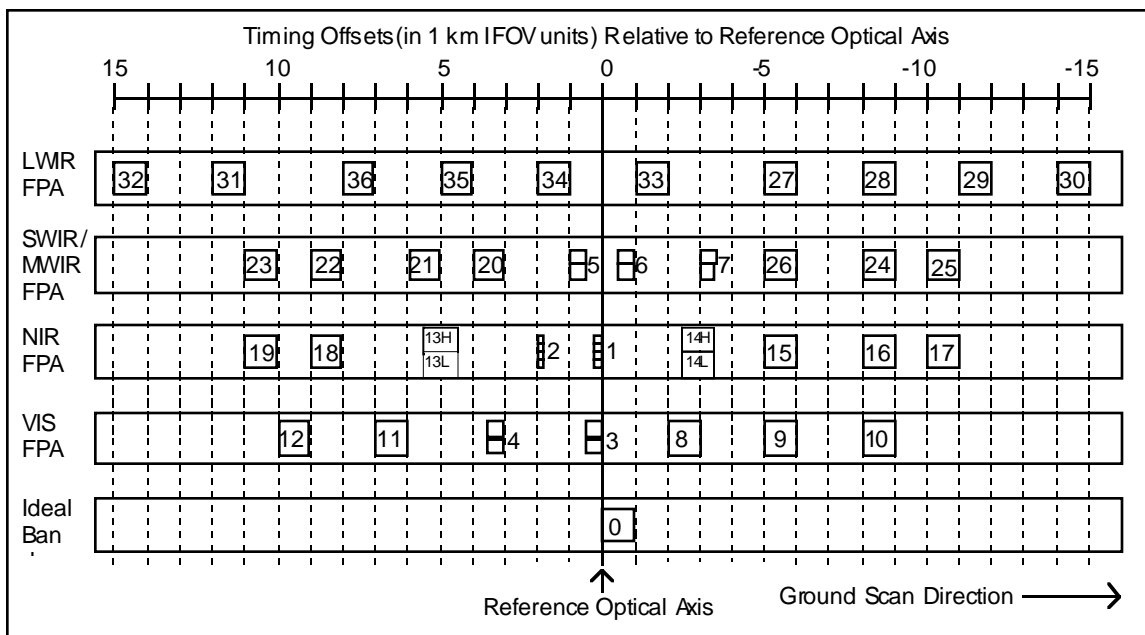


**Figure 3-11. Offset of Each Band Relative to the Reference Optical Axis**

The actual locations of each of the bands without the optical distortions will be measured both preflight and in-flight. The location  $(x_{i,j}, y_{i,j})$  of the center of detector  $i$  in band  $j$  is:

$$x_{i,j} = x_{\text{cen } j} + x_{\text{res } i,j}$$

$$y_{i,j} = y_{\text{cen } j} + y_{\text{space } j} \left[ i - \frac{1}{2}(N_{\text{det } j} + 1) \right] + y_{\text{res } i,j}$$

where (see Figure 3-12):

- $(x_{\text{cen } j}, y_{\text{cen } j})$  - Location of the center of band  $j$  relative to the optical axis
- $N_{\text{det } j}$  - Number of detectors for band  $j$
- $y_{\text{space } j}$  - Spacing between detectors for band  $j$
- $(x_{\text{res } i,j}, y_{\text{res } i,j})$  - Residual distortion for detector  $i$ , band  $j$
- $i = 1, \dots, N_{\text{det } j}$  - Detector number for band  $j$  (see Table 3-2)

For calculations involving ideal band the values for these quantities are:

$$(x_{\text{cen}}, y_{\text{cen}}) = (270 \mu\text{m}, 0)$$

$$N_{\text{det}} = 10$$

$$y_{\text{space}} = 540 \mu\text{m}$$

$$(x_{\text{res}}, y_{\text{res}}) = (0, 0)$$

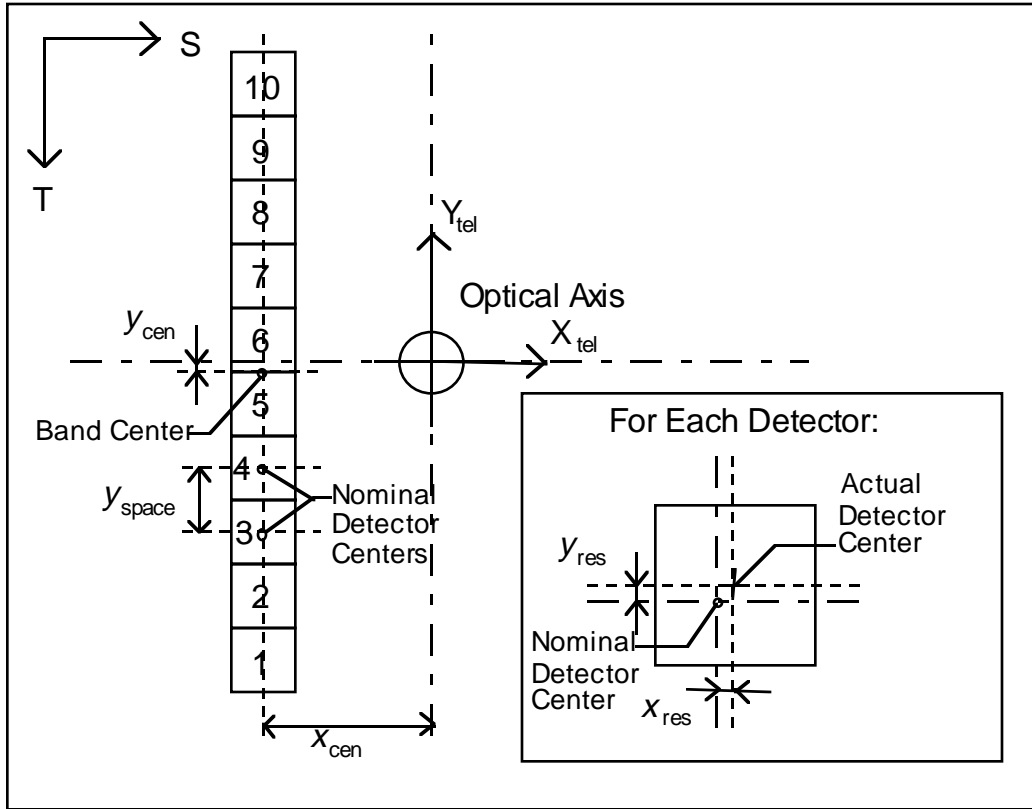


**Figure 3-12. Measurements of Detector Locations on Focal Plane**

**Detector Readout and Formatting**

A new frame of data is generated every 333.333  $\mu$ sec (exactly 3 kHz). The sample time, integration time, and number of samples per frame for each of the bands are given in Table 3-4. The integration time is 10  $\mu$ sec less than the sample time to allow for the readout of the detectors. Bands 27 to 30 are over-sampled by 4 times and averaged by the on-board computer into a single sample per frame.

**Table 3-4. Detector Sampling**

Bands	Sample Time	Integration Time	Number of Samples per Frame
1, 2	83.333 $\mu$ sec	73.333 $\mu$ sec	4
3 to 7	166.667 $\mu$ sec	156.667 $\mu$ sec	2
8 to 26	333.333 $\mu$ sec	323.333 $\mu$ sec	1
27 to 30	333.333 $\mu$ sec	4 x 73.333 $\mu$ sec	4 avg. to 1
31 to 36	333.333 $\mu$ sec	323.333 $\mu$ sec	1

The samples for each band are delayed by an appropriate amount so that all samples in a frame of data start at the same point on the ground. Figure 3-13 illustrates the integration area for the four different sampling rates and ground resolution.

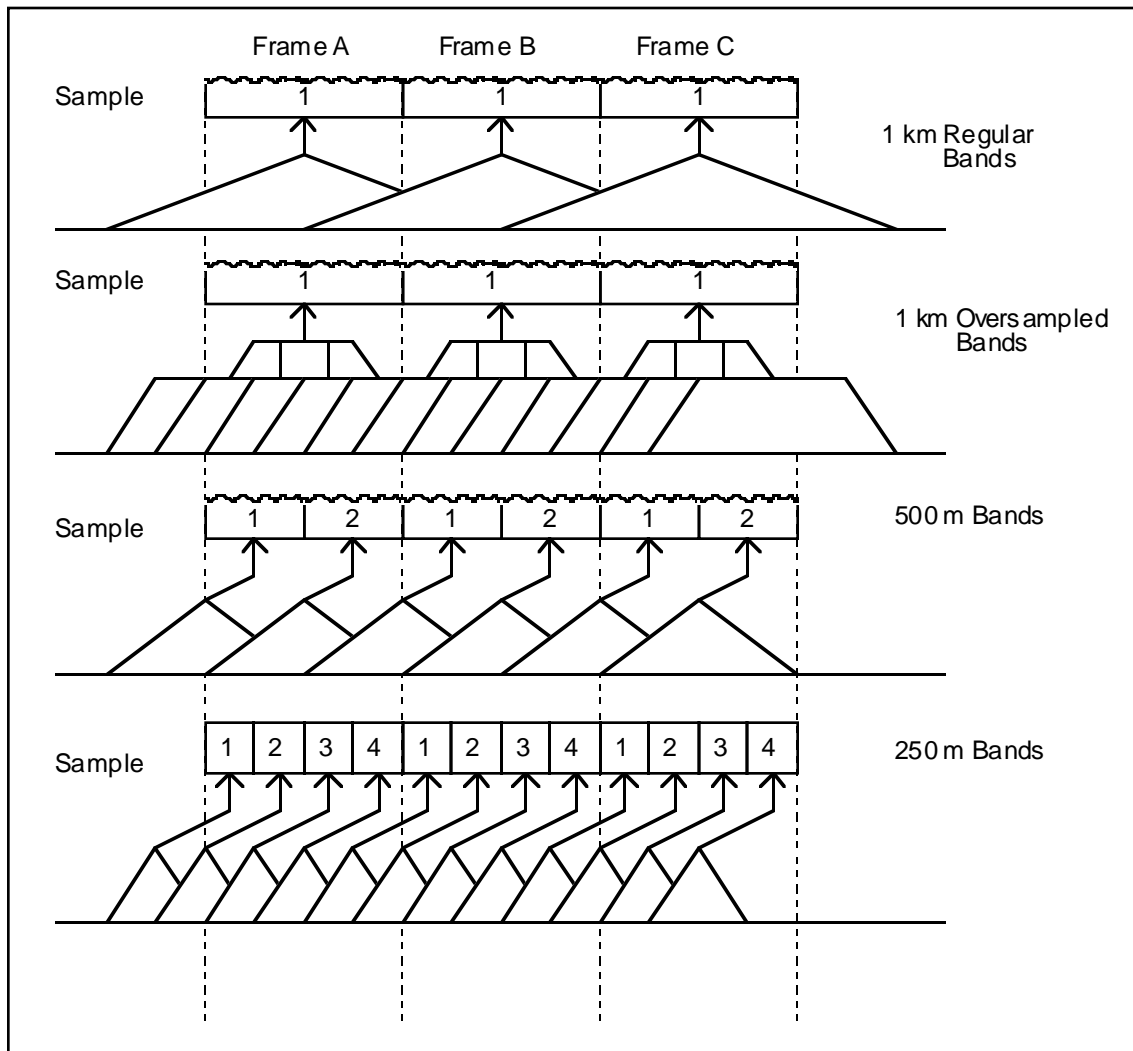


**Figure 3-13. Integration Area for Different Sampling Rates and Ground Resolution**

### Time of the Start of the Earth View Sector

There are 1354 frames of science data that are collected in the Earth view sector. The time code corresponding to the beginning of sensor data collection is recorded in the Consultative Committee on Space Data Systems (CCSDS) headers for all data frames in the sector. This time code  $t_0$  corresponds to the time when band 30 starts to sample for the first frame (Figure 3-14 or 3-15).

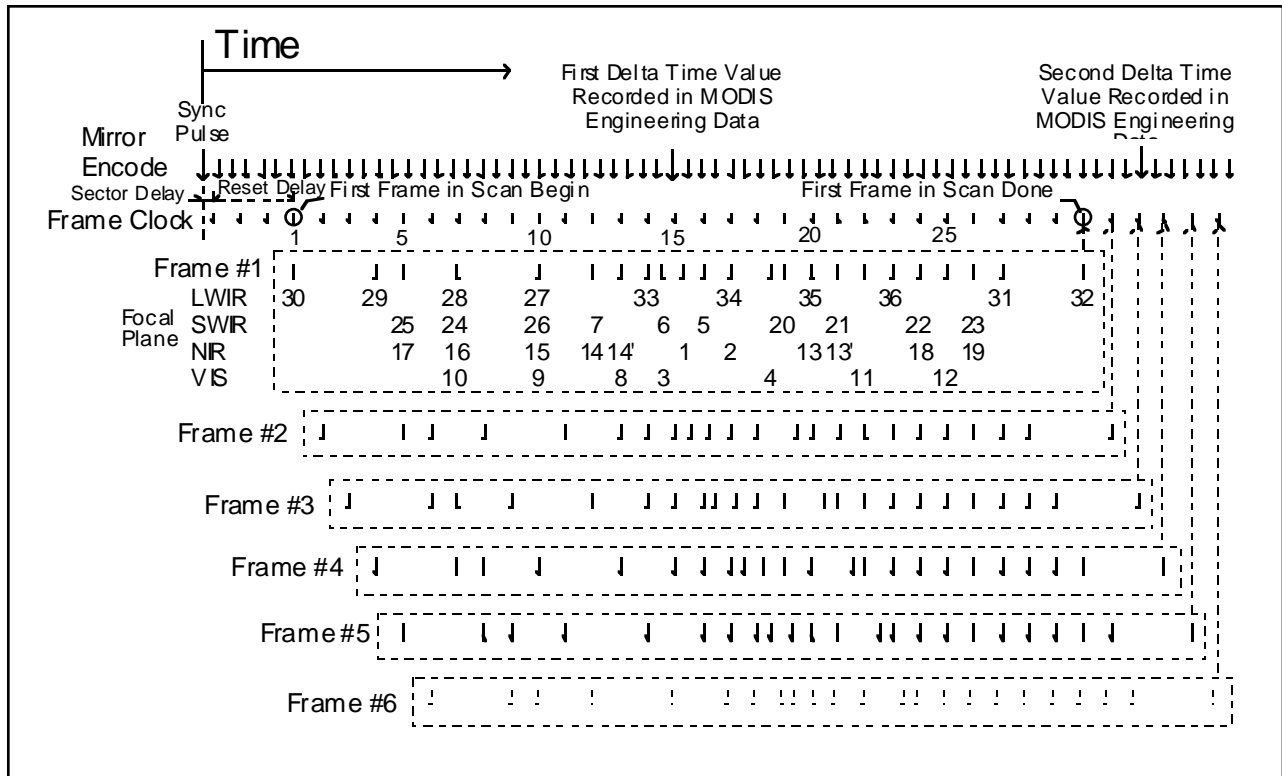


Figure 3-14. Time of Start of Earth View Sector

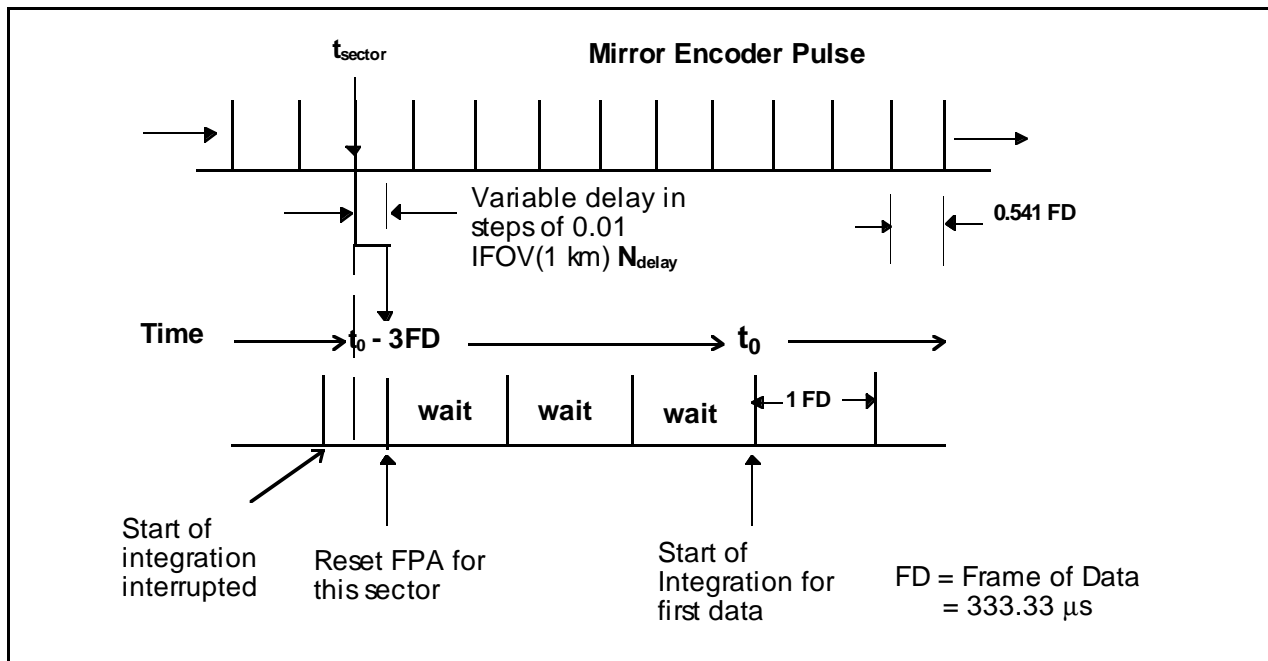


Figure 3-15. Frame Start Timing for Earth View Sector Around  $t_0$

When the scan mirror reaches the Earth view start position (as defined in the sector definition table), the encoder assembly generates a sync pulse to re-synchronize the frame clock. This is programmable but will be normally fixed and stored in a system parameter table for use by the processing software. This encoder position is related to a particular viewing direction (viewing vector) based on the preflight calibration.

The first frame is delayed a programmable fraction of a frame clock cycle, from 0.00 to 0.63 clock cycles. The value  $N_{\text{delay}}$ , in the number of hundreds of frame clock cycles (called vernier counts) will also be stored in the MODIS system parameter table.

Sensor data collection begins a programmable number  $N_{\text{reset}}$  (default = 3) of frame clock cycles after the mirror sync pulse to allow the focal plane output to stabilize following the reset. The leading band (band 30) data from the first sample will go into the first Earth scan data frame. The number of clock cycles ( $N_{\text{reset}}$ ) to wait to begin taking data will be fixed and stored in the system parameter table (see Figure 3-15 for details).

The Earth view sector start time  $t_{\text{sector}}$  is calculated from:

$$t_{\text{sector}} = t_0 - T_{\text{frame}} \left( N_{\text{reset}} + \frac{N_{\text{delay}}}{100} \right)$$

where:

$t_0$  - Frame time at start of the Earth view (start of band 30)

$T_{\text{frame}}$  - Frame time (333.333  $\mu\text{sec}$ )

$N_{\text{delay}}$  - Vernier counts (multiple of 0.01 Frame time)

### **Time of Individual Samples in Each Band**

Detector samples are stored in a buffer 30 frames deep to align the bands by time delay. The actual time for each of the samples within a frame is dependent on each band's location on the focal plane relative to the center of the focal plane.

1. The time  $t_{\text{latch}_{0,k}}$  at which the sample for the ideal band (0) was sampled (latched) in frame  $k$  is:

$$t_{\text{latch}_{0,k}} = t_0 + T_{\text{frame}} (k - F_{30}) \quad k = 1, \dots, 1354$$

where:

$t_0$  - Frame time at start of the Earth view (start of band 30)

$F_j$  - Location of band  $j$  trailing edge relative to optical axis in Instantaneous Field of View (IFOV) units (see Table 3-3 where  $F_{30} = -14$ ).

2. Calculate the offset  $t_{\text{offset},j}$  for the first sample (the only sample for the 1 km bands) in band  $j$  from the time when ideal band was sampled:

$$t_{\text{offset},j} = T_{\text{frame}}(F_j - F_{\text{offset}}) \quad j = 1, \dots, 36$$

where:

$F_{\text{offset},j}$  - Offset in IFOV units to get time of first sample for band  $j$ ; see table below

Band ( $j$ )	$F_{\text{offset}}$	$N_{\text{samp}}$
1, 2 (250 m)	3/4	4
3 to 7 (500 m)	1/2	2
8 to 36 (1 km)	0	1

The time offsets  $t_{\text{offset},i,j}$  for the remaining samples  $i$  of higher resolution bands are:

$$t_{\text{offset},i,j} = t_{\text{offset},j} + T_{\text{frame}} \left( \frac{i-1}{N_{\text{samp},j}} \right) \quad i = 2, \dots, N_{\text{samp},j}$$

where:

$N_{\text{samp},j}$  - Number of samples band  $j$ ; see table above

3. Then the time  $t_{\text{latch},i,j,k}$  when sample  $i$  of band  $j$  in frame  $k$  is latched is:

$$t_{\text{latch},i,j,k} = t_{\text{latch},0,k} + t_{\text{offset},i,j} \quad i = 2, \dots, N_{\text{samp},j}, \quad k = 1, \dots, 1354$$

4. In addition to the latch time of each band it is important to know the time when the center of the sample was imaged. This time is simply:

$$t_{\text{center},j,k} = t_{\text{latch},j,k} - \frac{1}{2}(T_{\text{samp},j} - T_{\text{reset}})$$

where:

$t_{\text{center},j,k}$  - Time when the center of sample  $i$  was imaged for band  $j$ , frame  $k$

$t_{\text{latch},j,k}$  - Latch time of sample  $i$ , band  $j$ , frame  $k$

$T_{\text{samp},j}$  - Sample time(dwel time) for band  $j$  (see Table 3-4)

$T_{\text{reset}}$  - Time to read out and reset the detectors at the beginning of the sample (10  $\mu\text{sec}$ )

A sample time of 333.333  $\mu\text{sec}$  will be used for the ideal band.

### **Scan Mirror Assembly Model**

The scan mirror assembly consists of a double-sided oval-shaped mirror and the motor-encoder assembly. The scan mirror assembly geometric specifications are listed in Table 3-5 (from Reference 11) with the corresponding mirror wedge angles and axis errors shown (exaggerated) in Figure 3-16.

**Table 3-5. Scan Mirror Assembly Geometric Specifications**

<b>Characteristic</b>	<b>Specification</b>
Wedge Angle $\alpha$	$\leq 145 \mu\text{rad}$ (30.0 arcsec)
Wedge Angle $\beta$	$\leq 145 \mu\text{rad}$ (30.0 arcsec)
Axes Error $\gamma$	$\leq \pm 48.5 \mu\text{rad}$ (10.0 arcsec)
Axes Error $\delta$	$\leq \pm 9 \text{ mrad}$ (0.5 deg)
Along-Track Mirror Axis Dynamic Error (jitter); equivalent to axis error $\gamma$	$\pm 47.5 \mu\text{rad}$ (9.8 arcsec) (3 $\sigma$ )
Mirror Rotation Period	$2.95433 \pm 0.003 \text{ sec}$ (3 $\sigma$ )
Mirror Angular Velocity	$2.12677 \pm 0.0021 \text{ rad/sec}$ (3 $\sigma$ )
Absolute Position Along-Scan	$< 90 \mu\text{rad}$ (18.6 arcsec) (3 $\sigma$ )
Scan Timing and Encoder Errors (dynamic)	$< 54 \mu\text{rad}$ (11.1 arcsec) (3 $\sigma$ )

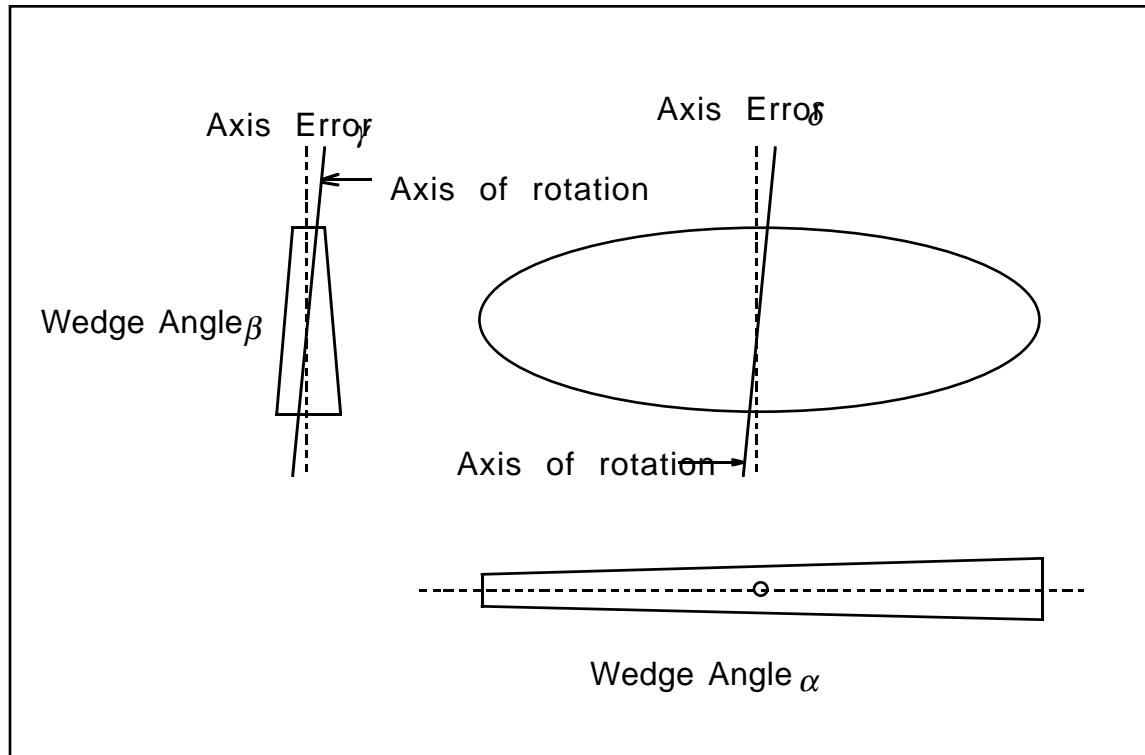


**Figure 3-16. Mirror Wedge Angles and Axis Errors Definitions**

The wedge angle  $\alpha$  is the non-parallelism of the scan mirror in the along-scan axis and creates an along-scan offset between scans from mirror sides 1 and 2. The wedge angle  $\beta$  is the non-parallelism of the mirror in the along-track axis and creates an along-track offset (conical scan). The axis error  $\gamma$  is the misalignment of the mirror center line through the depth of the mirror and the axis of rotation in the along-scan direction. The dynamic along-track axis error is similar but is the dynamic motion caused by the bearings. These axis errors cause a scan-to-scan along-track overlap or under-lap. The axis error  $\delta$  does not have a direct geometric effect. Of these errors, the wedge angles and the non-dynamic axis errors are static errors that will be measured preflight and are not expected to change in-flight. The dynamic along-track axis error will be characterized preflight and may be a function of the scan mirror angular position.

The normal vectors for each of the scan mirror surfaces can be determined from these axis and wedge errors. Figure 3-17 illustrates the construction of the normal vectors in the scan mirror coordinate system with zero rotation of the mirror. The normal vectors are:

$$\hat{\mathbf{n}}_{\text{side1}} = \begin{bmatrix} -\sin\left(\frac{\beta}{2} + \gamma\right) \\ \sin\left(\frac{\alpha}{2}\right)\cos\left(\frac{\beta}{2} + \gamma\right) \\ \cos\left(\frac{\alpha}{2}\right)\cos\left(\frac{\beta}{2} + \gamma\right) \end{bmatrix}$$

$$\hat{\mathbf{n}}_{\text{side2}} = \begin{bmatrix} -\sin\left(\frac{\beta}{2} - \gamma\right) \\ \sin\left(\frac{\alpha}{2}\right)\cos\left(\frac{\beta}{2} - \gamma\right) \\ -\cos\left(\frac{\alpha}{2}\right)\cos\left(\frac{\beta}{2} - \gamma\right) \end{bmatrix}$$

These equations assume a sign convention for  $\alpha$ ,  $\beta$  and  $\gamma$  as shown in Figure 3-17.

The scan mirror rotates about the scan mirror coordinate system X axis. The following rotation matrix is used to rotate a mirror normal vector through a scan mirror angle of  $\theta$ .

$$\mathbf{T}_{\text{rot}}(\theta) = \begin{bmatrix} 1 & 0 & 0 \\ 0 & \cos(\theta) & -\sin(\theta) \\ 0 & \sin(\theta) & \cos(\theta) \end{bmatrix}$$

Each of the mirror normal vectors is only relevant when the mirror side is facing toward the telescope. When the mirror is rotated -38 degrees the line of sight from the telescope reflected off mirror side 1 is pointed toward nadir. The following equation is used to compute the scan mirror normal  $\hat{\mathbf{n}}_{\text{mirr}}$  at any angle  $\theta$  for the appropriate mirror side  $i$ :

$$\hat{\mathbf{n}}_{\text{mirr}} = \mathbf{T}_{\text{rot}}(\theta)\hat{\mathbf{n}}_{\text{side}_i}$$

where  $i = 1$  when  $-128 < \theta \leq 52$  and  $i = 2$  when  $52 < \theta \leq 232$ .

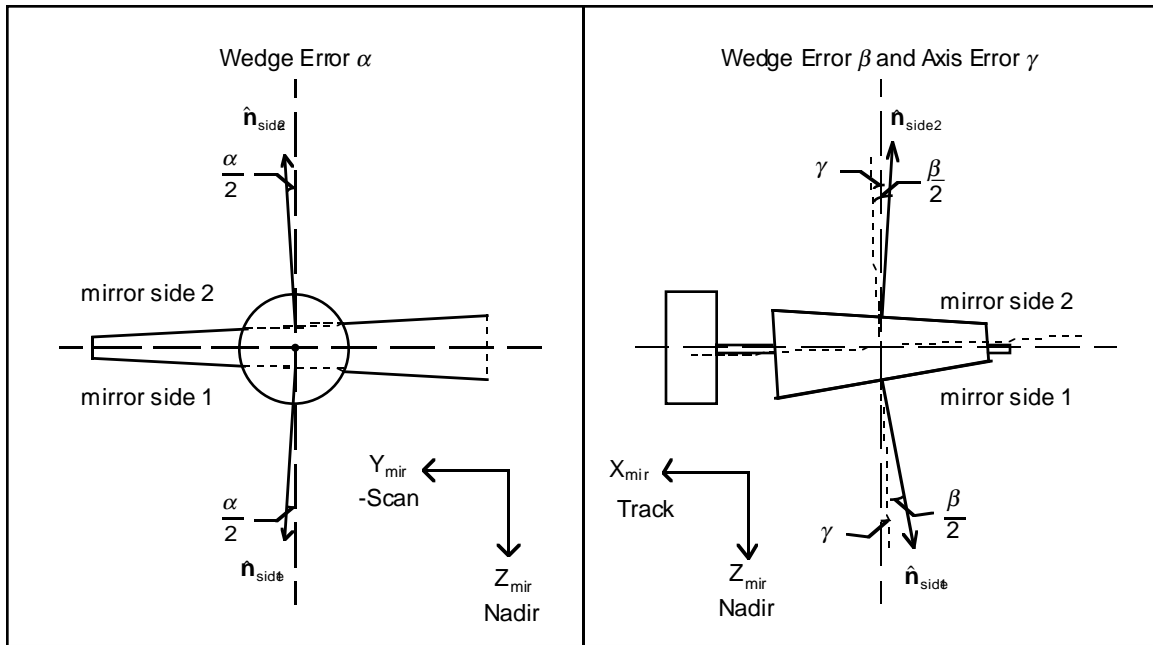


**Figure 3-17. Scan Mirror Normal Vectors**

**Scan Mirror Encoder Assembly**

The scan mirror encoder assembly measures the mirror position. Constants for the scan mirror encoder are listed in Table 3-6 with derived values in Table 3-7.

**Table 3-6. Scan Mirror Encoder Geometric Constants**

Characteristic	Value
Encoder Pulses (per rotation)	16,384
Number of Mirror Time Samples	24
Encoder Pulses per Mirror Time Sample	100

**Table 3-7. Scan Mirror Encoder Geometric Derived Values**

Characteristic	Derived Value
Rotation per Encoder Pulse	383.4 $\mu$ rad (79.1 arcsec)
Rotation per Mirror Time Samples	38349 $\mu$ rad (7910 arcsec)
Time per Encoder Pulse	180.3 $\pm$ 0.2 $\mu$ sec ( $3\sigma$ )
Time per Mirror Time Samples	18032 $\mu$ sec

The mirror scan angle  $\theta$  (in degrees) versus encoder position  $n_{\text{enc}}$  will be measured during preflight testing. SBRC will provide either a parametric model or a set of angles versus encoder number. Until this is available a polynomial model will be used:

$$\theta = A_0 + A_1 n_{\text{enc}} + A_2 n_{\text{enc}}^2 + \dots$$

Where:

$$\theta \leq n_{\text{enc}} < 16384$$

The time at which every 100<sup>th</sup> mirror encoder pulse occurs after the start of the Earth view is transmitted as part of the instrument telemetry. A total of 24 mirror time samples, in  $\mu\text{sec}$ , are collected during the Earth view. These relative times  $t_{\text{pulsere}i}$  must be added to the Earth view sector start time  $t_{\text{sector}}$  (computed above) to generate the absolute mirror time samples  $t_{\text{pulse}i}$ .

$$t_{\text{pulse}0} = t_{\text{sector}}$$

$$t_{\text{pulse}i} = t_{\text{sector}} + t_{\text{pulsere}i} \quad i = 1, \dots, 24$$

To determine the angle at any time  $t$  after the start of the Earth view it is necessary to interpolate between the encoder times in the spacecraft telemetry. The Chebyshev polynomials interpolation technique will be used in the initial model. A more physically based model may be used in later versions of the software.

Given:

- $n_{\text{enc}0}$  - Encoder position at start of the Earth view sector(fractional)
- $t_{\text{pulse}i}$  - Mirror pulse absolute times;  $i = 0, \dots, 24$

then the encoder locations corresponding to the time samples are:

$$n_{\text{enc}i} = n_{\text{enc}0} + 100i$$

The final encoder interpolation method is still under study. Until this final method is determined, we are using the Chebyshev polynomials. The Chebyshev polynomials  $f_{\text{enc}}$  which will be used to calculate the encoder position  $n_{\text{enc}}$  at time  $t$  is:

$$n_{\text{enc}} = f_{\text{enc}}(t, \mathbf{n}_{\text{enc}}, \mathbf{t}_{\text{pulse}})$$

where:

$$\mathbf{n}_{\text{enc}} = [n_{\text{enc}0} \quad \dots \quad n_{\text{enc}24}]^t$$

$$\mathbf{t}_{\text{pulse}} = [t_{\text{pulse}0} \quad \dots \quad t_{\text{pulse}72}]^t$$

Figure 3-18 illustrates the interpolation of the encoder times. The non-linear motion of the mirror is exaggerated in this figure.

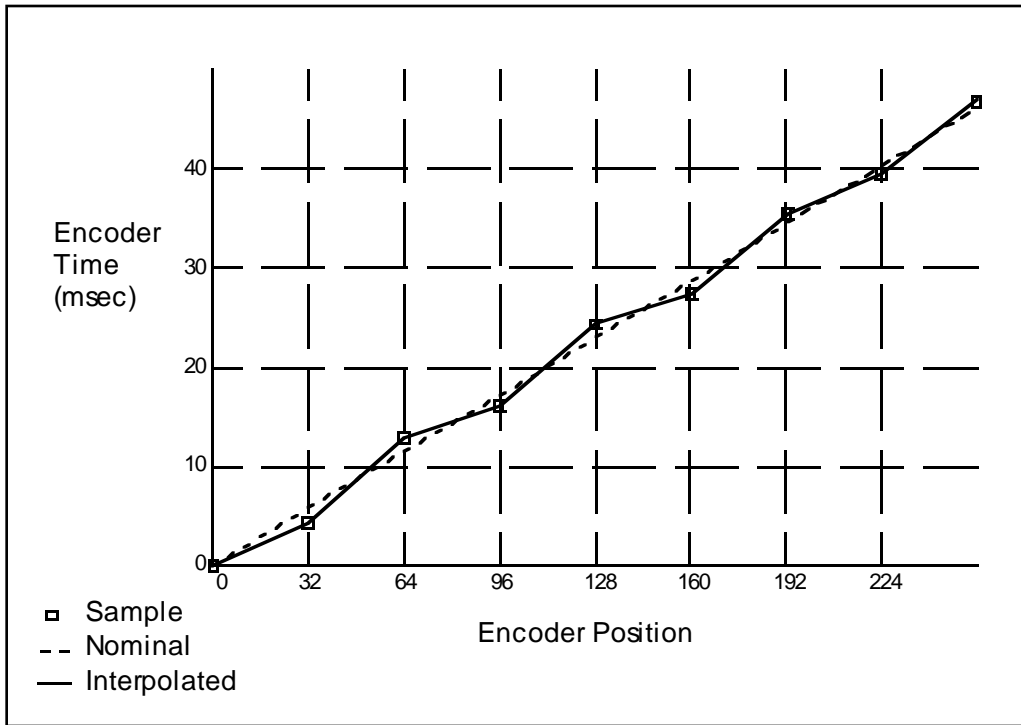


**Figure 3-18. Encoder Time Sample Interpolation**

**Table of Contents**  
**(ATBD-3)**

3.1.4.2	Earth Location Algorithm.....	30
3.1.4.3	Sub-pixel Approximate Ground Location Model .....	38
3.1.5	Variance or Uncertainty Estimates .....	45
3.2	Practical Considerations .....	51
3.2.1	Numerical Computation Considerations .....	51
3.2.2	Programming/Procedural Considerations.....	52
3.2.3	Algorithm Verification.....	52
3.2.3.1	Verification Standard.....	53
3.2.3.2	Preflight Verification .....	53
3.2.3.3	In-flight Verification.....	54
3.2.3.4	Verification of Inputs .....	55
3.2.4	Product Validation.....	58
3.2.5	Quality Control and Diagnostics.....	59
3.2.6	Exception Handling.....	59
3.3	ERROR ANALYSIS ALGORITHMS.....	60
3.3.1	Land Control Point Matching and Correlation Algorithm.....	60
Figure 3-19.	Ellipsoidal Viewing Vector Intersection.....	31
Figure 3-20.	Terrain Intersection Search Geometry .....	35
Figure 3-21.	Ideal Band Projection on the Ground .....	40
Figure 3-22.	Biquadratic Interpolation 3 x 3 Grid .....	40
Figure 3-23.	Earth Location Error (meters).....	49
Figure 3-24.	Earth Location Error (1 km pixel fraction).....	50
Figure 3-25.	Earth Location Error (in 1 km pixel fraction) Resulting from Various Terrain Height Errors as a Function of Scan Angle .....	51
Table 3-8.	Unique Center Locations in One Spatial Element .....	39
Table 3-9.	Geolocation Impact of 2 Sigma Spacecraft Position Errors.....	46
Table 3-10.	Geolocation Impact of 2 Sigma EOS AM Platform Attitude Knowledge Error Components.....	47
Table 3-11.	Geolocation Impact of 2 Sigma Instrument Pointing Knowledge Error Components.....	47
Table 3-12.	Total Combined 2 Sigma RSS Geolocation Error .....	48
Table 3-13.	In-flight Algorithm Verification Activities.....	54



## Generation of the Object Viewing Vector

This section summarizes the generation of an object viewing vector. For any focal plane location  $(x, y)$  the following can be used to generate an object space viewing vector  $\mathbf{u}_{\text{inst}}$  in the instrument coordinate system at time  $t$ . Typically, the focal plane location will be the center of a spatial element or detector and the time  $t$  will be the time  $t_{\text{center}}$  when the center of the sample was imaged.

1. Generate the image space viewing  $\mathbf{u}_{\text{tel}}$  in telescope coordinates from the focal plane location  $(x, y)$  and the focal length  $f$ .

$$\mathbf{u}_{\text{foc}} = [x \quad y \quad f]^T$$

2. Transform the view vector from the focal plane to the telescope coordinate system:

$$\mathbf{u}_{\text{tel}} = \mathbf{T}_{\text{tel foc}} \mathbf{u}_{\text{foc}}$$

3. Transfer the viewing vector from the telescope to instrument coordinate system:

$$\mathbf{u}_{\text{img}} = \mathbf{T}_{\text{inst/tel}} \mathbf{u}_{\text{tel}}$$

4. Compute the encoder position  $n_{\text{enc}}$  at time  $t$ .

$$n_{\text{enc}} = f_{\text{enc}}(t, \mathbf{n}_{\text{enc}}, \mathbf{t}_{\text{pulse}})$$

5. Compute the scan mirror angle  $\theta$  from the encoder position  $n_{\text{enc}}$ :

$$\theta = A_0 + A_1 n_{\text{enc}} + A_2 n_{\text{enc}}^2 + \dots$$

6. Compute the scan mirror normal vector  $\hat{\mathbf{n}}_{\text{mirr}}$  using the scan mirror angle  $\theta$  and the normal  $\hat{\mathbf{n}}_{\text{side}_i}$  for the appropriate mirror side  $i$ .

$$\hat{\mathbf{n}}_{\text{mirr}} = \mathbf{T}_{\text{rot}}(\theta) \hat{\mathbf{n}}_{\text{side}_i}$$

7. Transfer the scan mirror normal vector from the scan mirror to the instrument coordinate system and normalize it:

$$\mathbf{n}_{\text{inst}} = \mathbf{T}_{\text{inst/mirr}} \hat{\mathbf{n}}_{\text{mirr}} \quad \hat{\mathbf{n}}_{\text{inst}} = \frac{\mathbf{n}_{\text{inst}}}{|\mathbf{n}_{\text{inst}}|}$$

8. Reflect the viewing vector  $\mathbf{u}_{\text{img}}$  off the mirror to generate the viewing vector  $\mathbf{u}_{\text{inst}}$  in object space:

$$\mathbf{u}_{\text{inst}} = \mathbf{u}_{\text{img}} - 2\hat{\mathbf{n}}_{\text{inst}}(\mathbf{u}_{\text{img}} \cdot \hat{\mathbf{n}}_{\text{inst}})$$

### 3.1.4.2 Earth Location Algorithm

The MODIS Earth location algorithm computes the Earth location and other ancillary parameters for a viewing vector. There are three sections describing this calculation: the standard algorithm for intersection with the Earth ellipsoid; the terrain intersection algorithm; and the algorithm to generate the satellite and sun viewing angles and the satellite range.

#### **Basic Earth Ellipsoid Intersection Algorithm**

Given an object viewing vector  $\mathbf{u}_{inst}$  in the instrument coordinate system and a corresponding time  $t$ , the basic Earth ellipsoid intersection algorithm proceeds as follows:

1. Compute the required coordinate transformations:
  - a. Get instrument-to-spacecraft alignment matrix  $\mathbf{T}_{sc/inst}$ . [Construct the instrument-to-spacecraft alignment matrix based on the time  $t$  if a time varying model is needed.]
  - b. Interpolate the spacecraft attitude to time  $t$  and construct the spacecraft to orbital coordinate transformation matrix  $\mathbf{T}_{orb/sc}$ .
  - c. Interpolate the ECI spacecraft position  $\mathbf{P}_{eci}$  and velocity  $\mathbf{V}_{eci}$  to time  $t$  and construct the orbital to ECI transformation matrix  $\mathbf{T}_{eci/orb}$ .
  - d. Construct the ECI to ECR rotation matrix  $\mathbf{T}_{ecr/eci}$  from the sampling time  $t$ .
  - e. Construct the composite transformation matrix:

$$\mathbf{T}_{ecr/inst} = \mathbf{T}_{ecr/eci} \mathbf{T}_{eci/orb} \mathbf{T}_{orb/sc} \mathbf{T}_{sc/inst}$$

2. Transform the viewing vector and spacecraft position vector to the ECR coordinate system:
  - a. Rotate the viewing vector  $\mathbf{u}_{inst}$  to the ECR coordinate system:

$$\mathbf{u}_{ecr} = \mathbf{T}_{ecr/inst} \mathbf{u}_{inst}$$

- b. Rotate the spacecraft position vector to the ECR coordinate system:

$$\mathbf{p}_{ecr} = \mathbf{T}_{ecr/eci} \mathbf{p}_{eci}$$

3. Intersect the ECR viewing vector with the WGS84 (or other EOS Data and Information System (EOSDIS) standard) Earth ellipsoid:

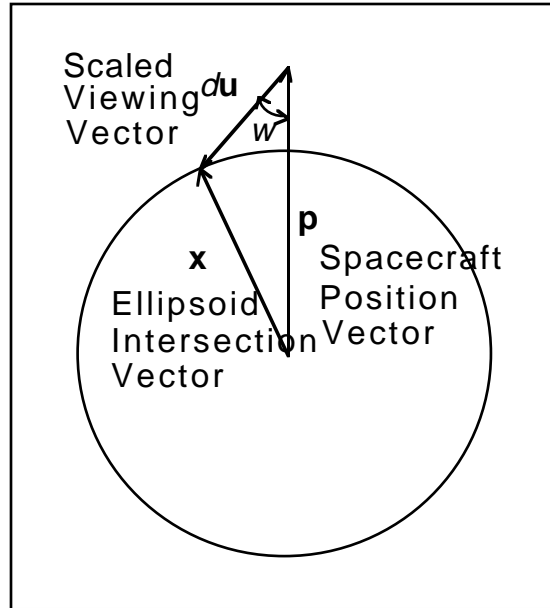


**Figure 3-19. Ellipsoidal Viewing Vector Intersection**

Note: These equations do not account for light travel time or aberration due to spacecraft motion or relativistic effects. These effects cause a systematic bias of 7 m at nadir and 14 m at the edges of the scans.

- a. Re-scale the viewing vector and satellite vector using the ellipsoid semi-major  $a$  and semi-minor  $b$  axis dimensions ( $a, a, b$ ):

$$\mathbf{u}' = \begin{bmatrix} u_1 / a \\ u_2 / a \\ u_3 / b \end{bmatrix} \quad \mathbf{p}' = \begin{bmatrix} p_1 / a \\ p_2 / a \\ p_3 / b \end{bmatrix}$$

Note:

$$\mathbf{x}' = \begin{bmatrix} x_1 / a \\ x_2 / a \\ x_3 / b \end{bmatrix} \quad \text{- the unknown ground point vector (re-scaled)}$$

- b. Solve for the scaling  $d$  of  $\mathbf{u}'$  which intersects the unit sphere:

From the law of cosines:

$$|\mathbf{x}'|^2 = |d \mathbf{u}'|^2 + |\mathbf{p}'|^2 - 2 |d \mathbf{u}'| |\mathbf{p}'| \cos(w)$$

Using the dot-product, the cosine of the acute angle  $w$  between  $\mathbf{u}'$  and  $-\mathbf{p}'$  is:

$$\cos(w) = -(\mathbf{u}' \cdot \mathbf{p}') / (|\mathbf{u}'| |\mathbf{p}'|)$$

By definition  $|\mathbf{x}'| = 1$  so:

$$1 = d^2 |\mathbf{u}'|^2 + |\mathbf{p}'|^2 + 2d |\mathbf{u}'| |\mathbf{p}'| (\mathbf{u}' \cdot \mathbf{p}') / (|\mathbf{u}'| |\mathbf{p}'|)$$

Simplifying and rearranging:

$$d^2 |\mathbf{u}'|^2 + 2d (\mathbf{u}' \cdot \mathbf{p}') + |\mathbf{p}'|^2 - 1 = 0$$

This can be solved for  $d$  using the quadratic formula:

$$d = \frac{-(\mathbf{u}' \cdot \mathbf{p}') - \sqrt{(\mathbf{u}' \cdot \mathbf{p}')^2 - |\mathbf{u}'|^2 (|\mathbf{p}'|^2 - 1)}}{|\mathbf{u}'|^2}$$

This is the smaller of the two solutions for  $d$ , the intersection closest to the satellite. If the solution is not real, then there is no intersection.

c. Use  $d$  to compute  $\mathbf{x}'$  and  $\mathbf{x}$ :

$$\mathbf{x}' = \mathbf{p}' + d\mathbf{u}'$$

$$\mathbf{x} = \begin{bmatrix} x'_1 a \\ x'_2 a \\ x'_3 b \end{bmatrix} = \begin{bmatrix} (p'_1 + du'_1) a \\ (p'_2 + du'_2) a \\ (p'_3 + du'_3) b \end{bmatrix} = \begin{bmatrix} p'_1 a + du'_1 a \\ p'_2 a + du'_2 a \\ p'_3 b + du'_3 b \end{bmatrix}$$

$$\mathbf{x} = \mathbf{p} + d\mathbf{u}$$

4. Convert the ECR ellipsoid pierce point to geodetic coordinates (special case direct solution):

$$lon = \tan^{-1} \left( \frac{x_2}{x_1} \right)$$

$$lat = \tan^{-1} \left( \frac{x_3 / (1 - e^2)}{\sqrt{x_1^2 + x_2^2}} \right)$$

$$h = 0$$

## Terrain Intersection Algorithm

The terrain intersection algorithm refines the earth ellipsoid intersection to account for the local terrain parallax. The method uses the ECR coordinate system and geodetic coordinate system and obtains geodetic coordinates where the view vector from the satellite intersects the terrain.

1. Compute the local ellipsoid normal unit vector from the geodetic latitude and longitude:

$$\hat{\mathbf{n}} = \begin{bmatrix} \cos(\phi) \cos(\lambda) \\ \cos(\phi) \sin(\lambda) \\ \sin(\phi) \end{bmatrix}$$

at  $\mathbf{x}$  on the Earth ellipsoid.

2. Compute the ECR unit vector from the ground point  $\mathbf{x}$  to the satellite:

$$\hat{\mathbf{u}} = -\frac{\mathbf{u}}{|\mathbf{u}|}$$

3. Compute the component of the satellite vector which is in the local vertical direction:

$$\cos \nu = \hat{\mathbf{u}} \cdot \hat{\mathbf{n}}$$

4. Compute the distance along the satellite vector ( $D_{\max}$ ) we must move to achieve a height of  $H_{\max}$  where  $H_{\max}$  is a pre-computed value representing the highest local terrain height:

$$D_{\max} = \frac{H_{\max}}{\cos \nu}$$

5. Compute the ECR coordinates of the point along the viewing vector that corresponds to  $H_{\max}$ :

$$\mathbf{x}_{\max} = \mathbf{x} + D_{\max} \hat{\mathbf{u}}$$

6. Compute the distance along the satellite vector ( $D_{\min}$ ) we must move to achieve a height of  $H_{\min}$  where  $H_{\min}$  is a pre-computed value representing the lowest local terrain height:

$$D_{\min} = \frac{H_{\min}}{\cos \nu}$$

7. Compute the ECR coordinates of the point along the viewing vector that corresponds to  $H_{\min}$ :

$$\mathbf{x}_{\min} = \mathbf{x} + D_{\min} \hat{\mathbf{u}}$$

8. Convert  $\mathbf{x}_{\max}$  to geodetic coordinates (iterative general solution), with coordinates  $(\phi_{\max}, \lambda_{\max}, H_{\max})$ ,

9. Define points  $\mathbf{s}_{\max}$  on the ellipsoidal surface from point  $\mathbf{x}_{\max}$  by:  
 $(\phi_{\max}, \lambda_{\max}, 0)$

10. Perform terrain intersection iterations (see Figure 3-20):

$$\mathbf{s}_0 = \mathbf{s}_{\max} = (\phi_{\max}, \lambda_{\max}, 0) \quad - \quad (\text{Geodetic coordinates})$$

$$h_0 = \text{DEM}(\mathbf{s}_0) \quad (\text{DEM at } \mathbf{s}_0)$$

$$H_0 = H_{\max}$$

$$ds = (\text{nominally } 1/2 \text{ km})$$

$$dD = \frac{ds}{\sin v}$$

$$i = 0$$

$$D_0 = D_{\max}$$

do until  $(h_i \geq H_i)$

$$i = i + 1$$

$$D_i = D_{i-1} - dD$$

$$\mathbf{x}_i = \mathbf{x} + D_i \hat{\mathbf{u}}$$

$$\mathbf{x}_i \Rightarrow (\phi_i, \lambda_i, h'_i) \quad (\text{Convert from ECR to geodetic})$$

$$\mathbf{s}_i = (\phi_i, \lambda_i, 0)$$

$$h_i = \text{DEM}(\mathbf{s}_i)$$

end do

$$D = D_i$$

11. Compute the precise terrain intersection from the last two iterations:

The final terrain intersection height can be expressed:

$$h_{\text{final}} = \alpha h_i + (1 - \alpha) h_{i-1} = \alpha h'_i + (1 - \alpha) h'_{i-1}$$



The database used for performing the terrain correction is the global 1 km Platte Carre EOS DEM. Height information is retrieved from the DEM database, which is called by the SDP Toolkit (see Reference 18), by performing linear interpolation to the specified geographic location from the four nearest-neighbor DEM data points. The DEM values are given over a geoid model and values from the Toolkit must be adjusted with the geoid to obtain the height values over the WGS84 ellipsoid.

It should be noted that the terrain correction will not be performed if the sensor zenith angle  $\nu$  (angle between  $\hat{\mathbf{n}}$  and  $\hat{\mathbf{u}}$ ) is greater than 85 degrees, which only occurs during the spacecraft maneuvers.

The use of alternative methods can be used to find the final geodetic coordinates simplifying some of the above processing. In Appendix B, part of Step 10 was rewritten to describe a simplified approach.

### **Computing Additional Parameters**

The remaining Earth location parameters can now be calculated from the final geodetic coordinates. These parameters are the zenith and azimuth angles to the satellite, the range to the satellite and the zenith and azimuth angles to the Sun. Also the sun vector from the satellite/Solar Diffuser is provided in addition to the lunar vector. The solar and lunar vectors are useful in the instrument calibration.

Given the final geodetic position latitude, longitude and height  $(\varphi, \lambda, h)$ , ECR coordinates  $(x, y, z) (= \mathbf{X}_{ecr})$  can be expressed (as given at the beginning of section 3.1.3.9) by:

$$x = (N + h) \cos \varphi \cos \lambda \quad (1)$$

$$y = (N + h) \cos \varphi \sin \lambda \quad (2)$$

$$z = (N(1 - e^2) + h) \sin \varphi \quad (3)$$

$$N = a / (1 - e^2 \sin^2 \varphi)^{1/2}$$

$$e^2 = 1 - \frac{b^2}{a^2}$$

1. Compute the unit normal vector  $\hat{\mathbf{n}}$  at the final geodetic position  $(\varphi, \lambda, h)$  by differentiating equations (1), (2), and (3) with respect to  $h$  and evaluate at  $(\varphi, \lambda, h)$ :

$$\hat{\mathbf{n}} = \begin{bmatrix} \cos(\varphi) \cos(\lambda) \\ \cos(\varphi) \sin(\lambda) \\ \sin(\varphi) \end{bmatrix}$$

2. Compute a unit vector  $\hat{\mathbf{E}}$  in the east direction at the geodetic position by differentiating equations (1), (2), and (3) with respect to  $\lambda$  and evaluate at the position:

$$\hat{\mathbf{E}} = \begin{bmatrix} -\sin\lambda \\ \cos\lambda \\ 0 \end{bmatrix}$$

3. Compute a unit vector  $\hat{\mathbf{N}}$  in the north direction at the geodetic position by computing the cross product of  $\hat{\mathbf{n}}$  and  $\hat{\mathbf{E}}$ :

$$\hat{\mathbf{N}} = \hat{\mathbf{n}} \times \hat{\mathbf{E}}$$

4. Generate the range to the spacecraft  $r_{sc}$  and the ground to spacecraft unit vector  $\hat{\mathbf{v}}_{sc}$ :

$$\mathbf{v}_{sc} = \mathbf{p}_{ecr} - \mathbf{x}_{ec}$$

$$r_{sc} = |\mathbf{v}_{sc}|$$

$$\hat{\mathbf{v}}_{sc} = \frac{1}{r_{sc}} \mathbf{v}_{sc}$$

5. The zenith angle  $\zeta_{sc}$  is the angle between the spacecraft view vector and the normal:

$$\cos(\zeta_{sc}) = \hat{\mathbf{n}} \cdot \hat{\mathbf{v}}_{sc}$$

6. Compute the azimuth angle  $\alpha_{sc}$ :

- a. Compute two directional cosines by:

$$l = \mathbf{v}_{sc} \cdot \hat{\mathbf{E}} \quad m = \mathbf{v}_{sc} \cdot \hat{\mathbf{N}}$$

- b. Using the following relationship between the azimuth angle and the directional cosines  $l$  and  $m$ , determine the angle.

$$\tan(\alpha_{sc}) = \frac{l}{m}$$

7. The following steps are used to generate the solar vectors from the ground and from the spacecraft/Solar Diffuser after retrieving the ECI solar vector  $\mathbf{s}_{eci}$  based on the time  $t$  at the middle of the Solar Diffuser Scan(product Generation System(PGS) Toolkit call).

- a. In the ECR coordinate system, rotate the solar vector at time  $t$  by:

$$\mathbf{s}_{ecr} = \mathbf{T}_{ecr/eci} \mathbf{s}_{eci}$$

For the solar zenith and azimuth angles, use steps 5 and 6.

b. In the instrument coordinate system,

$$\mathbf{s}_{inst} = \mathbf{T}_{instsc} \mathbf{T}_{sdorb} \mathbf{T}_{orbeci} \mathbf{s}_{eci}$$

c. In the Solar Diffuser coordinate system using the inverse of the rotation matrix  $\mathbf{T}_{instSD}$  of section 3.1.3.4.

$$\mathbf{s}_{SD} = \mathbf{T}_{SD/inst} \mathbf{s}_{inst}$$

d. Azimuth and zenith angles in the SD coordinate system by:

$$\phi_i = \tan^{-1} \frac{s_{SDy}}{s_{SDx}}$$

$$\theta_i = \cos^{-1} s_{SDz}$$

where  $\mathbf{s}_{SD} = (s_{SDx}, s_{SDy}, s_{SDz})^T$ .

See Figure 3-5 for more details.

8. Similarly the following steps are used to generate the lunar vector  $\mathbf{m}_{inst}$  from the spacecraft in the instrument coordinate system after retrieving the ECI lunar vector  $\mathbf{m}_{eci}$  based on the time  $t$  (product Generation System (PGS) Toolkit call).

In the instrument coordinate system,

$$\mathbf{m}_{inst} = \mathbf{T}_{instsc} \mathbf{T}_{sdorb} \mathbf{T}_{orbeci} \mathbf{m}_{eci}$$

### 3.1.4.3 Sub-pixel Approximate Ground Location Model

This section describes a method for calculation of the sub-pixel approximate ground location. The full set of equations above may be used to describe the ground location corresponding to any focal plane location at any time. There are 81 unique center locations within one spatial element (Table 3-8). To do the full calculation for every sample for each detector in each band for every frame of data would be very expensive computationally.

**Table 3-8. Unique Center Locations in One Spatial Element**

Resolution	Bands	Detectors	Samples	Total
1 km	29	1	1	29
500 m	5	2	2	20
250 m	2	4	4	32
Total				81

To make this process easier several approximations can be made that allow the ground locations to be calculated with slightly less accuracy.

The sub-pixel ground location may be the actual location of the center of any detector in any individual band or the location of any other point within the detector. Care should be taken when using these equations to calculate points other than the center of the detector since the dynamic point spread function of the detector is not taken into account.

The method uses the knowledge of all the ground points projected from the ten detectors of the ideal band for a scan. The projection (mapping) is then expanded to the detectors of all bands. The mapping is expressed by three sets of biquadratic polynomials.

### **General Concept**

The ideal band is created to make the sub-pixel approach easier and to minimize error, which will reduce computational expenses. Although in reality the first frame of a scan begins with band 30, the ideal band is created so that every band can be adjusted and aligned to it. The ideal band is placed at the center of the focal planes, and its trailing edges of the all detectors are aligned to y-axis of the focal plane coordinate system (see Figure 3-11 for its location). Let  $\mathbf{u}_0 = [x_0, y_0, f_0]^T$  be the ideal band's image space viewing vector of a particular detector. The vector  $\mathbf{u}_0$  is mapped to the ground at  $\mathbf{x}_0$  expressed by:

$$\mathbf{x}_0 = f_{ground}(t_0, \mathbf{u}_0)$$

All 10 detectors of the ideal band are mapped to the ground at time point 1 through 1354. This can be viewed as a mapping of a uniform grid  $10 \times 1354$  to the distorted earth grid, where time points move with interval  $t_{samp}$  of 333.33  $\mu$  seconds. The mapping is illustrated in Figure 3-21. All the real bands are mapped to the locations of the ideal band by adjusting sampling time. To find where all bands are projected on the ground, a sub-pixel approximation is needed.

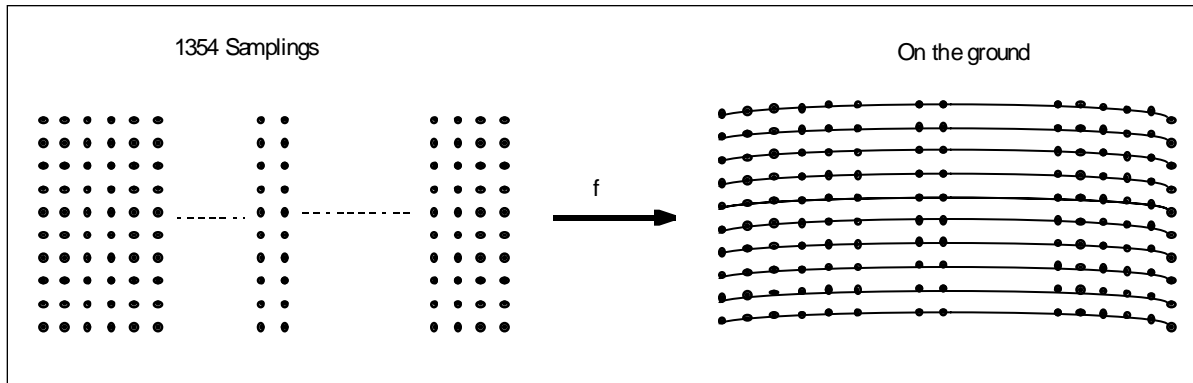


**Figure 3-21. Ideal Band Projection on the Ground**

**A Biquadratic Interpolation Method Around  $(x_0, y_0)$**

The  $10 \times 1354$  grid is mapped on the ground as shown in Figure 3-21. By shifting the  $3 \times 3$  grid within the  $10 \times 1354$  grid, we can think of a mapping from the  $3 \times 3$  imaginary grid to the  $3 \times 3$  ground points around time  $t$ . The coordinates of the  $3 \times 3$  grid are shown below:

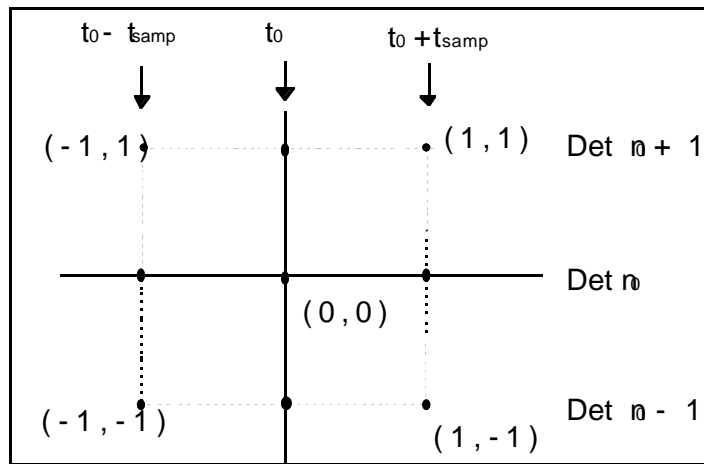


**Figure 3-22. Biquadratic Interpolation 3 x 3 Grid**

### Computation of subpixel offset along-scan and along-track offsets in IFOV

Let the ground location  $\mathbf{x}_0$  be calculated at sampling time  $t_0$  for an ideal band spatial element with center located at  $(x_0, y_0)$  and the ideal band focal length  $f_0$  be given by:

$$\mathbf{x}_0 = f_{ground}(t_0, \mathbf{u}_0)$$

Let  $x$  and  $y$  be the coordinates of a detector center of a band. Then the along-scan offset in 1 km IFOV is given by:

$$\Delta x = x' \frac{x_{space} - x_0}{x_{space}} - t_{offset} / t_{samp} \quad (1)$$

where  $x' = x \frac{f_0}{f}$ ,

$t_{offset}$ : time to bring back the detector's view on the ground to the ideal band.

For example, for band 30 in an ideal case, we have:

$$\begin{aligned} x' &= 1 \frac{x_{space}}{x_{space}} \\ x_0 &= 0 \\ t_{offset} &= 1 \frac{t_{samp}}{t_{samp}} \end{aligned}$$

This gives  $\Delta x = 0$ .

For band 2 in an ideal case, we have:

$$\begin{aligned} x' &= -2 \frac{x_{space}}{x_{space}} \\ x_0 &= 0 \\ t_{offset} &= \left( -2 - \frac{n}{4} + \frac{3}{4} \right) t_{samp} \quad \text{for } n = 0, \dots, 3 \end{aligned}$$

This gives  $\Delta x = -3/4, -1/2, -1/4,$  and  $0$  at four sampling time points (see Figure 3-13 for different band ground views).

The along-track offset is given by:

$$\Delta y = y' \frac{y_{space} - y_0}{y_{space}} \quad (2)$$

$$y' = y \frac{f_0}{f}$$

These along-scan and along-track offsets  $\Delta x$  and  $\Delta y$  are fed into three biquadratic polynomials to calculate ground coordinates of the sub-pixel location. It is necessary to calculate coefficients of the quadratic polynomials from 9 ground points. The following section describes how to calculate these coefficients.

### Computation of Interpolation Coefficients

The simplified  $3 \times 3$  grid is mapped to the ground points by a biquadratic equation of the form:

$$z(x, y) = \sum_{i,j=0}^2 a_{ij} x^i y^j \quad (3)$$

where  $x = -1, 0, \text{ or } 1$  and  $y = -1, 0, \text{ or } 1$ .  $z$  is one of three coordinates used for the ground point. Note that  $a_{00}$  is determined by  $z(0,0)$ .

Given  $3 \times 3$  grid points  $(x, y)$  and  $z$ , a set of coefficients  $a_{ij}$  can be chosen to fit exactly the values of  $z$  at the locations  $(x, y)$ .

Using the above simplified grid, we can derive a generic solution to the interpolation coefficients. The polynomial coefficients  $a_{ij}$  can be rearranged as a vector with element  $a'_k$ , where:

$$\begin{aligned} k &= 3i + j \\ a'_k &= a_{ij} \\ \mathbf{A} &= [a'_k]. \end{aligned} \quad (4)$$

Likewise, the input values  $x, y, z$  can be rearranged as vectors, where the ordering of  $(x_i, y_i)$  pairs is  $\{(-1,-1), (-1, 0), \dots, (1, 1)\}$ . For example,  $(x_0, y_0) = (-1, -1), \dots, (x_8, y_8) = (1, 1)$ . The solution for  $\mathbf{A}$  can then be expressed as the matrix equation:

$$\mathbf{MA} = \mathbf{Z} \quad (5)$$

where

$$\mathbf{M} = [m_{lk}] = x_l^{k/3} y_l^{(k \bmod 3)} \quad (6)$$

$$\mathbf{Z} = [z_l],$$

$$\text{for } l = 0, 1, \dots, 8, \quad k = 0, 1, \dots, 8$$

Note that  $k$  is the same as in equation (4) and the exponents of  $x_i$  and  $y_i$  in equation (6) are merely reproducing the indices  $i$  and  $j$ . The solution for the vector  $\mathbf{A}$  uses the inverse of matrix  $\mathbf{M}$  by:

$$\mathbf{A} = \mathbf{M}^{-1}\mathbf{Z} \quad (7)$$

and the interpolated value of  $z$  for any  $x$  and  $y$  is given by:

$$z = \sum_0^8 a'_k x^{k/3} y^{(k \bmod 3)} \quad (8)$$

Note that the value  $x$  and  $y$  are relative to the center location of the input values  $x_i$  and  $y_i$ . Also note that the matrix  $\mathbf{M}$  and therefore inverse  $\mathbf{M}^{-1}$  will be a constant since the values of  $x_i$  and  $y_i$  are defined as constants. The actual values of  $\mathbf{M}$  and  $\mathbf{M}^{-1}$  are given at (14) and (15).

In this particular application, there will be 3 sets of input values (one for each geolocation field) which all have the same values of  $x$  and  $y$  from the same 3 x 3 grid, and which need to be interpolated to the same value of  $x$ , and  $y$ . This allows for further simplification. Equation (8) can be expressed as a vector scalar product by expressing the products of powers of  $x$  and  $y$  as a vector  $\mathbf{v}$ :

$$v_k = x^{k/3} y^{(k \bmod 3)} \quad (9)$$

$$z = \mathbf{v} \cdot \mathbf{A} \quad (10)$$

Combining equation (7) and (8), gives

$$z = \mathbf{v} \cdot (\mathbf{M}^{-1}\mathbf{Z}) = (\mathbf{v}^T \cdot \mathbf{M}^{-1}) \cdot \mathbf{Z} \quad (11)$$

The vector /matrix product in the second parentheses can be computed once for a given value of  $x$  and  $y$ . Note again that  $\mathbf{M}^{-1}$  is a constant matrix. The resulting vector  $\mathbf{C}(x,y)$  coefficients can be used to interpolate all the  $x$  and  $y$  geolocation fields.

$$\mathbf{C} = \mathbf{v}^T \cdot \mathbf{M}^{-1} \quad (12)$$

$$z = \mathbf{C}\mathbf{Z} \quad (13)$$

Thus the computation of  $\mathbf{A}$  is unnecessary, and the interpolation can be performed directly with the input values  $\mathbf{Z}$  using vector  $\mathbf{C}$ .

It should be noted that if a detector of a band which corresponds to a spatial element of the ideal band's detector 1 or 10, or at the beginning of the scan or end of the scan,  $z$  will be extrapolated using the coefficients  $\mathbf{A}$ .

Values of  $\mathbf{M}$  and  $\mathbf{M}^{-1}$

As specified above,  $\mathbf{M}$  is a  $9 \times 9$  matrix computed from  $x_i$  and  $y_i$  using equation (6):

$$\mathbf{M} = [m_k] = x_i^{k/3} y_i^{(k \bmod 3)}$$

The values of  $x_i$  and  $y_i$  are:

$$x_i = (-1, -1, -1, 0, 0, 0, 1, 1, 1)$$

$$y_i = (-1, 0, 1, -1, 0, 1, -1, 0, 1)$$

This produces the following values for  $\mathbf{M}$ :

$$\mathbf{M} = \begin{bmatrix} 1 & -1 & 1 & -1 & 1 & -1 & 1 & -1 & 1 \\ 1 & 0 & 0 & -1 & 0 & 0 & 1 & 0 & 0 \\ 1 & 1 & 1 & -1 & -1 & -1 & 1 & 1 & 1 \\ 1 & -1 & 1 & 0 & 0 & 0 & 0 & 0 & 0 \\ 1 & 0 & 0 & 0 & 0 & 0 & 0 & 0 & 0 \\ 1 & 1 & 1 & 0 & 0 & 0 & 0 & 0 & 0 \\ 1 & -1 & 1 & 1 & -1 & 1 & -1 & -1 & 1 \\ 1 & 0 & 0 & 1 & 0 & 0 & 0 & 0 & 0 \\ 1 & 1 & 1 & 1 & 1 & 1 & 1 & 1 & 1 \end{bmatrix} \quad (14)$$

Inverting  $\mathbf{M}$  results in the following:

$$\mathbf{M}^{-1} = \begin{bmatrix} 0 & 0 & 0 & 0 & 1 & 0 & 0 & 0 & 0 \\ 0 & 0 & 0 & -5 & 0 & 5 & 0 & 0 & 0 \\ 0 & 0 & 0 & 5 & -1 & 5 & 0 & 0 & 0 \\ 0 & -5 & 0 & 0 & 0 & 0 & 0 & 5 & 0 \\ .25 & 0 & -25 & 0 & 0 & 0 & -25 & 0 & 0.25 \\ -25 & 5 & 1-25 & 0 & 0 & 0 & 25 & -5 & 0.25 \\ 0 & 5 & 0 & 0 & -1 & 0 & 0 & 5 & 0 \\ -25 & 0 & .25 & 5 & 0 & -5 & -25 & 0 & .25 \\ .25 & -5 & .25 & -5 & 1 & -5 & 25 & -5 & .25 \end{bmatrix} \quad (15)$$

It is worth noting that 36 of the 81 elements of  $\mathbf{M}$  are non-zero. Thus it may be more efficient to expand the matrix multiplication into a set of equations which use only the non-zero matrix elements.

Even if the above equations are used with the ellipsoid locations, it is still necessary to transfer the offsets calculated to the terrain locations of the points. The algorithm described below is based on the bi-linear interpolation technique, which requires a rectangular area. Since the areas should be very close to rectangular and the Earth curvature effects are small over the area of a single pixel, this algorithm is expected to perform well.

1. Initially, the ellipsoid ground locations of the four points surrounding the sub-pixel ground locations  $\mathbf{x}_{\text{ellip}}$  are found.

$$\mathbf{x}_{\text{ellip}11}, \mathbf{x}_{\text{ellip}12}, \mathbf{x}_{\text{ellip}21}, \mathbf{x}_{\text{ellip}22}$$

These points correspond to the upper left, upper right, lower left, and lower right points, respectively.

2. Compute the top and left side vectors,  $\mathbf{b}_1$  and  $\mathbf{b}_2$ , and the vector  $\mathbf{c}$  from the ground location to the upper left corner:

$$\mathbf{b}_1 = \mathbf{x}_{\text{ellip}12} - \mathbf{x}_{\text{ellip}11}$$

$$\mathbf{b}_2 = \mathbf{x}_{\text{ellip}21} - \mathbf{x}_{\text{ellip}11}$$

$$\mathbf{c} = \mathbf{x}_{\text{ellip}} - \mathbf{x}_{\text{ellip}11}$$

The relative length of the components of  $\mathbf{c}$  projected onto the top and left sides are then:

$$\alpha_1 = \frac{\mathbf{c} \cdot \mathbf{b}_1}{\mathbf{b}_1 \cdot \mathbf{b}_1} \quad \text{and} \quad \alpha_2 = \frac{\mathbf{c} \cdot \mathbf{b}_2}{\mathbf{b}_2 \cdot \mathbf{b}_2}$$

3. The relative distances are used to generate the area based weights:

$$w_1 = (1 - \alpha_1)(1 - \alpha_2) \quad w_2 = \alpha_1(1 - \alpha_2)$$

$$w_3 = (1 - \alpha_1)\alpha_2 \quad w_4 = \alpha_1\alpha_2$$

4. These weights are then used to interpolate between the terrain corrected ground locations:

$$\mathbf{x}_{\text{terr}} = w_1\mathbf{x}_{\text{terr}11} + w_2\mathbf{x}_{\text{terr}12} + w_3\mathbf{x}_{\text{terr}21} + w_4\mathbf{x}_{\text{terr}22}$$

### 3.1.5 Variance or Uncertainty Estimates

The fundamental measure of uncertainty of interest for the Earth location algorithm is the locational accuracy of the geodetic coordinates computed for each spatial element. This accuracy is limited by the uncertainty in the spacecraft, instrument, and elevation data provided to the algorithm.

A complete analysis of MODIS Earth location error is presented in "An Analysis of MODIS Earth Location Error" (Reference 2). That document presents a detailed breakdown of the anticipated sources of error in the EOS AM spacecraft ephemeris and attitude knowledge, and in the MODIS instrument pointing knowledge. It also demonstrates the effects these errors and errors in the ancillary digital elevation data have on the resulting data product Earth location accuracy. The current best estimates of the contributing errors provided by the spacecraft and instrument builders, as well as the spacecraft and instrument specification requirements, were used in that analysis. What follows is extracted from that report.

The sensitivity of the output product accuracy to the uncertainty in the input data varies with scan angle. Plots depicting this sensitivity for spacecraft position, spacecraft attitude pointing, and instrument pointing knowledge errors are presented in Reference 2.

The three error components, spacecraft position, spacecraft attitude, and instrument pointing knowledge, were analyzed separately with all contributing errors classified as either static or dynamic. Static errors are unknown constant offsets caused by imprecise knowledge of the instrument or spacecraft geometry, or by geometric distortions occurring before or in-flight. These error components, though initially unknown, should not change with time in-flight. Estimates of these constant offsets or biases will be computed using the geometric parameter estimation and algorithm verification procedures described in Section 3.2.3. The dynamic error components are time varying and cannot be easily modeled. Tables detailing the various error sources and their expected magnitudes are presented in Reference 2. Tables 3-9, 3-10, and 3-11 summarize the impact on Earth location of the various error sources. The three case studies were: the Current Design Specification case; the Likely Built case; and the Likely Built Bias Removed case. Table 3-12 shows the combined effect (Root Sum Square (RSS)) of all of the components.

**Table 3-9. Geolocation Impact of 2 Sigma Spacecraft Position Errors**

Spacecraft Position	X-Axis Platform Position Error	Corresponding Along-Track Earth Location Error		Y-Axis Platform Position Error	Corresponding Along-Scan Earth Location Error		Z-Axis Platform Position Error	Corresponding Along-Scan Earth Location Error	
		scan = 0°	scan = 55°		scan = 0°	scan = 55°		scan = 0°	scan = 55°
Current Spec	100.0 m	90.0 m (0.090 pixels*)	88.5 m (0.044 pixels*)	100.0 m	90.0 m (0.090 pixels*)	90.0 m (0.019 pixels*)	100.0 m	0.0 m	197.3 m (0.041 pixels*)
Likely Built	44.3 m	39.0 m (0.039 pixels*)	38.4 m (0.019 pixels*)	24.0 m	21.6 m (0.022 pixels*)	21.6 m (0.004 pixels*)	6.7 m	0.0 m	13.2 m (0.003 pixels*)

Likely Built Bias Removed	44.3 m	39.0 m (0.039 pixels*)	38.4 m (0.019 pixels*)	24.0 m	21.6 m (0.022 pixels*)	21.6 m (0.004 pixels*)	6.7 m	0.0 m	13.2 m (0.003 pixels*)
---------------------------	--------	---------------------------	---------------------------	--------	---------------------------	---------------------------	-------	-------	---------------------------

\* using a 1 km resolution pixel

**Table 3-10. Geolocation Impact of 2 Sigma EOS AM Platform Attitude Knowledge Error Components**

Platform Attitude	Roll Pointing Error	Corresponding Along-Scan Earth Location Error		Pitch Pointing Error	Corresponding Along-Track Earth Location Error		Yaw Pointing Error	Corresponding Along-Track Earth Location Error	
		scan = 0°	scan = 55°		scan = 0°	scan = 55°		scan = 0°	scan = 55°
Current Spec	60.0 arcsec	205.1 m (0.205 pixels*)	990.5 m (0.205 pixels*)	60.0 arcsec	205.1 m (0.205 pixels*)	235.9 m (0.118 pixels*)	60.0 arcsec	0.0 m	336.9 m (0.168 pixels*)
Likely Built	36.7 arcsec	125.3 m (0.125 pixels*)	605.3 m (0.125 pixels*)	51.5 arcsec	175.9 m (0.176 pixels*)	202.4 m (0.101 pixels*)	32.3 arcsec	0.0 m	181.2 m (0.090 pixels*)
Likely Built Bias Removed	7.3 arcsec	25.1 m (0.025 pixels*)	121.1 m (0.025 pixels*)	9.3 arcsec	31.9 m (0.032 pixels*)	36.7 m (0.018 pixels*)	6.1 arcsec	0.0 m	34.1 m (0.017 pixels*)

\* using a 1 km resolution pixel

**Table 3-11. Geolocation Impact of 2 Sigma Instrument Pointing Knowledge Error Components**

Instrument Pointing	Roll Pointing Error	Corresponding Along-Scan Earth Location Error		Pitch Pointing Error	Corresponding Along-Track Earth Location Error		Yaw Pointing Error	Corresponding Along-Track Earth Location Error	
		scan = 0°	scan = 55°		scan = 0°	scan = 55°		scan = 0°	scan = 55°
Current Spec	60.0 arcsec	205.1 m (0.205 pixels*)	990.5 m (0.205 pixels*)	60.0 arcsec	205.1 m (0.205 pixels*)	235.9 m (0.118 pixels*)	60.0 arcsec	0.0 m	336.9 m (0.168 pixels*)
Likely Built	57.1 arcsec	195.3 m (0.195 pixels*)	943.2 m (0.195 pixels*)	44.0 arcsec	150.4 m (0.150 pixels*)	173.0 m (0.086 pixels*)	46.9 arcsec	0.0 m	263.6 m (0.131 pixels*)
Likely Built Bias Removed	30.4 arcsec	103.9 m (0.104 pixels*)	501.9 m (0.104 pixels*)	17.3 arcsec	59.0 m (0.059 pixels*)	67.9 m (0.034 pixels*)	20.7 arcsec	0.0 m	116.1 m (0.058 pixels*)

\* using a 1 km resolution pixel

**Table 3-12. Total Combined 2 Sigma RSS Geolocation Error**

	Total RSS Along-Scan Earth Location Error (2 sigma)		Total RSS Along-Track Earth Location Error (2 sigma)	
	(Y-Axis Spacecraft Position) (Z-Axis Spacecraft Position) (Platform Roll ) (Instrument Roll)		(X-Axis Spacecraft Position) (Platform Pitch) (Instrument Pitch) (Platform Yaw) (Instrument Yaw)	
	scan = 0°	scan = 55°	scan = 0°	scan = 55°
Current Spec	303.7 m (0.304 pixels*)	1417.5 m (0.294 pixels*)	303.7 m (0.304 pixels*)	588.4 m (0.293 pixels*)
Likely Built	233.0 m (0.233 pixels*)	1121.0 m (0.232 pixels*)	234.7 m (0.235 pixels*)	417.9 m (0.208 pixels*)
Likely Built Bias Removed	109.0 m (0.109 pixels*)	516.9 m (0.107 pixels*)	77.6 m (0.078 pixels*)	148.5 m (0.074 pixels*)

\* using a 1 km resolution pixel

Figure 3-23 and 3-24 show these combined Earth location errors graphically. In the first figure, the six error ellipses correspond to the three cases at two different scan angles, 0 and 55 deg with the error given in meters. The second figure shows nine error ellipses representing the three case and three scan angles with the error given in fractions of a 1 km resolution pixel.

The accuracy impact of the digital elevation data is also a function of scan angle with no effect on Earth location at nadir and a greater than one-to-one correspondence between height and position errors at high scan angles. Figure 3-25 shows the impact of three different terrain accuracies on the Earth location accuracy in fractions of a 1 km pixel. In each graph, the Earth location error in pixel fraction reaches a peak and drops down after that point. Although both the Earth location error and ground pixel size increase as the scan angle increases, the rate of increase in the pixel size is slower than the one in the Earth location error at the beginning but later it becomes faster than the other and their ratio drops down. See Figure 3-1 for growth of the pixel size on the ground. In the context of image-to-image registration, the displacement due to terrain errors is self-canceling if the two data sets are taken from approximately the same viewing geometry but are arithmetically added if the views are from different directions. The effect of the input elevation model on the product accuracy is further complicated by the relationship between elevation accuracy and terrain roughness. In rugged areas, elevation variations of hundreds of meters can occur within a single MODIS spatial element. Assigning a single geodetic coordinate to such a spatial element using a

representative elevation masks the true complexity of the terrain and the real differences in what is being viewed from different directions.

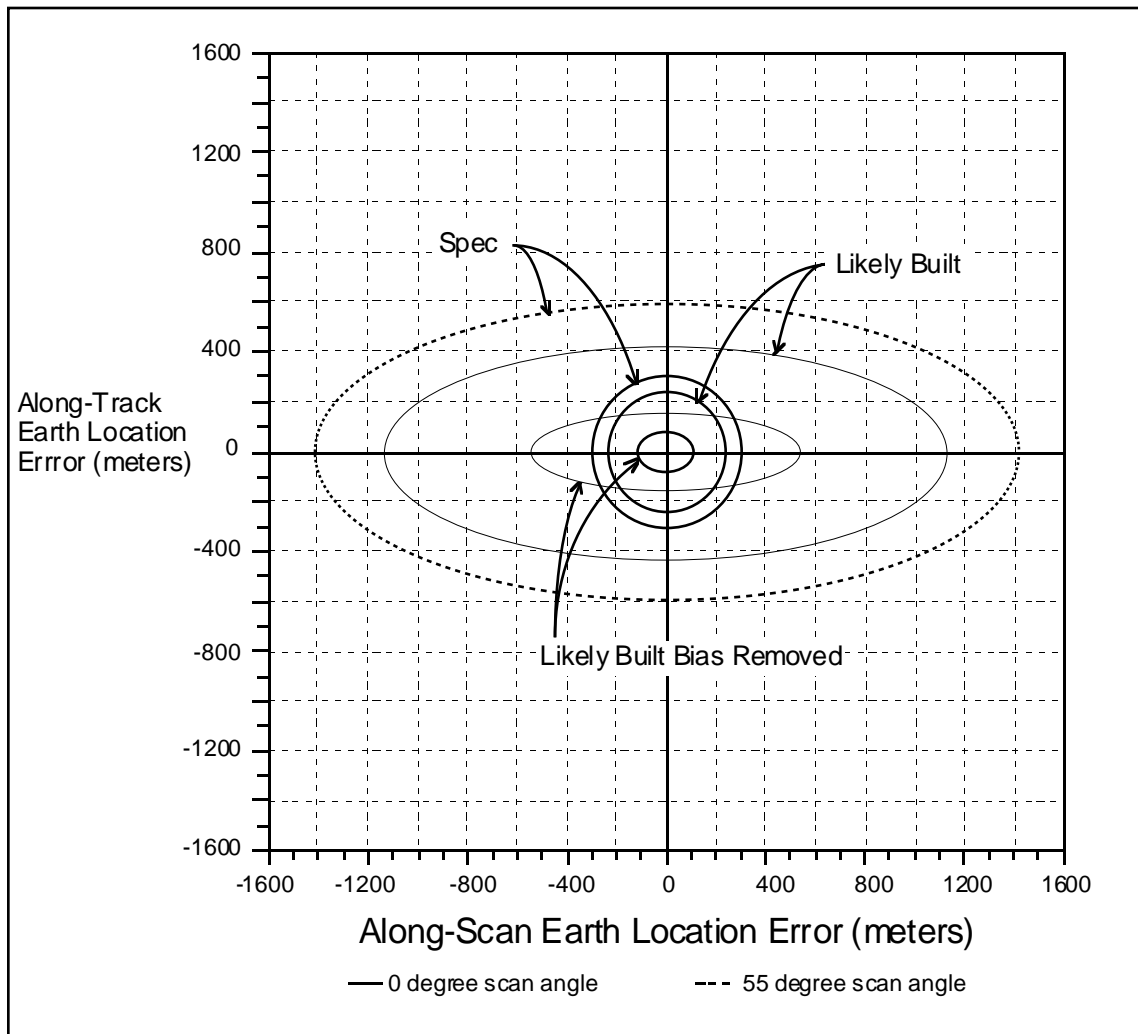
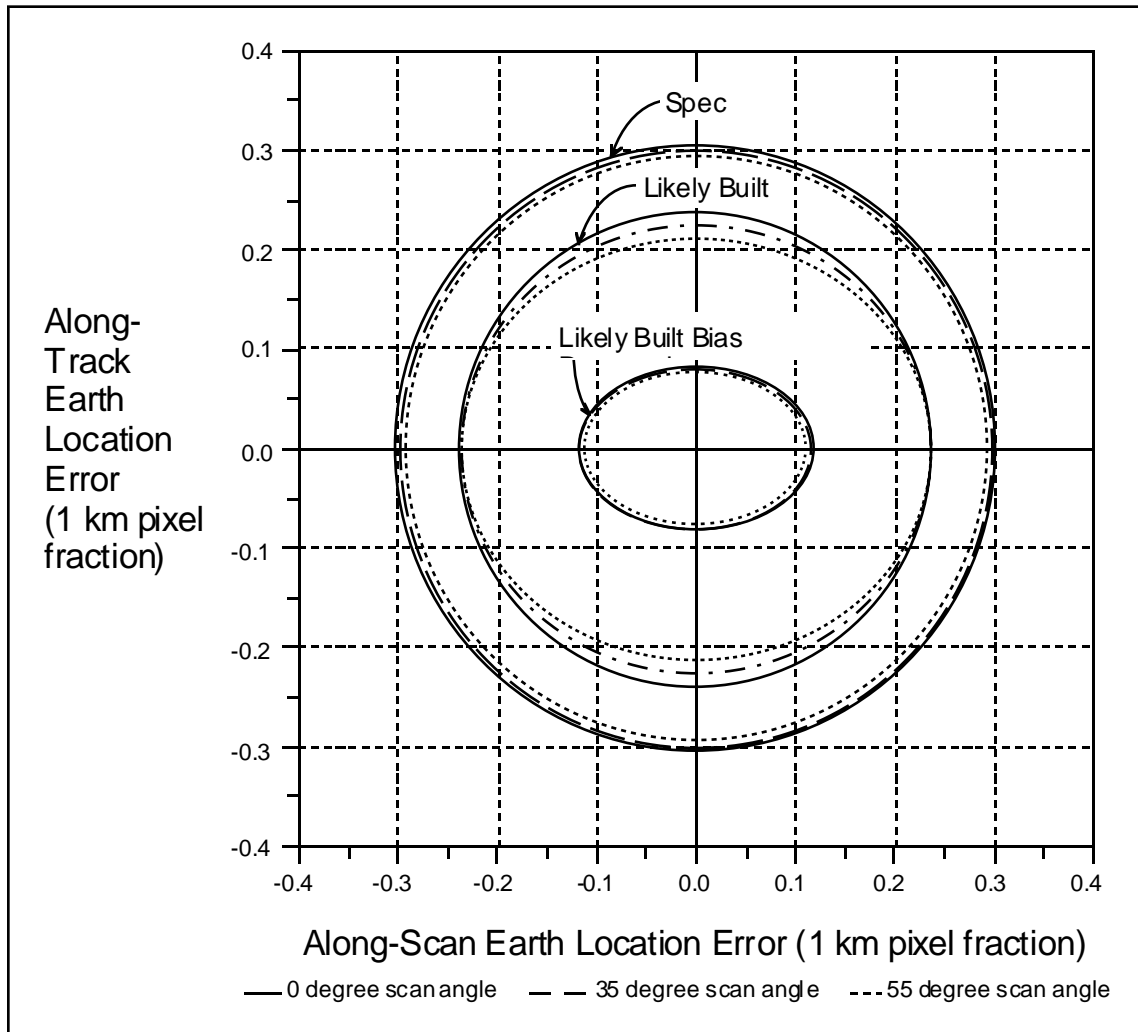
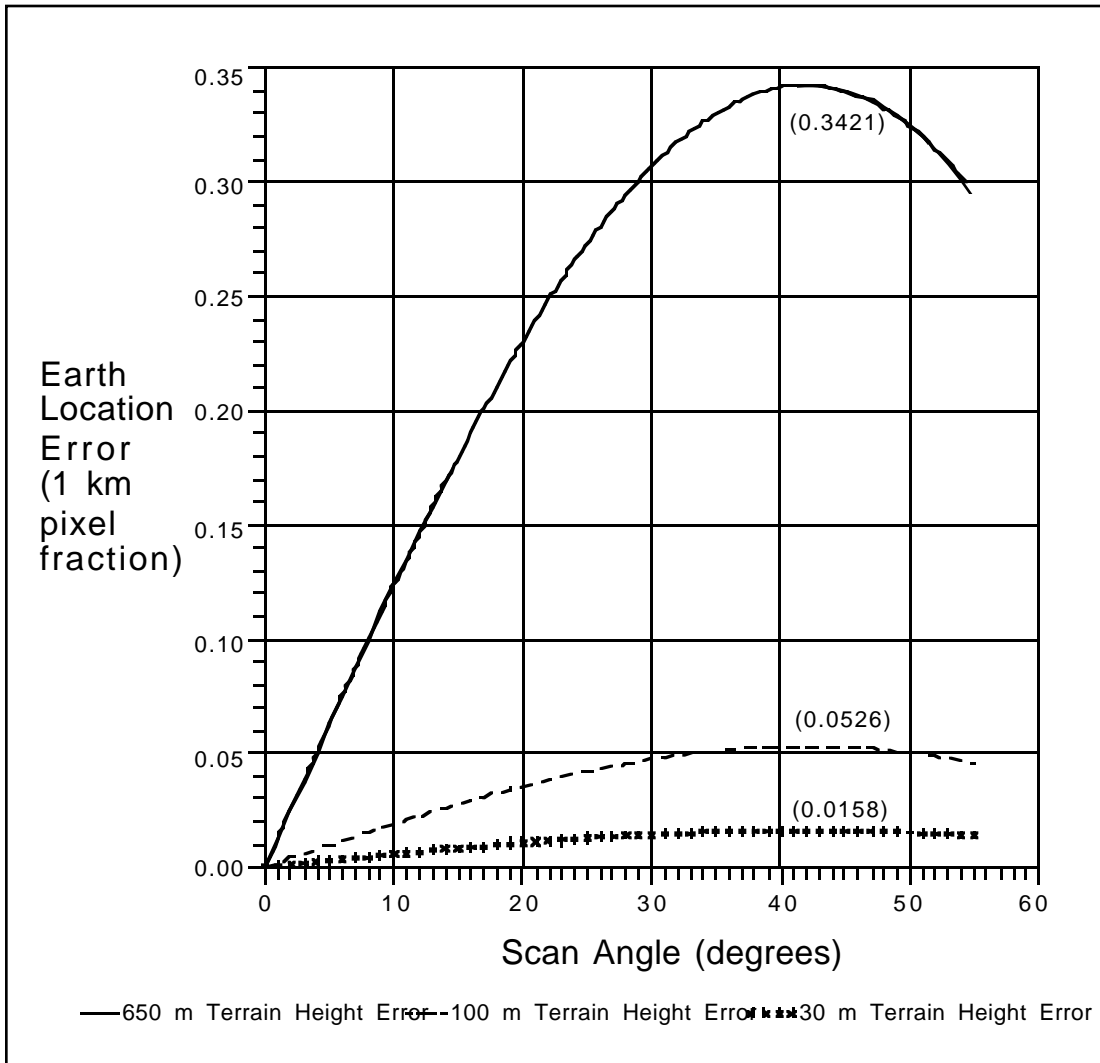


Figure 3-23. Earth Location Error (meters)



**Figure 3-24. Earth Location Error (1 km pixel fraction)**



**Figure 3-25. Earth Location Error (in 1 km pixel fraction) Resulting from Various Terrain Height Errors as a Function of Scan Angle**

### 3.2 Practical Considerations

The following sections discuss practical implementation and operational considerations including numerical stability, computational efficiency, algorithm verification, product validation, automated quality control and metadata generation, and possible processing exception conditions.

#### 3.2.1 Numerical Computation Considerations

The MODIS Earth location algorithm incorporates two iterative procedures that must be implemented carefully to ensure convergence. The first of these is the general iterative conversion from ECR to geodetic coordinates. This procedure is straightforward and robust. This is performed through a call to the SDP Toolkit (see Reference 18).

The second iterative procedure is the detection of the MODIS line of sight intersection with the terrain. Simple approaches to implementing this algorithm break down at high off-nadir angles due to the possibility of multiple intersections of the line of sight with the terrain surface. Under these conditions, care must be taken to ensure that the algorithm converges to the correct terrain intersection point (i.e. the intersection closest to the satellite). This is achieved here by searching from above to find the first (highest) terrain intersection. The iteration proceeds down monotonically until the viewing vector is below the terrain surface so that convergence is not a problem. The precision of the final terrain intersection determination is a function of the local relief. The degree to which this approximation breaks down is a function of the height range searched and the satellite look angle. These statistics will be monitored for quality control purposes as described in Section 3.2.4.

### ***3.2.2 Programming/Procedural Considerations***

The computational burden imposed by the MODIS Earth location algorithm arises primarily from the terrain intersection computation. Current estimates indicate that approximately 80% of the Earth location processing load is used by the terrain correction step. Within this procedure the conversion from ECR to geodetic coordinates consumes the bulk of the processing.

In the ECR to geodetic conversion the main computational driver is the number of trigonometric functions that must be performed. One way to achieve efficiency in these computations is to carefully apply small angle approximations and Taylor series expansions when the angles involved change very little between invocations. Another approach is to implement the standard sine and cosine functions as look-up tables that have been pre-computed based on the required precision of the calling routine. The tradeoff of computational precision for computational performance would have to be carefully weighed before implementing any of these approximations.

### ***3.2.3 Algorithm Verification***

The purpose of the algorithm verification process is to verify that the algorithm will accurately calculate the location of MODIS samples. This verification process will verify the accuracy of the algorithms presented here in this document as well as the algorithm's implementation in software. Initially at launch there will be systematic biases in the model that will be removed by the geometric parameter estimation process. It is expected that over time the algorithm will converge to an accurate solution which will be stable and repeatable in both scene to scene and scene to ground measurements.

There are three steps in the verification process. First, the software implementation of the Earth location model must match the algorithm. Second, the algorithm implementation must correctly represent the instrument. Third, the software implementation should match the end-to-end system, which verifies both the instrument model and the satellite and Earth models. The tools for measuring the accuracy will be tested as part of the verification process.

Once the algorithm has been verified, care must be taken that, as the algorithm evolves, the chain of verification is not broken. This process will involve careful feedback of model changes, both to the algorithm and constants. This will be done by verifying that the new model increases the accuracy from the previous baseline for multiple products.

### *3.2.3.1 Verification Standard*

The MODIS accuracy testing involves two types of related measurements, absolute and relative. The former measures how well the MODIS instrument matches a location on the Earth. The latter measures how well multiple images from the same area on the ground match one another. If two images have an absolute accuracy of 100 m, then the relative accuracy of the images is better than 200 m and would be around 141 m if the errors are uncorrelated and normally distributed. A measurement of relative accuracy does not necessarily give any information about the absolute accuracy; two scenes that are well registered to one another could be off by a large amount in an absolute sense.

The absolute error is very important in using MODIS data with other data sets, such as maps and other satellite data. The standard by which the absolute accuracy is based is the World Geodetic System of 1984 (WGS84), an international standard model of the Earth. This standard is based on a number of physical constants, including the origin and orientation of an Earth centered and fixed Cartesian coordinate system, a standard ellipsoid model of the Earth, and a definition of mean sea level. Many countries are now basing their new maps on this standard and there are standard transformations from most older maps to this standard.

The relative measurement is very important in determining what changes occur between images. Since the mission is to look at global change, measuring season-to-season and year-to-year variations are very important. There is no standard for the relative accuracy measurements. It is expected that by achieving the absolute accuracy goal, the relative accuracy requirements will be met.

### *3.2.3.2 Preflight Verification*

The MODIS algorithms will be verified preflight by prototyping key Earth location subsystems to develop and refine geometric models, and data processing and analysis techniques using both preflight data and data from other instruments such as AVHRR.

The verification that the software matches the theoretical algorithm will be performed by software walk through and unit testing of individual parts of the algorithm. Separate hand calculations will be performed to verify that the unit testing is correct. The second step is to verify the instrument part of the model. This will be done by verifying that the results from the instrument model match those from live data from the engineering model. The third step will be done both preflight and in-flight. The preflight part will be done using satellite data from other instruments such as AVHRR. Parts of the software model, which are common to both MODIS and AVHRR, will be tested by verifying the Earth location of the AVHRR data. This will not be a complete test of the software

primarily because of the poor quality and lack of ancillary data, the orbit, and attitude data. In addition, simulated MODIS data will be available to test the algorithm preflight.

### 3.2.3.3 In-flight Verification

The in-flight accuracy of the MODIS Earth location data will be verified using automated control point correlation methods coupled with off-line analysis. Control point measurement will be built into the MODIS Level 1A production system but, operationally, will only be applied to a subset of the Level 1A products based on control availability and cloud cover. This product verification activity is described in more detail below.

The schedule for in-flight Earth location/geometric verification activities is less well defined than the preflight phase. The planned activities are divided into Short-Term (conducted in the first three months after activation), Medium-Term (conducted in the first year of operation), and Long-Term (ongoing sustaining activities) in Table 3-13.

**Table 3-13. In-flight Algorithm Verification Activities**

<b>Time Frame</b>	<b>Activity</b>
Short-Term (first three months)	Verify Earth location algorithm performance as soon as operational data becomes available.  Look for constant bias terms in control point QA results to assess accuracy of instrument alignment knowledge.
Medium-Term (first year)	Estimate refinements to instrument alignment knowledge using control point QA data.  Analyze ancillary digital terrain data accuracy using orbit-to-orbit tie points.  Analyze control point QA results to characterize repeatable errors correlated with scan angle and/or mirror side.  Use control point QA results to detect repeatable within-orbit trends such as thermal effects.  Use data from multiple instruments to estimate spacecraft position and attitude accuracy performance.
Long-Term (sustaining activities)	Analyze control point QA data for trends to monitor stability of instrument geometric parameters.  Refine geometric models for mirror and thermal effects as appropriate based on longer data record.

The performance of the automatic correlation procedure will be verified through interactive control point mensuration. The performance of interactive control point mensuration method is expected to be less accurate than the automatic procedure but will be used to provide a double check of the algorithm. The image internal geometric accuracy will be verified by correlating multiple MODIS products from the same orbital path. This will include looking for even/odd scan artifacts due to differences in the two

scan mirror sides. The control chips and neighborhoods will be used to verify the performance of the control point mensuration procedure itself, while the measured distortions will be used in anomaly detection, trend analysis, and to build up a statistical record of Earth location performance.

#### *3.2.3.4 Verification of Inputs*

The verification of the inputs to the MODIS Earth location process must be performed to enable the overall process to be verified. It is expected that the inputs to the MODIS Earth location algorithms will have systematic biases in them. As part of the verification process, these inputs will be verified and biases removed. These inputs include information about the geometric characterization and calibration of the instrument and spacecraft, information about the spacecraft position, velocity, attitude, mirror encoder data, ground control points, and the DEM. For the computational saving, the geolocation calculation is performed only for the ideal band. All real bands' locations on the ground are derived from the ideal band location as described in section 3.1.4.3. Because of this, the control point residual calculation relies on the approximated values. The approach will create some systematic or random error for the ground control point residual error calculation.

#### **Instrument and Spacecraft Data Verification**

The geometric characterization and calibration of instrument, spacecraft, and ancillary data are integral to the verification process. Geometric calibration activities that are being performed by the instrument and spacecraft contractors will be carried out in accordance with their contract schedules. Specifically, the preflight MODIS instrument geometric calibration will be performed by the SBRC according to their calibration plan. The MODIS Characterization Support Team (MCST) is responsible for the oversight of these measurements. Of particular interest to the Earth location model are the absolute orientation, mirror positioning, MTF, and band-to-band registration tests. Preflight measurements of the instrument-to-spacecraft alignment will presumably be carried out during the instrument/spacecraft integration phase per the EOS-AM1 development schedule. The accuracy error analysis work performed by the MODIS SDST is documented in the Earth location error report referred to previously. The second version of this document is currently available and will be updated and ultimately released as a National Aeronautics and Space Administration (NASA) Technical Memorandum.

In-flight measurements of the SRCA calibration data will be used to estimate refinements to the preflight focal plane alignment and the relative band/detector locations will be performed by MCST. This would be done by using the SRCA reticule patterns, or well defined image features that appear in multiple bands, to measure the sub-pixel mis-registration of bands from the same and different focal planes.

The verification of the spacecraft pointing knowledge and position information will be performed by the spacecraft builder Lockheed Martin and NASA. The science and

telemetry data from the instrument and the telemetry data from the spacecraft, up to the point where it is input into the Earth location model, must also be verified.

Refinements to the knowledge of the alignment between the various parts of the instrument, and the instrument to the spacecraft, will be done as part of the geometric parameter estimation process.

The input data stream to be used for geolocation of MODIS products will be read from the MODIS engineering packets and validated, which includes the spacecraft orbit position and velocity, attitude angles and rates, and the mirror encoder times. The scan start times and mirror side indicators, which are also required for geolocation, will be unpacked and converted by the Level 1A unpacking software. It is assumed that any validation required for those data has been performed prior to geolocation. The validation tests to be performed fall into four basic categories: absolute limits, delta limits, consistency, and sanity.

1. The absolute limit test checks individual measurements against a specified range. For a value  $V$  and lower and upper limits  $L$  and  $U$ , the test requires that

$$L \leq V \leq U$$

2. The delta limit test checks the differences between successive values of an individual measurement against a specified range. For a delta limit  $\delta$ , the test requires that

$$|V_{j+1} - V_j| \leq \delta \quad \text{for } j\text{-th and } j+1 \text{ th sample of } V.$$

3. Consistency tests compare different measurements within a general category to verify consistency among the measurements.
4. Sanity tests involve computing additional quantities from the measurements, which can be checked against absolute limits such as magnitude of position and velocity vectors. These are performed to take advantage of our knowledge of the mission limits or the physical processes involved.

The application of the four approaches for orbit, attitude, and mirror encoder data is described in Appendix C.

### **Ground Control Verification**

There are two methods for verifying the accuracy of the ground control point information. The first method is to internally verify the control using information from either MODIS or other satellites. The second is to use some other type of verification such as an accurate map base or points from the Global Positioning System (GPS). In either case, there will be some prior knowledge of the accuracy of the control point information based on the source.

To use satellite data for validating the control points, it will be assumed that the error in the position of the satellite is random and that the pointing knowledge errors do not systematically vary over any single location. If both these assumptions were true, it would be easy to take the large number of measurements of the points and then improve the knowledge of the control points using this information. However, only the first is true. The pointing knowledge errors are expected to have some systematically varying component, which we plan to remove as part of the geometric parameter estimation. If only the EOS-AM satellite or satellites with similar orbit characteristics are used, the same type of bias may occur in all of the measurements. This would prevent the separation of the ground control bias from the systematically varying component of the pointing knowledge. So, it is not possible to use only the satellite data to validate the ground control points.

One problem in verifying the absolute accuracy of the MODIS instrument is with the original maps and other sources which to be used in collecting control point information. In some well mapped areas of the world such as the United States of America (USA), it is easy to acquire highly accurate maps. In the continental USA, Canada, Europe, and some other areas, typical maps have a low enough vertical and horizontal error to be used as sources for absolute control point location information. The rest of the world is not as well mapped. In some areas the only maps available are 1:250,000, or even 1:1,000,000 scale maps. The accuracy of these maps is typically from 125 to 450 m horizontally and 50 to 200 m vertically. In areas of the world where there exist inaccurate maps, the locations of the ground control points could have a significant uncertainty in the measurement process.

Using an accurate map base or GPS has some appeal but there are also problems with this approach. First, the availability of accurate maps throughout the world is limited and the collection of GPS verified control points is likely to be expensive. Even once the ground control has been identified there is still the problem of transferring this knowledge to the image. Typically, a control point can only be identified in an image to the nearest 1/2 pixel by an operator. This should not be much of a problem with MODIS because the control points are being identified in higher resolution images.

The correlation process may introduce a systematic bias into the process since it relies on correlation of an area and not the location of a single point. One bias may be caused by a change in elevation over the correlation area; the second may be caused by temporal changes in the scene or in the viewing geometry of the scene. In the case of errors introduced by elevation, correlation techniques rely on locking up on unique strong features in the correlation area. In the case when there is only a single strong feature at the center of the correlation area, this is not a problem. Many times, however, there are a number of less strong features in the area, which, if they are at a different elevation than the main feature, may cause the correlation process to be biased. To minimize this type of effect, efforts will be made to pick control points in areas that are relatively flat, or to orthorectify the control points before use. Then the MODIS viewing geometry will be simulated as described in section 3.3.1.

Temporal changes and changes in the viewing geometry may cause other biases. Both may cause the correlation to fail completely. If a correlation is successful, there is a possibility that a systematic bias may be introduced by changes in the scene. For instance, if the correlation is occurring on a large lake in which the shallow end is partially covered by ice in the winter, the correlation of this area would tend to be biased toward the deep end of the lake. A different viewing geometry may also cause a similar bias. Suppose the image is of a volcanic island and the original image of the ground control point is taken when the shadows are to the left of the mountain. If, when the point is later imaged, the viewing conditions are such that the shadow has moved to the right side of the mountain, there is a good possibility the correlation will be biased.

One solution that has been used in the past to alleviate this problem with correlation has been to use a large number of control points. If many control points of different types are used then this error can be treated as a random error. In any case, statistics should be kept for each control point. Moreover, care should be taken to use the good control points in the geometric parameter estimation, and to include the control point correlation statistics in the solution as well as any measured mean shift in the location.

### **Digital Elevation Model Verification**

The terrain correction accuracy will be verified and areas of poor DEM data will be identified by measuring tie points between overlapping MODIS products. The DEM will be verified in two ways. First, the provider of the DEM will perform quality checks to verify its accuracy. It is expected that the DEM provided will have, at worst, a 1 km resolution with 100 m uncertainty in vertical direction. Second, image data from MODIS, and possibly other instruments/satellites (such as MISR), will be used to provide some additional verification.

Once the images have been correctly navigated, the image data will be rectified and then areas from overlapping orbits will be correlated. The tie points would be generated automatically, possibly using an interest operator to generate "good" tie points. Once this is done a sufficient number of times, there may be certain areas of the world where there is a systematic bias between every image pair. It is expected that biases covering large areas may be found using this method but the vertical accuracy when correlating the 250 m bands is expected to be, at best, 125 m (1 sigma) and the horizontal spacing between 500 m and 750 m. Particular care should be taken to do this type of correlation only after sufficient systematic biases have been removed from the pointing knowledge. Lack of sufficient high frequency information in the DEM will cause residual high frequency errors in the MODIS Earth location knowledge. It will not be possible to remove these errors until a higher resolution DEM becomes available.

#### ***3.2.4 Product Validation***

The validation process will examine the end result of the process (the Earth location product) and not the mechanism for producing the product. This process will be done independently of the verification process. A number of products will be selected and measurements will be performed independently of the production software. This

process will not necessarily be a global process but sufficient number of measurements will be made so that there is a high level of confidence in product accuracy for the entire globe. This validation process will be done with some regularity, either biannually or annually, and after any significant modifications to the production software or constants occur. Both the absolute and relative accuracy of the products will be validated.

The validation measurement tools will be developed independently of the production tools. Ground control information will also be independently collected for measurements of absolute accuracy. Of course, the same source material, maps, etc., may be used for ground control information.

### **3.2.5 Quality Control and Diagnostics**

The MODIS Earth location procedure will accumulate performance indicators during the normal course of processing for inclusion in the Level 1A product metadata as quality control information. Numeric performance indicators include the number of suspect ephemeris points replaced and the number of suspect attitude points replaced. Other quality control fields include quality information taken from the ancillary input data sets such as the DEM and possibly the ephemeris and attitude data if it came from a source other than the Level 0 data itself.

These quality control fields will be included in the Level 1A product metadata along with other descriptive data such as a record of the ancillary data lineage (e.g., data set version number and date, preprocessing history).

### **3.2.6 Exception Handling**

The Earth location algorithm will provide mechanisms for gracefully handling the following three known exception conditions:

1. There are missing ephemeris or attitude data,
2. There are missing DEM data, and
3. The instrument line of sight does not intersect the Earth (e.g., during a lunar view).

The input ephemeris and attitude data will be checked for consistency and completeness by the Level 1A processing software. These checks will be first order only and will primarily remove blunders. For example, the magnitude of the position and velocity must be close to the nominal values and the instrument must be pointing downward, etc. If these ancillary data are completely missing or unusable, an error message will be generated and Earth location data will be filled by interpolation (using PGS Toolkit routines, if provided) with appropriate quality control information entered into the product metadata. In the case of missing input DEM data, the Earth location will proceed using the Earth ellipsoid as the reference terrain surface. A warning message will be generated and an appropriate notation added to the product metadata. If the line of sight intersection algorithm detects a viewing vector that does not intersect the Earth ellipsoid, the geodetic position fields will be populated with fill values, a

warning message will be generated, and a notation will be added to the product metadata.

### **3.3 Error Analysis Algorithms**

After the Level 1B production is done for a granule, the error analysis begins. Initially only for those 250 m and 500 m resolution MODIS bands will be used in conjunction with sets of ground control points to validate the accuracy of the MODIS Earth location data. Ground control points will be used to estimate residual errors in the spacecraft ephemeris and attitude. Small geolocation errors are mainly caused by errors in these parameters. Other parameter errors are difficult to analyze. However, through long term trend analysis, we are hoping to expand error analysis to the focal plane, telescope geometry, and mirror assembly geometry. The ground control matching algorithm is divided into a land part and an island part. In the following sections, the land control point matching algorithm is first explained and then the island. The trend and bias analysis follows.

#### ***3.3.1 Land Control Point Matching and Correlation Algorithm***

The Control Point Matching software will use the control points to automatically collect the raw verification data (in the form of ground control point residual errors). This data will then be analyzed off-line at the MODIS Team Leader Science Computing Facility (TLCF).

#### **General Background and Preprocessing**

The 250 m resolution MODIS bands will be used in conjunction with preassembled sets of ground control points to validate the accuracy of the MODIS Earth location data. The known position of the control point can be used to extract an image neighborhood from the new MODIS data at the location predicted by the Earth location data. Nominal radiometric calibration parameters will be applied to the MODIS neighborhood to remove radiometric artifacts (detector to detector striping). A simple cloud detection algorithm (e.g. thresholding) will also be used to identify areas that are not suitable for image correlation. This product validation will be scheduled after the Level 1B radiometric correction and cloud detection algorithm have been performed so that the simple radiometric correction, snow, sea ice and cloud detection algorithm would be skipped. In either case, the control point image chip can then be correlated with the MODIS neighborhood to measure the sub-pixel displacement between its predicted and observed locations. The control data image chips will be processed to simulate the effects of the MODIS viewing geometry including the elevation-related parallax and correlated with the real 250 m resolution image data. This will include applying the MODIS modulation transfer function (MTF) to the higher resolution control chips. The extracted MODIS data will be shifted along the image lines and pixel counts over the control point chip. At each fraction of shift in the positive or negative direction, the MTF is applied over this higher resolution control point chip and matched with the MODIS resolution. The measured image displacement on shift or error angles, along with the

extracted MODIS neighborhoods, will then be passed to the MODIS TLCF for off-line analysis.

**Table of Contents**  
**(ATBD -4)**

3.3.2 Island Control Point Matching Algorithm ..... 3-71

3.3.3 Error Analysis and Parameter Estimation Algorithm ..... 3-76

**4. CONSTRAINTS, LIMITATIONS, ASSUMPTIONS..... 4-1**

**APPENDIX A: ACRONYMS AND ABBREVIATIONS ..... A-1**

**APPENDIX B: ALTERNATIVE APPROACH FOR TERRAIN CORRECTION ..... A-3**

**APPENDIX C: DATA VALIDATION..... A-4**

**APPENDIX D: INVERSE MAPPING ALGORITHM ..... A-6**

Figure 3-26. Three Satellite Locations .....62

Figure 3-27. Connecting Parts of 3 Scans .....63

Figure 3-28. The  $\alpha$ - $\beta$  coordinate system reference planes .....66

Figure 3-29. Thematic Mapper Pixel.....67

Figure 3-30. Triangular Weighting Function.....68

Figure 3-31. Triplet Islands Matching .....75

Figure 3-32. Satellite Position and Ground Control Point .....77

Figure 3-33. Look Vector Angles .....79

Figure 3-34. Cross Track Geometry .....81

Figure 3-35. Along Track Geometry.....83

Figure 3-36. Linear Estimate of dx as a Function of dt Generated from Control Points85

(No tables in ATBD4)



## **Control Point Image Chips and Control Scenes**

Control point image chips will consist of arrays containing georectified and terrain corrected Landsat Thematic Mapper (TM) pixel radiances. In the U.S. the 30 m spatial resolution of DEM will be used for the TM images while 100 m spatial resolution will be expected outside the U.S. Associated with each TM pixel will be a geolocation (latitude, longitude, and terrain height), resampled in the UTM (Universal Transverse Mercator) coordinate system. Associated with each control point chip as a whole will be the location of the key feature, control point, expressed as a latitude and longitude and as row and column (possibly fractional) in the array of pixels.

A MODIS control scene, in terms of MODIS 250 m resolution pixels, consists of an array of  $P$  rows by  $Q$  columns, where  $16 \leq P \leq 64$  and  $16 \leq Q \leq 64$ . The scene is a sub-image of a MODIS scene and may contain pixels from more than one scan. It is taken around a predicted control point location corresponding to a given TM chip. The values of  $P$  and  $Q$  will be decided based on experience. It is planned to set  $P$  and  $Q$  to the same value.

In Thematic Mapper pixels, the dimensions of a control point chip will be at least  $12P$  by  $14Q$  TM pixels ( $192 \leq 12P \leq 768$  and  $224 \leq 14Q \leq 896$ ). If a TM pixel is 28.5 m resolution, it requires more than 8 of them along each dimension to make up a 250 m resolution MODIS pixel. In addition, at scan angles up to 30 degrees, the MODIS pixels are enlarged nearly 25 percent vertically and nearly 50 percent horizontally, raising the required number of TM pixels by those percentages.

The term feature will be used here to mean a single, identifiable, geographical point on the earth's surface, specified by exactly one set of coordinates: latitude, longitude, and elevation. Ideally, the latitude, longitude, and elevation values point to a stable geographical feature that is detectable in MODIS data. Each land control point chip will have exactly one key feature. Features that are close together may be used but they will be put into separate, possibly overlapping, control point chips.

## **General Strategy of Control Point Matching Algorithm**

The control point matching algorithm strategy used here is to fix a position of the spacecraft in space where the MODIS sensor scans through the ground from west to east (in case of descending path) within 0.451 seconds (although in reality the spacecraft is moving 6.755 km/s on the ground). A control point chip is viewed from that fixed point in space and coordinates of each pixel are expressed in terms of two angles. This will enable us to build a MODIS control scene and a new set of TM chips with MODIS resolution (250 m).

The relationships between the trace of a scan, projected ground locations of the satellite at the start, middle, and end scans (points 1, 2, 3) are illustrated in Figure 3-26 where all the locations are based on the ideal condition and no attitude errors are assumed. The inclination of the scan on the ground to the ground track is due to the rotation of the focal plane around the telescope optical axis (see Figure 3-9 for more details).



- (2) There are enough line segments to complete a P-by-Q control scene.
- (3) All the scan angles are within a given threshold.

Step 3. Extract line segments Q pixels long from the current scan containing its neighborhood,

Step 4. Extract an extra line segments from the above (and or below) the scan by the following procedure (see Figure 3-27 for notations):

- (1) Check coordinates of a pixel in the last line(northern most) along the 'feature pixel' (Pixel A),
- (2) Find a pixel in the first line of the previous scan which is closest to the pixel A (Pixel A'),
- (3) Extract additional line segments from the above scan aligning these two pixels together and fill the control scene,
- (4) Do a similar procedure from the next scan and complete a P-by-Q control scene.

Figure 3-27 shows schematically how a control scene would typically be created using three scans.

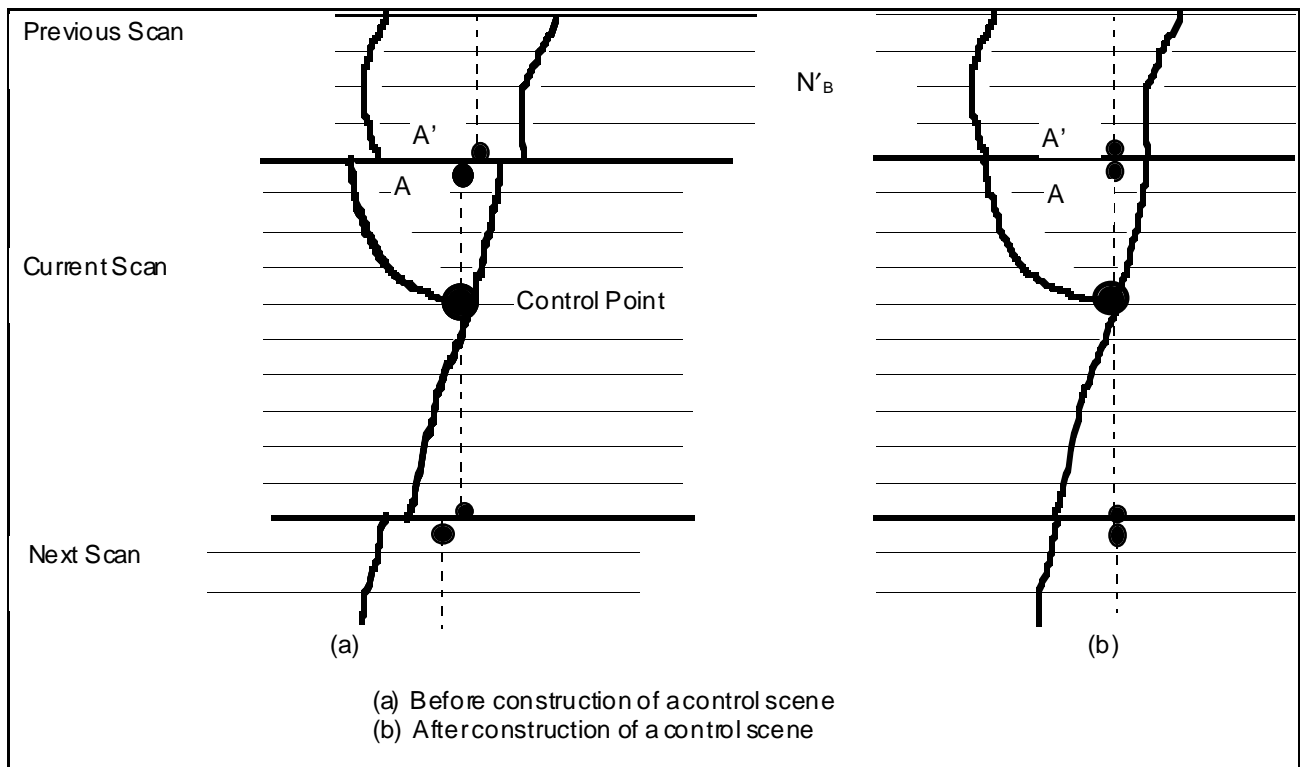


**Figure 3-27. Connecting Parts of 3 Scans**

The number of pixels is  $Q$  and line segment starting  $q_s$  and  $q_e$  given by:

$$q_s = q_0 - Q/2 + 1, \quad q_e = q_0 + Q/2 \quad (2)$$

These three numbers  $q_0$ ,  $q_s$ , and  $q_e$  may not be the same for the scan above or below.

Using extra line segments from the above ( $N'_B$  lines), pixel/line numbers are adjusted for  $p_0$ ,  $q_0$ ,  $p_H$  to obtain  $p'_0$ ,  $q'_0$ ,  $p'_H$  by:

$$p'_0 = p_0 + N'_B \quad q'_0 = q_0 - q_s + 1 \quad p'_H = p_H + N_B \quad (3)$$

$$\text{and} \quad 1 \leq p'_0, \quad p'_H \leq P \quad 1 \leq q'_0 \leq Q$$

The following section shows how a control scene and a TM control chip are viewed from a fixed point in space. At first some notations and geometry are defined.

### Points, Vectors and Planes

Let

$\mathbf{p} = (p_x, p_y, p_z)$  = position vector of the MODIS sensor in ECR (determined by interpolation between MODIS position at center of feature scan and position at center of previous or next scan)

$$TM_{ij} = (TM_{ij,x}, TM_{ij,y}, TM_{ij,z})$$

= position of the Thematic Mapper pixel in ECR at i-th row and j-th column of the control point chip which covers the MODIS control scene.

Along the column of pixels of the feature pixel, define:

$\mathbf{x}_1$  = Location of the first pixel in the column,  
( $x_{1,x}, x_{1,y}, x_{1,z}$ )

$\mathbf{x}_N$  = Location of the last pixel in the column  
( $x_{N,x}, x_{N,y}, x_{N,z}$ )

$\mathbf{x}_H$  = Location of the middle pixel in the column  
( $x_{H,x}, x_{H,y}, x_{H,z}$ )

Along the MODIS line segment, define:

$\mathbf{x}'_H$  = Location of the middle pixel in the first column of the control scene along scan line passing through  $\mathbf{x}_H$   
 $(x'_{H,x}, x'_{H,y}, x'_{H,z})$

$\mathbf{x}''_H$  = Location of the middle pixel in the last column of the control scene along the scan line passing through  $\mathbf{x}_H$   
 $(x''_{H,x}, x''_{H,y}, x''_{H,z})$

Let

$$\mathbf{u}_1 = \mathbf{x}_1 - \mathbf{p} \quad \mathbf{u}_N = \mathbf{x}_N - \mathbf{p} \quad \mathbf{u}_H = \mathbf{x}_H - \mathbf{p}.$$

Define a plane called 'β-plane', spanned by vectors  $\mathbf{u}_H$  and whichever of  $\mathbf{u}'_H$ ,  $\mathbf{u}''_H$  is closer to the center of the scan. The plane called 'α-plane' is defined by  $\mathbf{u}_H$  and  $\mathbf{u}_H \times \mathbf{u}'_H$  (or  $\mathbf{u}_H \times \mathbf{u}''_H$ ).

Figure 3-28 shows points, vectors, and planes used to define the MODIS sensor's view coordinate system using one row of pixels in a scan.

### α-β Coordinate System for a TM Chip

We generate simulated MODIS scenes around the feature pixel by mapping TM pixels (from the TM chip which covers the MODIS control scene) into the MODIS scan's reference frame, as determined by  $\mathbf{p}$ ,  $\mathbf{u}_H$ , and  $\mathbf{u}'_H$  or  $\mathbf{u}''_H$ . In order to assign coordinates for each TM pixel, the above two reference planes are used to calculate two angles,  $\alpha$  and  $\beta$ , that uniquely identify the direction in which the MODIS sensor views that pixel. Angle  $\alpha$  is measured in the along scan direction. Angle  $\beta$  is measured in the (approximately) along track direction. (The actual along track direction is at a slight angle to the  $\beta$  direction; the  $\beta$  direction may be thought of as the axis of rotation of the scan mirror.)

The algorithm for computing angles  $\alpha$  and  $\beta$  is described below. How angles  $\alpha$  and  $\beta$  are computed in mapping a Thematic Mapper pixel,  $TM_{ij}$ , into a simulated MODIS scene is illustrated in Figure 3-29.

(In this discussion, unit vectors will be represented as  $\hat{\mathbf{u}}$ . For example,  $\hat{\mathbf{n}} = \frac{\mathbf{n}}{\|\mathbf{n}\|}$ .)

Let  $\mathbf{u}_T$  be the vector from  $\mathbf{p}$  to  $TM_{ij}$ , i.e.,  $\mathbf{u}_T = (p_x - TM_{ij,x}, p_y - TM_{ij,y}, p_z - TM_{ij,z})$ .

Let  $\mathbf{n} = \mathbf{u}_H \times \mathbf{u}'_H$ . (If  $\mathbf{u}''_H$  is closer to the center of the scan than  $\mathbf{u}'_H$  is, then let  $\mathbf{n} = \mathbf{u}''_H \times \mathbf{u}_H$ .) Vector  $\mathbf{n}$  is perpendicular to both  $\mathbf{u}_H$  and  $\mathbf{u}'_H$  (or to both  $\mathbf{u}''_H$  and  $\mathbf{u}_H$ ).

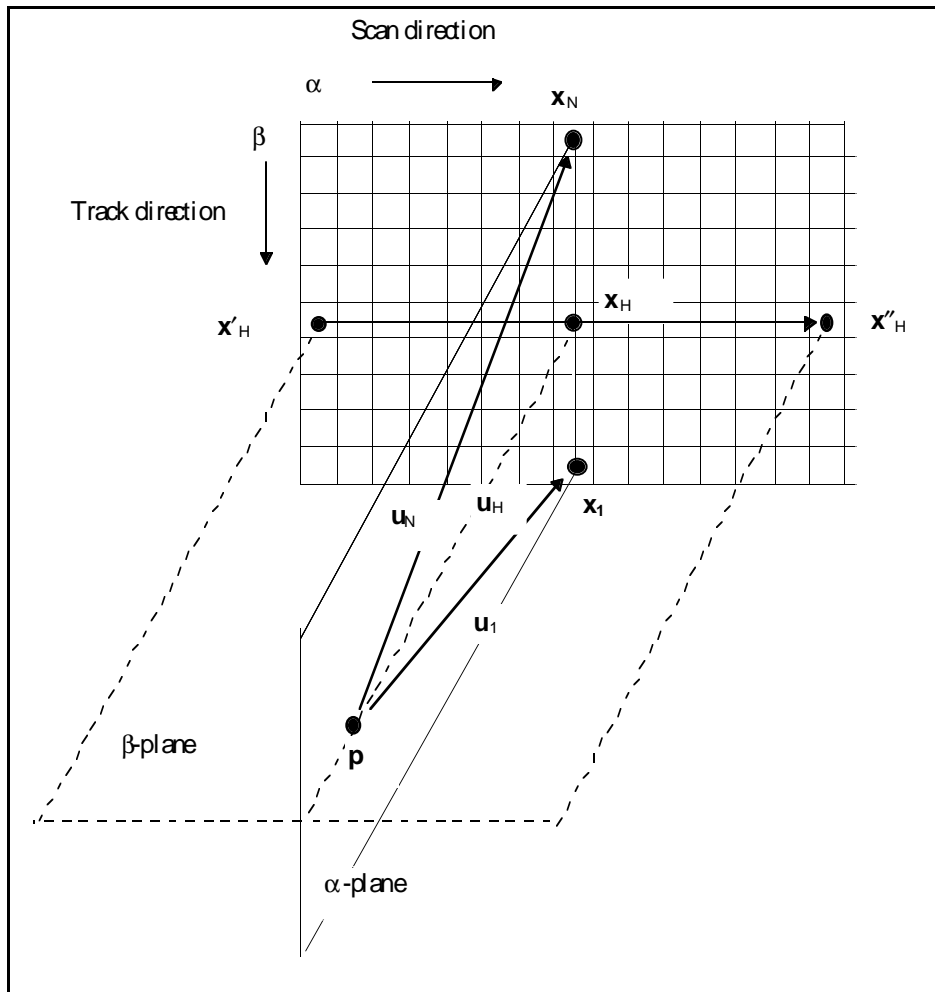


**Figure 3-28. The  $\alpha$ - $\beta$  coordinate system reference planes for one MODIS control scene**  
 (Feature Point in the column between pixels  $x_1$  and  $x_N$ , not shown.)

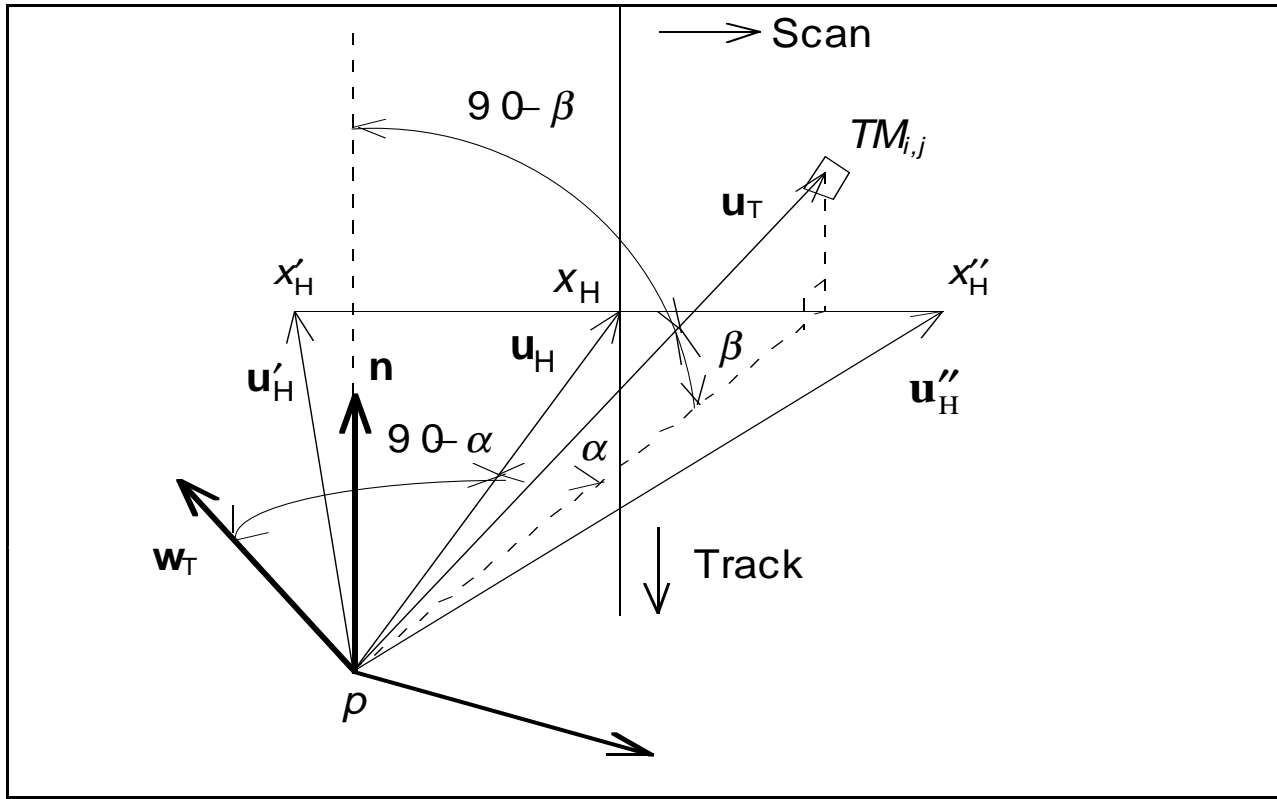


Figure 3-29. Thematic Mapper Pixel

We define the angle between  $\mathbf{n}$  and  $\mathbf{u}_T$  to be  $(90 - \beta)$ . Therefore  $\cos(90 - \beta) = \hat{\mathbf{n}} \cdot \hat{\mathbf{u}}_T$ . It follows that  $\sin \beta = \hat{\mathbf{n}} \cdot \hat{\mathbf{u}}_T$ , and finally,

$$\beta = \sin^{-1}(\hat{\mathbf{n}} \cdot \hat{\mathbf{u}}_T) \tag{4}$$

Next, let  $\mathbf{w}_T = \mathbf{n} \times \mathbf{u}_T$ . Vector  $\mathbf{w}_T$  is perpendicular to both  $\mathbf{n}$  and  $\mathbf{u}_T$ . We define the angle between  $\mathbf{w}_T$  and  $\mathbf{u}_H$  to be  $(90 - \alpha)$ . Therefore  $\cos(90 - \alpha) = \hat{\mathbf{w}}_T \cdot \hat{\mathbf{u}}_H$ . It follows that  $\sin \alpha = \hat{\mathbf{w}}_T \cdot \hat{\mathbf{u}}_H$ , and finally,

$$\alpha = \sin^{-1}(\hat{\mathbf{w}}_T \cdot \hat{\mathbf{u}}_H) \tag{5}$$

Note that values  $\alpha$  and  $\beta$  can be negative. If  $\alpha$  is negative, the pixel is in the west of the scene. If  $\beta$  is negative, the pixel is in the south of the scene.

To complete the scene in MODIS space,  $\alpha$  and  $\beta$  coordinates, expressed in radians, will be converted to MODIS pixel coordinates. First, the sign is changed on all of the  $\beta$

angles so that the origin of the scene will be in the upper left following the image processing conventions. Next, each angle is multiplied by a (constant) scaling factor,  $1/(0.354462 \text{ milliradians per pixel})$ , to convert from radians to pixels. Then a constant number of pixels is added, to translate the origin to the upper left corner of the scene.

### **Simulated MODIS Scenes with MODIS Pixel Resolution**

This section explains how a MODIS band 1 size pixel (250 m, 0.354462 mr) is generated from TM pixels.

When a MODIS detector in motion views TM pixels on the ground, the TM pixel radiances must be summed and put through the triangular weighting function to generate expected MODIS pixels. All of the TM pixels within a 2-MODIS-pixel wide rectangle are weighted and added together to get the MODIS pixel value, as shown in Figure 3-30, where geometry does not show possible terrain and scan angle effects.

In Figure 3-30, TM pixel locations 1 and 2 are contributing to MODIS pixel I and II, while No 3 and 4 are contributing to MODIS pixel II and III. The triangular weighting function and the two pixel wide set of TM pixels used to generate an expected MODIS pixel in bold outline.

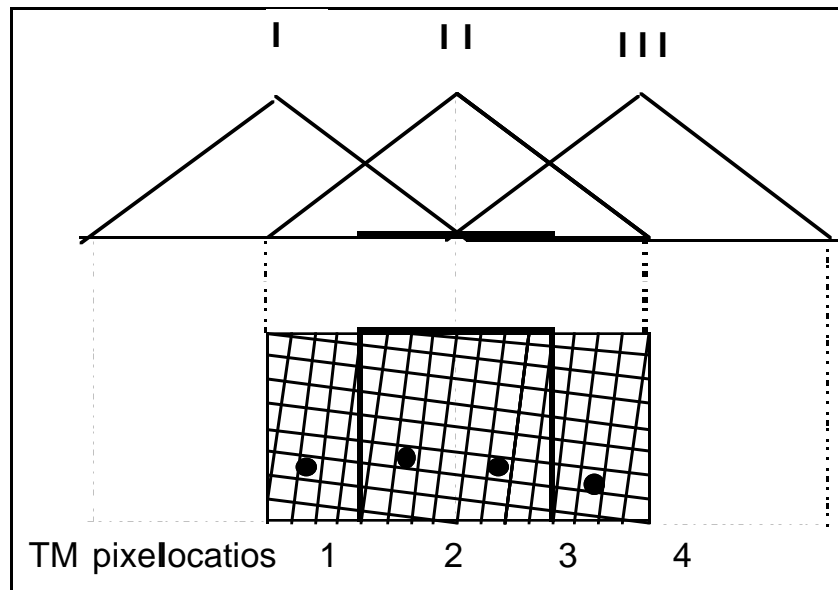


**Figure 3-30. Triangular Weighting Function**

To prepare for the correlation of TM and MODIS chips, multiple simulated MODIS scenes are generated with indices  $m, n$ , and notation  $T_{mn}$ , where:

$$m = -M, -(M-1), \dots, -1, 0, 1, 2, \dots, (M-1), M,$$

$$n = -N, -(N-1), \dots, -1, 0, 1, 2, \dots, (N-1), N$$

$$T_{mn} = \text{new TM chip radiances with indices } (m,n)$$

for some positive integers of  $M$  and  $N$ .

For each  $TM_{ij}$ , let  $r_\alpha$  be the fractional MODIS pixel number corresponding to angle  $\alpha_T$  that was computed by (5) and  $r_\beta$  be the fractional MODIS line number corresponding to angle  $\beta_T$  that was computed by (4).

Define

$$r_{\alpha,m} = r_\alpha + m\delta \quad \text{and} \quad r_{\beta,n} = r_\beta + n\delta$$

where:

$$\delta = \text{fractional increment in MODIS pixel count.}$$

Find two MODIS pixels  $(p,q)$ -th and  $(p, q+1)$ -th which view this TM pixel and add radiance to these two pixels for  $(m,n)$ -th scene by the following steps:

Step 1. Define

$$p = [p'_H + r_{\beta,n}] \quad \text{and} \quad q = [q'_0 + r_{\alpha,m}],$$

where  $p'_H$  and  $q'_0$  are defined by (3). The brackets are used to truncate the number to the next lowest integer.

Define

$$d_L = q'_0 + r_{\alpha,m} - q \quad \text{and} \quad d_R = q + 1 - (q'_0 + r_{\alpha,m}) \quad (11)$$

and define two weights by:

$$W_L = 1 - d_L \quad \text{and} \quad W_R = 1 - d_R \quad (12)$$

Note that  $d_L + d_R = 1$ , which is the MODIS pixel width.

Step 2. Add  $TM_{ij}$  radiance to all  $T_{mn}$  with triangular weights at MODIS pixel/line location  $(p,q)$  and  $(p,q+1)$  by:

$$T_{mn}(p,q) = T_{mn}(p,q) + Rad(TM_{ij})W_L \quad (13)$$

$$T_{mn}(p,q+1) = T_{mn}(p,q+1) + Rad(TM_{ij})W_R \quad (14)$$

Note that for TM pixels at location 1 and 2 in Figure 3-30,  $q$  corresponds to MODIS pixel I, while for pixels at 3 and 4,  $q$  corresponds to the MODIS pixel II.

For each expected MODIS pixel, a count of TM pixels is also maintained. After all the TM pixels are processed, each expected MODIS pixel's total TM radiance is divided by its TM pixel count to get its expected radiance level.

### **Correlation of Simulated MODIS Scenes and Actual MODIS Control Scene**

Let the actual MODIS radiance of the  $P \times Q$  array in the control scene be denoted  $M$ . Let  $S$  be the array of normalized radiances (i.e.,  $S(u,v) = M(u,v) - \bar{M}$  where  $\bar{M}$  is the mean value of array  $M$ ). Similarly, let  $T_{m,n}$  be a simulated MODIS scene, with shift parameters  $m$  and  $n$  and pixel radiances normalized to have a mean of zero. Using the array  $S$  and the arrays of simulated MODIS pixels  $T_{m,n}$  that have been constructed by the above algorithm for row and column pixel shift values  $m$  and  $n$ , the cross correlations will be performed using the normalized cross correlation function below. [See Reference 17 at page 683, equation 20.4-1.]

$$R(m,n) = \frac{\sum_u \sum_v S(u,v) T_{m,n}(u,v)}{\left[ \sum_u \sum_v [S(u,v)]^2 \right]^{1/2} \left[ \sum_u \sum_v [T_{m,n}(u,v)]^2 \right]^{1/2}} \quad (15)$$

for  $m = -M, \dots, -2, -1, 0, 1, 2, \dots, M$  and  $n = -N, \dots, -2, -1, 0, 1, 2, \dots, N$ .

In a shift pattern of ten steps of 1/10th of a pixel each ( $M = 5$  and  $N = 5$ ) and there are  $11 \times 11 = 121$  cross correlations to be performed. In the Version 2 system, all cross correlations will be computed. Methods for safely reducing this amount of computation may be explored after some experience with actual MODIS data.

After all of the  $T_{m,n}$  expected MODIS pixel arrays are constructed and all the cross correlations  $R(m,n)$  are computed, the  $m$  and  $n$  offsets that produce the maximum cross correlation are determined.

Let  $(m,n)$  be such best correlated indices and  $(\hat{p}, \hat{q})$  be the predicted location of the control point in the MODIS control scene. Then the actual location can be expressed by

$$(\hat{p} + m\delta, \hat{q} + n\delta).$$

From this information, the following values can be generated:

- (1) Actual location of the control point in the MODIS scene in terms of fractional line/pixel numbers.
- (2) Sensor view vector.

- (3) Systematically computed geodetic coordinates of the control point.
- (4) Residuals error for residual data base, along with the MODIS control scene.

### **Error Conditions**

The following conditions are regarded as errors:

- If the maximum cross correlation occurs at the edge of the shift region, then that set of geolocation residual error values should be flagged as suspect and as out of range.
- It is likely that either the cross correlations failed to detect the correct location of the feature in the image. or that the image correction needed is larger than what the algorithm is capable of measuring (e.g., larger than one MODIS 250 meter pixel).
- If a maximum cross correlation value occurs in two adjacent elements of R, then the residuals could be recorded as the average of the two corresponding values.
- If the maximum cross correlation value occurs in more than two (or more than one, TBD) element of the cross correlation matrix R, then no residuals will be recorded for that control scene.

### **Possible Enhancements to the Method**

- Adjustments To Radiance Values:
  - The TM radiance may be adjusted and corrected in several ways. They could be adjusted depending on scan angle, sun elevation and azimuth, etc.
  - Seasonal TM image chips could be used or seasonal adjustments made.
  - Geometrically, TM pixels that cross MODIS pixel boundaries could be proportionally allocated to the respective MODIS pixels.
  - Both TM and MODIS images can be enhanced using various techniques and compared.

#### ***3.3.2 Island Control Point Matching Algorithm***

The MODIS island control point matching algorithm is based on the approach developed for the SeaWiFS mission (see Reference 14 Patt, Gregg & Woodward 1996). The elements of this approach are:

- A classification algorithm is applied to the calibrated radiances in two of the visible bands on a per-pixel basis to determine whether the pixel is land, water, clouds or snow/ice.

- Islands are located within the classified data as contiguous groups of land pixels which are completely surrounded by water.
- Each located island is matched, if possible, with an island control point from a reference catalog and the position difference is computed.

The approach for each of these is described in the following subsections.

### 1. Classification Algorithm

The MODIS classification algorithm follows the same overall approach as developed for SeaWiFS but with one important difference: the classification of pixels as clouds, snow, or ice will have been performed using information from other MODIS products. The MODIS classification can be limited to land/water discrimination for pixels which have not already been excluded.

The algorithm uses calibrated reflectances for two bands at the extremes of the visible range: Band 3 at 469 nm, and Band 1 at 645 nm. The Band 3 resolution is 500m vs. 250m for Band 1 so the Band 1 data will be aggregated to 500m prior to the start of the algorithm. (As of this date the aggregated Band 1 data will be included in the MOD02 500m product and can be read directly by the island control point software.)

The classification is performed separately for each pixel which has not previously been excluded. There are three steps:

- The reflectances are normalized to a solar zenith angle of zero to correct for changes in illumination:

$$\hat{B}_1 = B_1 / \cos(\gamma)$$

$$\hat{B}_3 = B_3 / \cos(\gamma)$$

where  $B_1$  and  $B_3$  are the reflectances in Bands 1 and 3,  $\hat{B}_1$  and  $\hat{B}_3$  are the normalized reflectances in those bands, and  $\gamma$  is the solar zenith angle.

- A weighted difference is computed of the normalized reflectances:

$$B_{31} = \hat{B}_3 - W \cdot \hat{B}_1$$

where  $W$  is a weighting factor to be determined.

- The pixel is classified as land or water based on a threshold  $T_{\text{land}}$ :

if  $B_{31} > T_{\text{land}}$  pixel is land, otherwise pixel is water.

The weighting factor and land threshold will be initially set based on SeaWiFS data and determined post-launch using the MODIS flight data.

## 2. Island location

The island location algorithm involves identifying contiguous sets of land pixels which are completely surrounded by water and which are not contaminated by clouds, ice, or snow. For each island located in the data, the centroid and size are computed and saved for the matching algorithm.

The SeaWiFS approach for locating the islands involves two steps: scanning the pixels line-by-line to locate segments of land pixels bounded by water and determining which segments comprise a contiguous land pixel set. An upper limit is set on the island size (i.e., number of pixels in each direction).

The MODIS implementation of this algorithm is complicated by the bowtie effect. The initial implementation will avoid this problem by processing the data scan-by-scan, i.e., only islands which lie within a single scan will be located. This approach will be revisited in the post-launch era.

The segment comparison algorithm involves using a segment in the table as a starting point for locating a series of contiguous segments, starting with the first segment in the table. The indices for the set of contiguous segments are entered into a table as they are located; they are also flagged in the main segment table to avoid repeated checking.

Computation of centroid and size is as follows:

$$\phi_c = \frac{1}{N} \sum_{i=1}^N \phi_i$$

$$\lambda_c = \frac{1}{N} \sum_{i=1}^N \lambda_i$$

$$\phi_{size} = \text{Max}(\phi) - \text{Min}(\phi)$$

$$\lambda_{size} = \text{Max}(\lambda) - \text{Min}(\lambda)$$

where:  $\phi$  is the set of latitudes for the pixels in the island segments

$\lambda$  is the set of longitudes for the pixels in the island segments

$N$  is the number of pixels for the island

$\phi_c$  is the latitude of the island centroid

$\lambda_c$  is the longitude of the island centroid

$\phi_{size}$  is the extent of the island in latitude

$\lambda_{size}$  is the extent of the island in longitude

In addition, the relative uncertainty in the island location is estimated using the pixel size and the number of pixels:

$$U = S_{pix} / \sqrt{N}$$

where:  $U$  is the relative uncertainty

$S_{pix}$  is the average size of the pixels for the island.

The centroids and sizes for the located islands are saved, along with a time, scan line, and pixel number corresponding to each observation, and passed to the matching algorithm.

### 3. Island Matching

The matching algorithm attempts to match each island located in the data with an island control point from the reference catalog. This section describes first the catalog and then the matching algorithms.

The catalog consists of a set of reference island locations which were derived from World Vector Shoreline (WVS) data. It was generated for the SeaWiFS project and will be used as is for the MODIS island control point matching starting at launch. The information stored for each island is the same as computed for the islands located in the data: centroid location and maximum extent in latitude and longitude.

The SeaWiFS catalog currently contains about 6300 islands, which were selected based on the following criteria:

- Minimum island area of 0.5 square km, to ensure visibility;
- Maximum extent of about 50 km in latitude or longitude, to reduce the effects of along-scan pixel size variations;
- Minimum separation of 3 km (centroid to centroid) from nearest neighbors, to allow for unique identification.

The matching of located islands to control points can be performed using either direct-match (nearest neighbor) or triplet (geometric pattern) algorithms. The choice of algorithm depends on the expected geolocation areas vs. the catalog minimum separation criteria.

If the expected error is less than half of the minimum separation, then direct matching will be the most reliable; for larger errors the triplet algorithm is preferred.

It is known that locations of islands in WVS could have large errors and should be used with a great care.

## **Direct Matching**

The first step for both algorithms is to locate all of the control point candidates from the catalog for each located island using a specified search radius and size matching tolerance (i.e., if the angular separation arc-length between the island and the control point is less than the search radius and the difference in size is less than the size tolerance, the control point is considered a candidate for matching with the island). The search radius is chosen according to the expected geolocation error. Islands with no candidates are removed from further processing. This step can be made more efficient by initially generating a subset of the catalog which includes only the islands which lie within the geographic boundaries of the granule being processed.

In the next step, each island is matched with the candidate with the minimum angular separation (distance) from the island.

## **Triplet Matching**

The triplet algorithm attempts to match islands with candidates by use of geometric pattern matching (see Figure 3-31). Specifically, it compares the pattern represented by a group of three islands (i.e., a spherical triangle) to the corresponding patterns for all combinations of candidates in order to find the best match. This works well if the geolocation errors are nearly constant for a granule; the effect is that all of the island locations are shifted but the patterns remain unaltered. (This algorithm was originally developed by the GSFC Flight Dynamics Facility to match star observations using data from star trackers flown on satellites.)

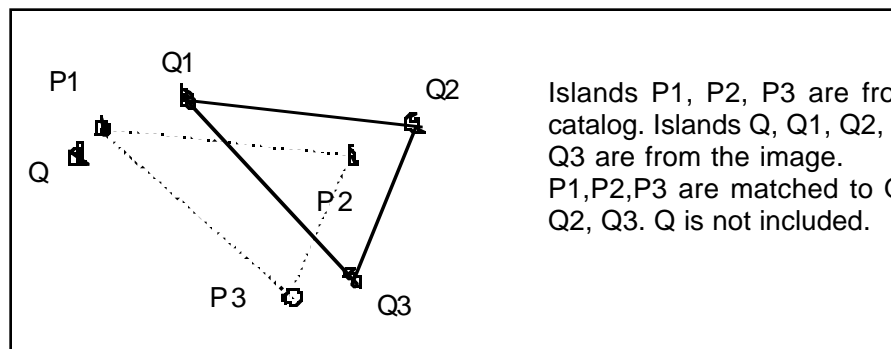


**Figure 3-31. Triplet Islands Matching**

The first step is to sort the table of located islands by the number of candidates (from least to most) and then by the location uncertainty for the island. This is based on the assumption that the probability of a correct match is highest for the islands with the fewest candidates and the most accurate locations. The islands are then processed in groups of three, starting at the top of the list. Each triplet is required to pass a collinearity test to improve the robustness of the algorithm. In this test, the included angle at each corner of the spherical triangle represented by the triplet must be greater than a specified minimum angle or the triplet is rejected. The pattern matching algorithm

involves comparing the angular separation(distance) of each pair of islands in the triplet with all possible combinations of candidates for the islands. If the angular separations agree to within a specified tolerance, then all three islands are matched with the corresponding candidates. Once the best match is found for a triplet, all other candidates are removed for those islands. This process is repeated until all possible combinations of triplets have been attempted. In Figure 3-31 two sets of islands plus one extra island are illustrated. Islands P1, P2, P3 are from the catalog, and Q, Q1, Q2, Q3 are from a MODIS image scene. A triplet P1,P2,P3 is matched with Q1,Q2,Q3. Q is not included in the matching even though it is closer to island P1 than Q1. The shape of triangle Q1, Q2, Q3 matches better to the shape of P1, P2, P3 after comparing distances between Ps and Qs.

When either matching algorithm is completed, the list of matched islands and the corresponding control points are saved to be written to the matchup file.

### ***3.3.3 Error Analysis and Parameter Estimation Algorithm***

The geolocation error comes from various sources including errors in satellite position, velocity, attitude, sensor misalignments, and scan mirror related errors. It may also be possible to have clock drift in the sensor data stream differing from the spacecraft's. Many of the sensor and mirror characteristics and internal temperature will be continuously collected and included in the telemetry. Some changes may appear in the form of such as attitude parameters and could be observed through the evaluation of control point residuals.

In this section, we describe the algorithm to estimate satellite position/velocity and attitude parameters through use of ground control points. It is assumed that some of the sensor misalignments and mirror error will be absorbed in the attitude parameter error.

From the control point matching algorithms, the following values are expected for each control point:

1. Time of control point observation,
2. Satellite position and velocity,
3. Attitude parameters  $\xi_r^0$ ,  $\xi_p^0$ ,  $\xi_y^0$  for roll, pitch, and yaw
4. Fractional scan line and pixel counts and a view vector in the spacecraft coordinate system pointing to the control point,
5. Systematic control point coordinates in the ECR coordinate system,
6. Control point coordinates in the ECR coordinate system,
7. Mirror side information(used in the trend analysis).

It is important to know that the error analysis depends on the accuracy of the control point matching results.

To express a ground control point and view vector, the following notations are used:

- $\mathbf{p}$  - True location of satellite(to be estimated),
- $\mathbf{p}_0$  - Satellite location from the systematic data,
- $\mathbf{x}_0$  - Ground control point location through the systematic data,
- $\mathbf{x}_{cp}$  - True ground control point location.

For their relationship, see Figure 3-32.

In this section, we do not expect any large errors in satellite positions, attitude, or instrument clock time. Even if the control point's location and predicted location is a few pixels off, the control point matching algorithm may not be able to detect and this algorithm cannot use any residual information.

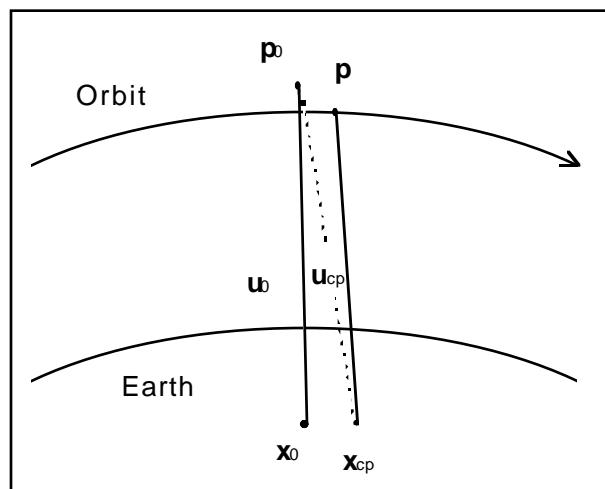


**Figure 3-32. Satellite Position and Ground Control Point**

Errors detected and calculated by the ground control point matching algorithm as described in Section 3.3.1 and 3.3.2 will be used in the error analysis algorithm. Assuming errors are small, we will follow a methodology used by Landsat 7 (see Reference 15) and refine our error estimate for correcting the parameters. In this approach, satellite position/velocity and attitude parameter residuals are estimated through use of the Earth and satellite geometry. The differences in the control point location and systematic point locations are used to construct a normal equation. By solving the normal equation, the error is estimated and the original parameter set is updated to create a new set of parameters. This process continues until it reaches a certain threshold.

The process is described in the following order:

1. Difference of Two View Vectors,
2. Definition of Observation Equations,
3. Building Coefficients for Observation Equations,
4. Further Decomposition of Bias over Time,
5. Best Estimate from a Normal Equation.

The satellite position and ground control point are illustrated in Figure 3-32.

### Construction of Normal Equation

#### • Difference of Two View Vectors

Let:

- $\mathbf{p}_0, \mathbf{v}_0$  - Satellite position/velocity vector
- $\mathbf{A}(\xi_r^0, \xi_p^0, \xi_y^0)$  - Satellite attitude matrix ( $=\mathbf{T}_{orb/sc}$  determined by  $\mathbf{p}_0, \mathbf{v}_0$ . See Section 3.1.3 Coordinate Transformations)( $=\mathbf{A}^0$ ),
- $\mathbf{A}(\xi_r^0 + d\xi_r, \xi_p^0 + d\xi_p, \xi_y^0 + d\xi_y)$ 
  - True satellite attitude matrix(to be estimated)
- $\mathbf{u}_{sc}$  - View vector to the ground control point in the spacecraft coordinate system(measured)
- $\mathbf{u}_0$  - View vector in the orbital coordinate system( $=\mathbf{A}^0\mathbf{u}_{sc}$ ),
- $\mathbf{T}_{ecr/orb}$  - Transformation matrix from orbital coordinate system to earth fixed coordinate system ( $=\mathbf{T}_{ecr/eci}\mathbf{T}_{eci/orb}$ . See Section 3.1.4.2 Earth Location Algorithm),
- $\mathbf{u}_{ecr}$  - Look vector to earth ( $=\mathbf{T}_{ecr/orb}\cdot\mathbf{u}_0$ ),
- $\mathbf{u}_{cp}$  - Look vector to the true control point from the spacecraft position  $\mathbf{p}_0$ .

$\mathbf{x}_0$  and  $\mathbf{x}_{cp}$  are as before. Note that  $\mathbf{x}_0$  is computed using  $\mathbf{u}_{sc}$  and systematic orbit and attitude parameters  $\mathbf{p}_0, \mathbf{v}_0, \xi_r^0, \xi_p^0, \xi_y^0$  as described in Section 3.1.4.2. Thus  $\mathbf{x}_0$  can be regarded as a function of these parameters:

$$\mathbf{x}_0 = \mathbf{F}(\mathbf{u}_{sc}, \xi_r^0, \xi_p^0, \xi_y^0, \mathbf{p}_0, \mathbf{v}_0) \quad (1)$$

Because of the possible error in the satellite orbital ephemeris data and attitude data, this calculated  $\mathbf{x}_0$  may be different from the true location  $\mathbf{x}_{cp}$ .

Set :

$$d\mathbf{x} = \mathbf{x}_{cp} - \mathbf{x}_0 = \mathbf{x}_{cp} - F(\mathbf{u}_{sc}, \xi_r, \xi_p, \xi_y, \mathbf{p}_0, \mathbf{v}_0) \quad (2)$$

Instead of comparing two points on the ground, they are pulled back to the orbital coordinate system and compared because the distance to the control point is not important.

First construct the unit vector to the actual control point location in the orbital coordinate system.

$$\mathbf{u}_{cp} = \mathbf{T}_{orb/ecf} \left( \frac{\mathbf{x}_{cp} - \mathbf{p}_0}{|\mathbf{x}_{cp} - \mathbf{p}_0|} \right) \quad (3)$$

Note that this vector only depends on the spacecraft position, while  $\mathbf{u}_0$  only depends on the attitude parameters.

We can compare two vectors  $\mathbf{u}_0$ ,  $\mathbf{u}_{cp}$  by:

$$d\mathbf{u} = \mathbf{u}_{cp} - \mathbf{u}_0 = \mathbf{T}_{orb/ecf} \left( \frac{\mathbf{R}_{cp} - \mathbf{P}_0}{|\mathbf{R}_{cp} - \mathbf{P}_0|} \right) - \mathbf{A}^0 \mathbf{u}_{sc} \quad (4)$$

The task of precision modeling is to calculate the ephemeris and attitude parameters so that the residuals  $\{d\mathbf{u}\}$  after corrections are minimized for all selected control points. This model shifts the satellite position/velocity in three directions and rotates the satellite to fit the control point measurements.

#### • Definition of Observation Equations

Let  $\mathbf{u} = (x_l, y_l, z_l)^T$  be a look vector (either  $\mathbf{u}_{cp}$  or  $\mathbf{u}_0$ ) in the orbital coordinate system.

Instead of computing  $d\mathbf{u}$ , the following two angles are compared:

$$\delta = \tan^{-1}(y_l / z_l)$$

$$\psi = \tan^{-1}(x_l / z_l)$$

See Figure 3-33 for a relationship among angles and look vector  $\mathbf{u}$ .

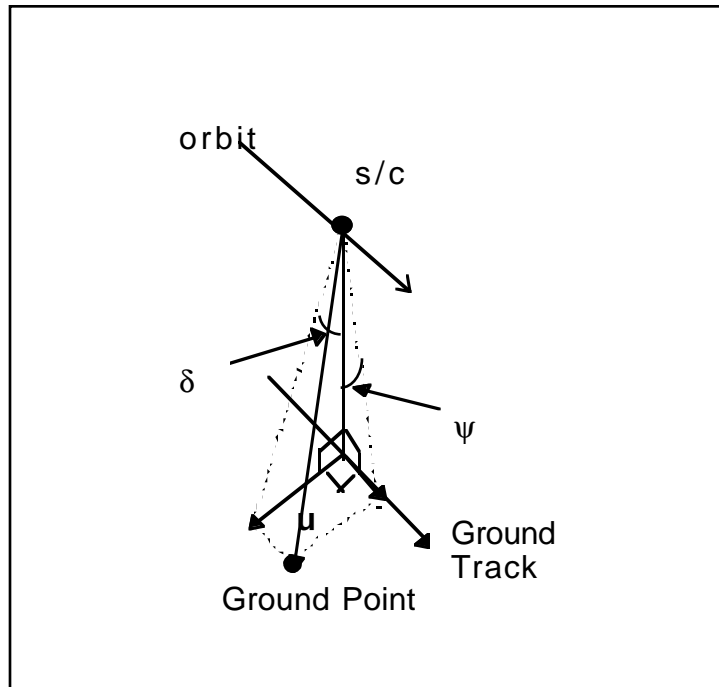


**Figure 3-33. Look Vector Angles**

Now compare the two sets of  $\delta$ ,  $\psi$  and estimate

$$\alpha = \delta_{cp} - \delta_{orb} \tag{5}$$

$$\beta = \psi_{cp} - \psi_{orb} \tag{6}$$

Note that from (3)  $\delta_{cp}$  and  $\psi_{cp}$  do not depend on satellite attitude. Also note that from (4),  $\delta_{orb}$  and  $\psi_{orb}$  do not depend on the spacecraft position.

First  $\alpha$  and  $\beta$  can be expressed in terms of small position corrections  $dx$ ,  $dy$ ,  $dz$  and small attitude corrections  $d\xi_r$ ,  $d\xi_p$ ,  $d\xi_y$ .

The basic idea of this scheme is as follows:

$\delta_{cp}$  and  $\psi_{cp}$  are a function of  $(x, y, z)$  and  $\delta_{orb}$  and  $\psi_{orb}$  are a function of  $(\xi_r, \xi_p, \xi_y)$ . These can be expanded around a known set of values. From (5), we obtain:

$$\begin{aligned} \alpha &= \alpha(X_0 + X) = \alpha(X_0) + d\alpha \\ &= \alpha(X_0) + d\delta_{cp} - d\delta_{orb} \end{aligned} \tag{7}$$

where  $X_0 = (0, 0, 0, \xi_r^0, \xi_p^0, \xi_y^0)$  at given attitude parameters  $\xi_r^0, \xi_p^0, \xi_y^0$  with the satellite at the origin  $(0,0,0)$  and  $X = (x, y, z, \xi_r, \xi_p, \xi_y)$ .

The function is expanded to a Taylor series at  $X = 0$  and taking only the first order terms:

$$\alpha = \alpha(X_0) + \frac{\partial\alpha}{\partial x}dx + \frac{\partial\alpha}{\partial y}dy + \frac{\partial\alpha}{\partial z}dz + \frac{\partial\alpha}{\partial \xi_r}d\xi_r + \frac{\partial\alpha}{\partial \xi_p}d\xi_p + \frac{\partial\alpha}{\partial \xi_y}d\xi_y \quad (8)$$

Note that all partials are evaluated at the origin.

$$\alpha(X_0) \text{ is given by: } \alpha(X_0) = \delta_{cp} - \delta_{orb} \quad (9)$$

The estimated solution can be found by setting  $\alpha = 0$  satisfying:

$$\delta_{cp} - \delta_{orb} = -\frac{\partial\alpha}{\partial x}dx - \frac{\partial\alpha}{\partial y}dy - \frac{\partial\alpha}{\partial z}dz - \frac{\partial\alpha}{\partial \xi_r}d\xi_r - \frac{\partial\alpha}{\partial \xi_p}d\xi_p - \frac{\partial\alpha}{\partial \xi_y}d\xi_y \quad (10)$$

A similar expression can be given by setting  $\beta = 0$ .

• **Building Coefficients for the Observation Equations**

Angle  $\delta_{cp}$  (simply  $\delta$ ) is illustrated in Figure 3-34.

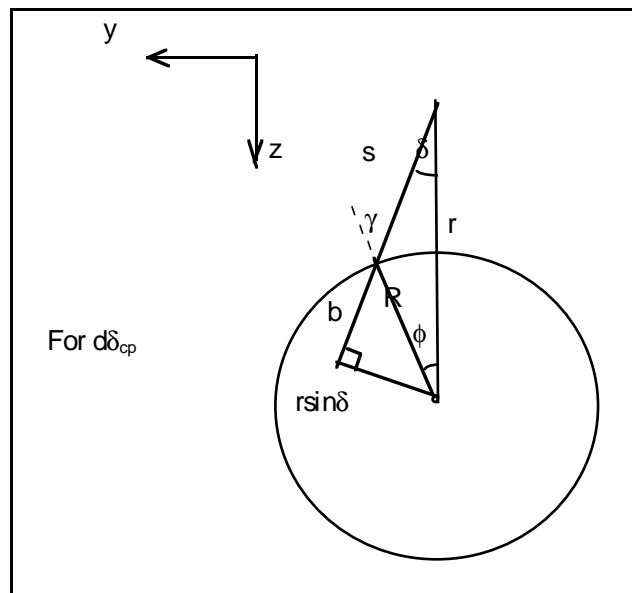


**Figure 3-34. Cross Track Geometry**

where R: Distance to the control point from the center of the Earth,  
 r: Distance to the satellite from the center of the Earth  
 h: Satellite altitude  
 s: Distance from satellite to the control point  
 $\delta$ : Along-scan angle of look vector  
 $\phi$ : Earth centered angle between the satellite and the control point  
 $\gamma$ : Zenith angle of the look vector at the control point  
 b:  $\sqrt{R^2 - r^2 \sin^2 \delta}$

From the above figure, we have a relationship:

$$R \sin(\delta + \phi) = r \sin \delta \quad (11)$$

Differentiating the equation (11) (holding R and r constant) yields:

$$R \cos(\delta + \phi)(d\delta + d\phi) = r \cos \delta d\delta \quad (12)$$

Note that  $\delta + \phi = \gamma$ ,  $d\phi = -dy/r$

Thus from (12),

$$d\delta = -\frac{b}{rs} dy \quad (13)$$

where  $b = R \cos \gamma = \sqrt{R^2 - (r^2 \sin^2 \delta)}$ ,  $s = r \cos \delta - b$ .

For the effect of altitude error, differentiating (11) with respect to  $\delta$  and r (holding  $\phi$  constant) and noting  $dr = -dz$ , we have

$$d\delta = \frac{\sin \delta}{s} dz \quad (14)$$

Combining (13) and (14), the total effect will be

$$d\delta = -\frac{b}{rs} dy + \frac{\sin \delta}{s} dz \quad (15)$$

For the calculation of  $\beta$ , use a relationship illustrated in Figure 3-35.

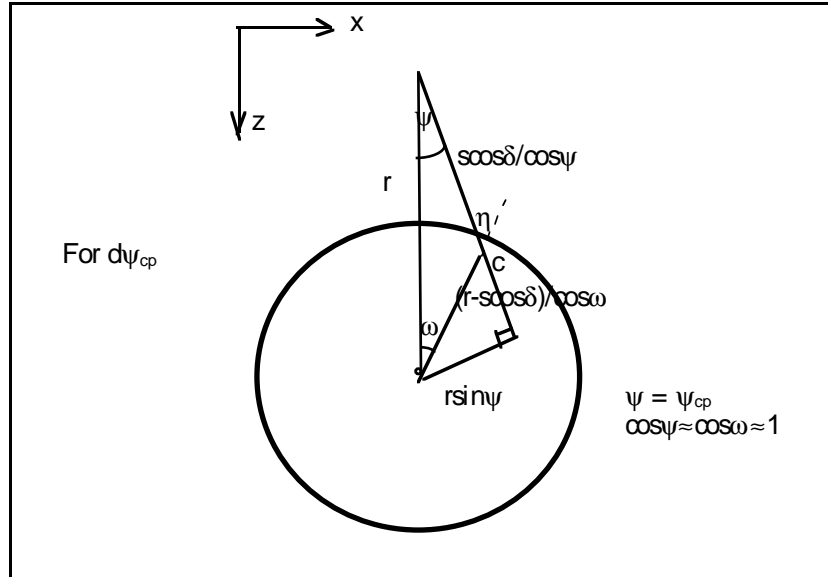


**Figure 3-35. Along Track Geometry**

- where  $\omega$ : Projection of angle  $\phi$  on x-z plane
- $\eta$ : projection of angle  $\gamma$  on x-z plane
- $c$ :  $r \cos \psi - s \cos \delta / \cos \psi$

Note that along-track angle  $\psi$  is assumed very small compared to cross-track angle  $\delta$ . That is,

$$\cos \psi \approx \cos \omega \approx 1.$$

From the Figure 3-35,

$$d\psi = -\frac{r - s \cos \delta}{rs \cos \delta} dx \tag{16}$$

Now we evaluate partials in (8) and (10), which are functions of attitude parameters.

Let  $\mathbf{u}_{sc} = (u_x, u_y, u_z)^T$ ,

$$\mathbf{A} = [a_{ij}] = [a_{ij}(\xi_r, \xi_p, \xi_y)]$$

$$\begin{pmatrix} x_l \\ y_l \\ z_l \end{pmatrix} = [a_{ij}] \mathbf{u}_{sc}$$

Then:

$$\tan(\delta_{orb}) = \frac{y_l}{z_l} = \frac{a_{21}u_x + a_{22}u_y + a_{23}u_z}{a_{31}u_x + a_{32}u_y + a_{33}u_z} \quad (17)$$

$$\tan(\psi_{orb}) = \frac{x_l}{z_l} = \frac{a_{11}u_x + a_{12}u_y + a_{13}u_z}{a_{31}u_x + a_{32}u_y + a_{33}u_z} \quad (18)$$

Then  $d\delta_{orb}$  and  $d\psi_{orb}$  can be expressed by:

$$d\delta_{orb} = A_\delta d\xi_r + B_\delta d\xi_p + C_\delta d\xi_y \quad (19)$$

$$d\psi_{orb} = A_\psi d\xi_r + B_\psi d\xi_p + C_\psi d\xi_y \quad (20)$$

where partial derivatives with respect to  $\xi_r, \xi_p, \xi_y$  to calculate  $A, B, C$  are all evaluated at  $\xi_r, \xi_p, \xi_y = 0$  and we obtain;

$$A_\delta = -1 \quad B_\delta = \frac{u_x u_y}{u_z^2 + u_y^2} \quad C_\delta = \frac{u_x u_z}{u_z^2 + u_y^2}$$

$$A_\psi = -\frac{u_x u_y}{u_z^2 + u_x^2} \quad B_\psi = 1 \quad C_\psi = -\frac{u_y u_z}{u_z^2 + u_x^2}$$

Thus from (8), (9) and (10):

$$\alpha = \delta_{cp} - \delta_{orb} - \frac{b}{rs} dy + \frac{\sin \delta}{s} dz - A_\delta d\xi_r - B_\delta d\xi_p - C_\delta d\xi_y \quad (21)$$

$$\beta = \psi_{cp} - \psi_{orb} - \frac{r - s \cos \delta}{rs \cos \delta} dx - A_\psi d\xi_r - B_\psi d\xi_p - C_\psi d\xi_y \quad (22)$$

From these by setting  $\alpha = 0, \beta = 0$ :

$$\delta_{cp} - \delta_{orb} = \frac{b}{rs} dy - \frac{\sin \delta}{s} dz - d\xi_r + \frac{u_x u_y}{u_z^2 + u_y^2} d\xi_p + \frac{u_x u_z}{u_z^2 + u_y^2} d\xi_y \quad (23)$$

$$\psi_{cp} - \psi_{orb} = \frac{r - s \cos \delta}{r \cos \delta} dx - \frac{u_x u_y}{u_z^2 + u_x^2} d\xi_r + d\xi_p - \frac{u_y u_z}{u_z^2 + u_x^2} d\xi_y \quad (24)$$

• **Further Decomposition of Bias over Time**

To include both bias and rate terms, we decompose each correction term into two parts:

$$dx = dx_0 + dx \dot{d} t \quad dy = dy_0 + dy \dot{d} t \quad dz = dz_0 + dz \dot{d} t \tag{25}$$

$$d\xi_r = d\xi_{r0} + d\xi_r \dot{d} t \quad d\xi_{sp} = d\xi_{sp0} + d\xi_{sp} \dot{d} t \quad d\xi_{sy} = d\xi_{sy0} + d\xi_{sy} \dot{d} t$$

where dt is measured from a reference time taken to be the average time of the control point observation. See Figure 3-36 for how a set of offsets(dx or dξ) could be expressed as a function of dt in terms of constant bias and rate using control point residuals.

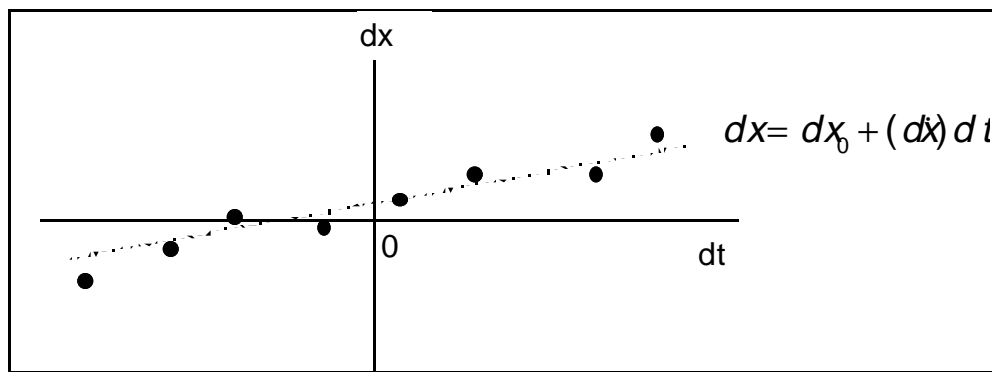


**Figure 3-36. Linear Estimate of dx as a Function of dt Generated from Control Points**

We now estimate vector X of :

$$[dx_0, dy_0, dz_0, d\xi_{r0}, d\xi_{sp0}, d\xi_{sy0}, dx \dot{d}, dy \dot{d}, dz \dot{d}, d\xi_r \dot{d}, d\xi_{sp} \dot{d}, d\xi_{sy} \dot{d}] \tag{26}$$

Considering system error  $V_\delta, V_\psi$  and using (26), the observation equations can be expressed by:

$$\begin{aligned} \delta_{cp} - \delta_{orb} = & \frac{b}{rs} dy_0 - \frac{\sin \delta}{s} dz_0 + A_\delta d\xi_{r0} + B_\delta d\xi_{sp0} + C_\delta d\xi_{sy0} \\ & + \left(\frac{b}{rs} dt\right) dy \dot{d} - \left(\frac{\sin \delta}{s} dt\right) dz \dot{d} + (A_\delta dt) d\xi_r \dot{d} + (B_\delta dt) d\xi_{sp} \dot{d} + (C_\delta dt) d\xi_{sy} \dot{d} + V_\delta \end{aligned} \tag{27}$$

$$\begin{aligned} \psi_{cp} - \psi_{orb} = & \frac{r - s \cos \delta}{r s \cos \delta} dx_0 + A_\psi d\xi_{r0} + B_\psi d\xi_{sp0} + C_\psi d\xi_{sy0} \\ & + \left(\frac{r - s \cos \delta}{r s \cos \delta} dt\right) dx \dot{d} + (A_\psi dt) d\xi_r \dot{d} + (B_\psi dt) d\xi_{sp} \dot{d} + (C_\psi dt) d\xi_{sy} \dot{d} + V_\psi \end{aligned} \tag{28}$$

## Solving Normal Equations

### • Best Estimate from Normal Equations

Combining these two observation equations for all control points, we obtain the following form of observation equations:

$$\mathbf{Y} = \mathbf{HX} + \mathbf{V} \quad (29)$$

where  $\mathbf{Y}$ : is look angles differences [left hand side of (27) and (28)] for all control points,

$\mathbf{H}$ : is a coefficients matrix for all control points

$\mathbf{X}$ : is to be estimated (26)

$\mathbf{V}$ : is the system noise for all control points given by:

$$\mathbf{V} = \begin{pmatrix} V_{\delta} \\ V_{\psi} \end{pmatrix} \quad (30)$$

Note that if the number control points is  $N$ , the total number of equations is  $2N$ .

Let:

$\mathbf{X}_a$  denote a mean a priori estimate of  $X$  with covariance matrix  $\mathbf{P}_a$ ,

$\mathbf{W}^{-1}$ : covariance matrix of the measurement noise  $\mathbf{V}$ .

Then the normal equation to the observation equation (29) can be given by:

$$(\mathbf{H}^T \mathbf{W} \mathbf{H} + \mathbf{P}_a^{-1}) \hat{\mathbf{X}} = [\mathbf{H}^T \mathbf{W} \mathbf{Y} + \mathbf{P}_a^{-1} \mathbf{X}_a] \quad (31)$$

See the section of Reference 20 on estimation theory.

Then solving the normal equation the best estimate of  $\hat{\mathbf{X}}$  is given by:

$$\hat{\mathbf{X}} = (\mathbf{H}^T \mathbf{W} \mathbf{H} + \mathbf{P}_a^{-1})^{-1} [\mathbf{H}^T \mathbf{W} \mathbf{Y} + \mathbf{P}_a^{-1} \mathbf{X}_a] \quad (32)$$

Residuals on the observations and a priori value can be computed from:

$$\mathbf{V} = \mathbf{Y} - \mathbf{H} \hat{\mathbf{X}} \quad \text{and} \quad \mathbf{V}_a = \mathbf{X}_a - \hat{\mathbf{X}} \quad (33)$$

Since observation equations are non-linear and linearized by computing partial derivatives, the entire process must be iterated until the correction parameters

converge. At each stage, a priori value and covariance matrix, weight matrix and coefficients matrix H will be determined and solved for residuals.

As indicated in Reference 15, along track residual and pitch residual in the observation equation may be correlated and may not be well separated. This will result in a singular normal matrix. To solve this problem, either the along track residual or pitch residual can be absorbed into the other. A similar problem may occur between the roll residual and cross-track residual. If we have enough priority information ( $\mathbf{P}_a$ ) on these parameters, they could be resolved without changing the normal matrix artificially in order to avoid ill-condition of the equation.

Summarizing these problems, we have:

1. Errors from the control point matching process can reduce the accuracy of residual error estimation,
2. Correlation among parameters:
  - Along track residual - pitch residual errors
  - Cross track residual - roll residual errors

To solve this problem,

- Absorb one parameter to the other,
- Find a reasonable a priori value and a priori covariance matrix ,
- Select well distributed control points over more than one granule.

Sensor misalignments and mirror errors will be studied using the current approach with a long term results. Later some of the parameters will be modeled. To understand and estimate a long term trend and bias for the parameters, the error analysis must be performed from a short arc of a granule to over a long period of time covering many granules.

It should be noted that band-to-band misalignments can not be studied since only band 1 or 2 (250 m resolution) scenes are to be used.

(This page intentionally left blank.)

#### 4. CONSTRAINTS, LIMITATIONS, AND ASSUMPTIONS

Several simplifying assumptions were made in the development of the MODIS Earth location algorithm. These assumptions and their justifications are as follows:

- Ignore atmospheric refraction of the line of sight - Recent analysis of the refraction (private communication with Peter Noerdlinger) indicates it may be as high as 30 m at the edge of a scan. Later versions of the software will take this refraction into account.
- Ignore light travel time - The maximum range to a terrestrial target seen by MODIS is about 1414 km. This corresponds to a light travel time of 4.7 msec. This is a significant effect that causes as much as a 14 m bias at the edges of the scans. Later versions of the software will take this effect into account.
- Ignore the instrument primary mirror offset from the spacecraft center of mass - The ephemeris position represents the spacecraft center of mass rather than the instrument optical origin, but this offset is a few meters at most, which is less than the accuracy of the ephemeris data and much less than a MODIS pixel.

The error analysis presented in Section 3.1.5 is based on Reference 2, which assumed that the individual contributors to the overall MODIS Earth location error were independent zero-mean Gaussian distributed random variables. This assumption is implicit in this document as well. In addition, the Earth location algorithm was developed under the assumption that the nature and magnitudes of the errors documented in Reference 2 are essentially correct. The quality of the available DEM data is assumed to conform to the characteristics specified in Reference 8, although this does not affect the algorithm itself, only its final performance.

The implementation of the MODIS Earth location algorithm described above is based on the final assumption that the output product data structure will be sufficiently flexible to permit the addition of eight new Earth location data fields for each spatial element and to allow the efficient extraction of control point neighborhoods from the 250m image bands for automated product validation.

(This page intentionally left blank.)

**APPENDIX A: ACRONYMS AND ABBREVIATIONS**

AC	Ambient Calibration and Testing
arcsec	arc second
ATBD	Algorithm Theoretical Basis Document
AVHRR	Advanced Very High Resolution Radiometer
BIH	Bureau International de l'Heure
CCSDS	Consultative Committee on Space Data Systems
CTS	Conventional Terrestrial System
deg	degree
DEM	Digital Elevation Model
DMA	Defense Mapping Agency
ECI	Earth Centered Inertial
ECR	Earth Centered Rotating
EDOS	EOS Data and Operations System
EOS	Earth Observing System
EOSDIS	EOS Data and Information System
EROS	Earth Resources Observation System
FPA	Focal Plane Assembly
GIIS	General Instrument Interface Specification
GPS	Global Positioning System
GSFC	Goddard Space Flight Center
IERS	International Earth Rotation Service
IFOV	Instantaneous Field of View
IMS	Information Management System
kHz	kilohertz
km	kilometer
LAC	Local Area Coverage (type of AVHRR data)
Landsat	Land Remote Sensing Satellite
LWIR	Long Wave Infrared (spectral bands)
m	meter
MCST	MODIS Characterization Support Team
MISR	Multi-angle Imaging Spectroradiometer
mm	millimeter
MODIS	Moderate-Resolution Imaging Spectroradiometer
MSS	Multi-spectral Scanner
mrad	milliradian
msec	millisecond

$\mu\text{m}$	micrometer
$\mu\text{rad}$	microradian
$\mu\text{sec}$	microsecond
MTF	Modulation Transfer Function
MWIR	Medium Wave Infrared
NASA	National Aeronautics and Space Administration
NIR	Near Infrared (spectral bands)
PGS	Product Generation System
QA	Quality Assurance
rad	radian
RSS	Root Sum Square
SBRC	Santa Barbara Research Center
sec	seconds
$\sigma$	standard deviation
SDST	Science Data Support Team
SeaWiFS	Sea Wide-Field Sensor
SOM	Space Oblique Mercator
SPOT	System pour l'Observation de la Terre
SRCA	Spectroradiometric Calibration Assembly
SWIR	Short-wave Infrared (spectral bands)
TLCF	Team Leader Science Computing Facility
TM	Thematic Mapper
TR	Technical Report
UIID	Unique Instrument Interface Document
USA	United States of America
USGS	United States Geological Survey
VIS	Visible (spectral bands)
WGS84	World Geodetic System 1984

## APPENDIX B: ALTERNATIVE APPROACH FOR TERRAIN CORRECTION

As described in the section of terrain intersection algorithm, the current approach is to use DEM through Toolkit calls at given geodetic coordinates with zero height and calculate the final intersection point with terrain in the ECR coordinates and then geodetic coordinates. Another approach is simply to use ground coordinates such as SOM map coordinates or geodetic coordinates with zero height. The alternative method will introduce more errors near the pole if done in geodetic coordinates but it greatly reduces computation time. The current method approaches the final point along the vector  $\hat{\mathbf{u}}$  looking at the points on the ellipsoid converting coordinates from ECR to geodetic, while the alternative method moves along the ellipsoid without any conversion.

Step 10 can be rewritten with the alternative map coordinates in the following way:

### Simplified Method

$$\mathbf{s} = \mathbf{s}_{\min} - \mathbf{s}_{\max} \quad (\text{alternative map coordinates})$$

$$\hat{\mathbf{s}} = \mathbf{s}/|\mathbf{s}|$$

$$\mathbf{s}_0 = \mathbf{s}_{\max}$$

$$h_0 = \text{DEM}(\mathbf{s}_0) \quad (\text{DEM at } \mathbf{s}_0)$$

$$h'_0 = H_{\max}$$

$$ds = (\text{nominally } 1/2 \text{ km})$$

$$dh' = \frac{ds(H_{\min} - H_{\max})}{|\mathbf{s}|}$$

$$i = 0$$

do until ( $h \geq h_i$ )

$$i = i + 1$$

$$\mathbf{s}_i = \mathbf{s}_{i-1} + ds\hat{\mathbf{s}}$$

$$h_i = \text{DEM}(\mathbf{s}_i)$$

$$h'_i = h'_{i-1} + dh'$$

end do

## APPENDIX C: DATA VALIDATION

As described in Section 3.2.3.4, the input data stream to be used for geolocation of MODIS products will be checked through four basic approaches: absolute limits, delta limits, consistency, and sanity. The actual data validation methodology for orbit, attitude and mirror encoder data is described below.

### Orbit Data

The orbit data validation will consist of absolute limit, consistency, and sanity checks. The consistency check will compare successive values of the individual components of the position and velocity, using the time difference, to establish consistency.

For the  $j$ -th sample of component  $i$ , the check to be performed is:

$$\left| p_{i,j+1} - P_{i,j} - (T_{j+1} - T_j) \cdot (V_{i,j+1} + V_{i,j}) / 2 \right| < d_0$$

where  $P$  is the position,  $V$  is the velocity,  $T$  is the time and  $d_0$  is the limit.

This equation uses the average of the velocity at the two times to estimate the change in position. Sanity checks will be performed on: the position vector magnitude, the velocity vector magnitude, and the orbit angular momentum. The first two will be performed by computing the magnitude of each vector and performing an absolute limit. The angular momentum (per unit mass) is computed as the cross product of the position and velocity vectors:

$$\mathbf{M} = \mathbf{P} \times \mathbf{V}$$

Absolute limit checks will be performed on both the magnitude of  $\mathbf{M}$ , which should be constant according to physics, and on the Z component of  $\mathbf{M}$ , which should be constant according to the orbit inclination.

Position absolute limits = -7100000, 7100000 meters

Velocity absolute limits = -7520, 7520 meters/second

Consistency limit = 10 meters

Position magnitude limits = 7070000, 7100000 meters

Velocity magnitude limits = 7480, 7520 meters/second

Angular momentum magnitude limits = 5.30E10, 5.32E10

Angular momentum Z component limits = -7.52E9, -7.50E9

### **Attitude Data**

The attitude data validation will consist of absolute limit, delta limit, and consistency checks. The consistency check will compare successive values of the individual attitude angles and angular velocity, using the time difference, to establish consistency.

For the  $j$ -th sample of component  $i$ , the check to be performed is:

$$\left| A_{i,j+1} - A_{i,j} - (T_{j+1} - T_j) \cdot (W_{i,j+1} + W_{i,j}) / 2 \right| < d_a$$

where:  $A$  is the angle

$W$  is the angular velocity

$T$  is the time

$d_a$  is the limit

Angle absolute limits = -1800, 1800 arcseconds

Rate absolute limits = -20, 20 arcseconds/second

Delta angle limit = 90 arcseconds

Delta rate limits = -5, 5 arcsecond/second

Consistency limit = 5 arcseconds

### **Mirror Encoder Data**

The mirror encoder samples the time of every 100th mirror encoder pulse beginning at the pulse which defines the start of the Earth sector. The mirror encoder times consist of time differences (in microseconds) between these time samples. The validation will consist of absolute and delta limit checks on the time differences.

Absolute limits = 18000, 18064 microseconds

Delta limits = 10 microseconds

## APPENDIX D: INVERSE MAPPING ALGORITHM

As described in the section of Land Control Point Matching Algorithm, given a ground point in geodetic coordinates (latitude or longitude), the inverse mapping algorithm will find pixel and line numbers within a MODIS granule.

The following notations are useful:

N: Total number of scans in the granule,  
**v**: Normalized ground point expressed by:

$$\mathbf{v} = \begin{bmatrix} \cos\lambda_g \cos\varphi_g \\ \cos\lambda_g \sin\varphi_g \\ \sin\lambda_g \end{bmatrix} \quad (1)$$

at the location  $(\varphi_g, \lambda_g)$

$\mathbf{s}_{S1}$ : Start of the first scan (unit vector)

$\mathbf{s}_{E1}$ : End of the first scan (unit vector)

$\mathbf{s}_{C1}$ : Sum of  $\mathbf{s}_{S1}$  and  $\mathbf{s}_{E1}$  given by:

$$\mathbf{s}_{C1} = \frac{\mathbf{s}_{E1} + \mathbf{s}_{S1}}{|\mathbf{s}_{E1} + \mathbf{s}_{S1}|} \quad (2)$$

$\mathbf{s}_{N1}$ : Cross product of  $\mathbf{s}_{S1}$  and  $\mathbf{s}_{E1}$  given by:

$$\mathbf{s}_{N1} = \frac{\mathbf{s}_{E1} \times \mathbf{s}_{S1}}{|\mathbf{s}_{E1} \times \mathbf{s}_{S1}|} \quad (3)$$

$\mathbf{s}_{S2}$ : Start of the last scan (unit vector)

$\mathbf{s}_{E2}$ : End of the last scan (unit vector)

Similarly define  $\mathbf{s}_{C2}$  and  $\mathbf{s}_{N2}$  from  $\mathbf{s}_{S2}$  and  $\mathbf{s}_{E2}$ .

The above vectors are illustrated in Figure D-1.

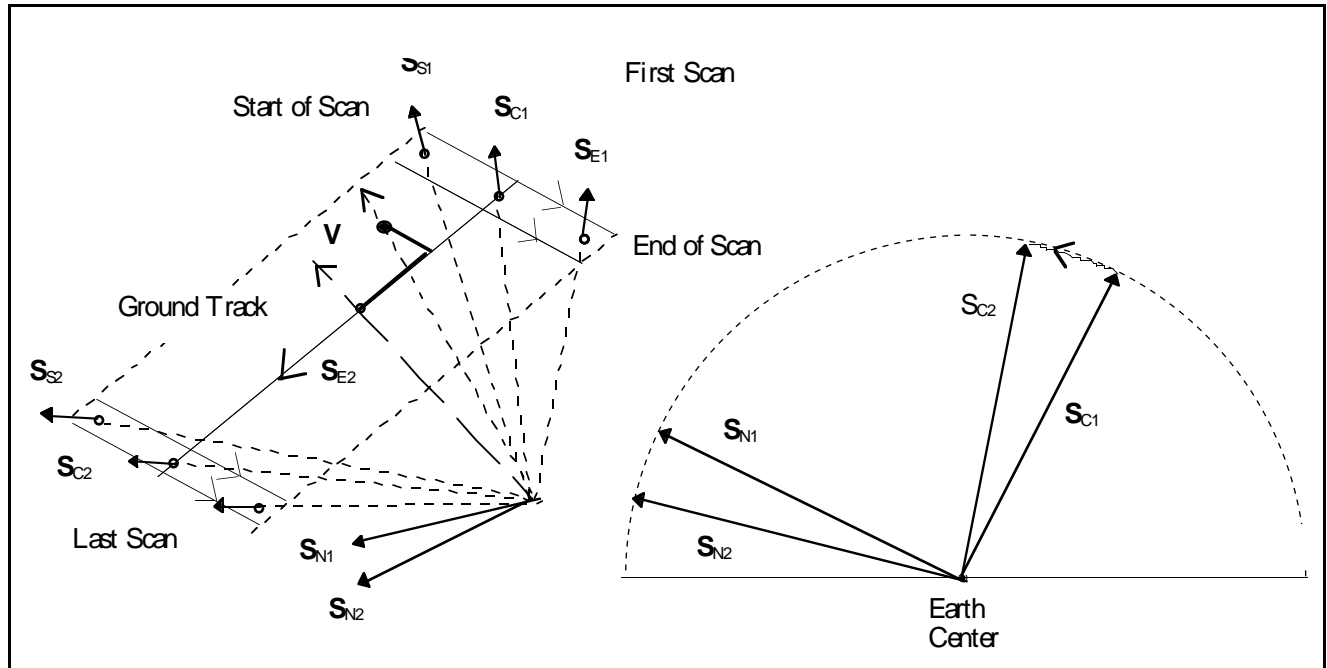


**Figure D-1. Vectors to the First and Last Scans**

Note that the sense of the cross product results in the scan normal being in the positive along-track direction.

Using small angle approximation, the scan number for the location  $\mathbf{v}$  can be estimated from the sine of the angle relative to the first scan:

$$n_s = N \frac{\mathbf{v} \cdot \mathbf{s}_{N1}}{\mathbf{s}_{C2} \cdot \mathbf{s}_{N1}} \tag{4}$$

where  $n_s$  is the estimated scan number.

Similarly, the estimation can be performed relative to the last scan:

$$n_s = N \left( 1 - \frac{\mathbf{v} \cdot \mathbf{s}_{N2}}{\mathbf{s}_{C1} \cdot \mathbf{s}_{N2}} \right) \tag{5}$$

Either of these expressions may be sufficiently linear for our purpose. However, we can improve the approximation by averaging the above two:

$$n_s = N \left( 0.5 + \frac{\mathbf{v} \cdot \mathbf{s}_{N1} + \mathbf{v} \cdot \mathbf{s}_{N2}}{\mathbf{s}_{C2} \cdot \mathbf{s}_{M1} - \mathbf{s}_{C1} \cdot \mathbf{s}_{N2}} \right) \quad (6)$$

knowing the fact that

$$\mathbf{s}_{C1} \cdot \mathbf{s}_{M1} \approx -\mathbf{s}_{C1} \cdot \mathbf{s}_{N2} \quad (7)$$

Rewriting (6), we obtain:

$$n_s = c_0 + c_1 \sin \lambda \quad (8)$$

where:

$$c_0 = N/2$$

$$c_1 = N \frac{|\mathbf{s}_{M1} + \mathbf{s}_{N2}|}{\mathbf{s}_{C2} \cdot \mathbf{s}_{N1} - \mathbf{s}_{C1} \cdot \mathbf{s}_{N2}} \quad (9)$$

$$\sin \lambda = \mathbf{v} \cdot \mathbf{c}_{N1}$$

$$\mathbf{c}_{N1} = \frac{\mathbf{s}_{M1} + \mathbf{s}_{N2}}{|\mathbf{s}_{M1} + \mathbf{s}_{N2}|}$$

In this sense,  $\lambda$  is the angle between the location specified by  $\mathbf{v}$  and the center scan plane, with negative  $\lambda$  representing the first half of the granule.

If  $n_s$  is not within the range 0 to  $(N-1)$ , we assume that  $\mathbf{v}$  is outside the granule.

To express a frame number for  $\mathbf{v}$ , a relationship among the scan angle, ground point, and Earth center will be used.

Let:

$\theta$ : sensor scan angle,

$\alpha$ : angle from the nadir frame to the viewed location on the earth surface,

$r$ : distance from the earth center to the spacecraft,

$R$ : Earth radius at the viewed location.

Then we obtain the following approximation:

$$\tan \theta = \frac{\sin \alpha}{(r/R - \cos \alpha)} \quad (10)$$

This is illustrated in Figure D-2.

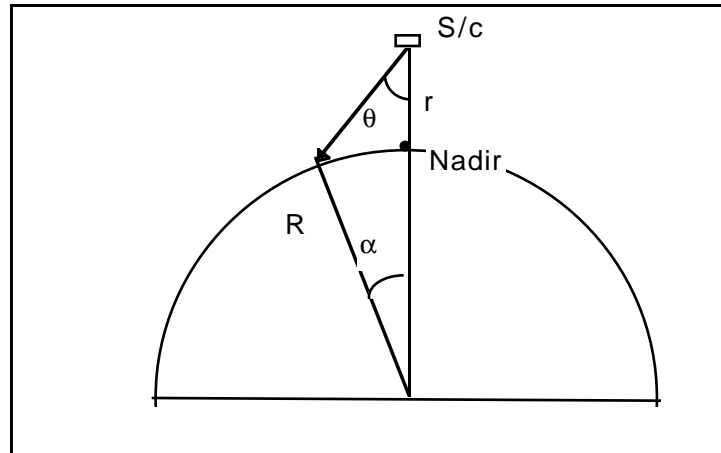


**Figure D-2. Scan and Earth Angle**

The sign of  $\alpha$  is chosen to be consistent with  $\theta$ .

A good approximation for this is given by:

$$\tan\theta = c_1 \sin\alpha + c_3 \sin^3\alpha$$

An expression for the sign of  $\alpha$  can be easily be derived using the same approach as for the scan number. We can compute the normal to a vector at the granule's center as follows:

$$\mathbf{c}_{N2} = \frac{\mathbf{s}_{C1} \times \mathbf{s}_{C2}}{|\mathbf{s}_{C1} \times \mathbf{s}_{C2}|} \quad (11)$$

The cross product is chosen to give  $\mathbf{c}_{N2}$  in the direction of positive scan angle.

Then set

$$\sin\alpha = \mathbf{v} \cdot \mathbf{c}_{N2} \quad (12)$$

Coefficients  $c_1$  and  $c_3$  can be given by:

$$c_1 = R / (r - R) \quad (13)$$

$c'_3$  can be computed to force agreement at the endpoints of the scan by computing the maximum value for  $\alpha$  by:

$$\sin(\alpha_{\max}) = \frac{\mathbf{c}_{N2} \cdot (\mathbf{s}_{E1} + \mathbf{s}_{E2})}{|\mathbf{s}_{E1} + \mathbf{s}_{E2}|} \quad (14)$$

and

$$c'_3 = \frac{\tan \theta_{\max} - c'_1 \sin \alpha_{\max}}{\sin^2 \alpha_{\max}} \quad (15)$$

where  $\theta_{\max}$  is normally 0.96(55 degrees) in radians. The final step is to compute the frame number from  $\theta$ :

$$n_f = 705 \theta + N_f / 2 \quad (16)$$

where  $N_f$  is normally 1354. Value 705 is the altitude of the spacecraft in km. We only consider the case where  $n_f$  is within a range 1 to  $N_f$ .

In the actual use, the information stored with the file is computed as follows:

First the vector  $\mathbf{c}_{N1}$  and  $\mathbf{c}_{N2}$  are computed as in (9) and (11) for the granule. Next, the values of the coefficients  $c_0$  and  $c_1$  and  $c'_1$  and  $c'_3$  are computed using (9), (13), and (15).

### **Determination of along-track and along-scan fractional offset**

This algorithm uses the coordinates for two scan lines and two consecutive frames in a scan to compute the along-track and along-scan indices for an input location. The first step is to convert the coordinates for the specified scan lines and frames to unit vectors using the equation (1) above. The following will be used to refer to unit vectors:

- $\mathbf{p}_{11}$  = first line, first frame
- $\mathbf{p}_{12}$  = first line, second frame
- $\mathbf{p}_{21}$  = second line, first frame; etc.

The distance between the input position  $\mathbf{v}$  and the first line and frame position is computed as a vector difference:

$$\Delta \mathbf{v} = \mathbf{v} - \mathbf{p}_{11} \quad (17)$$

The along-track offset  $\Delta$  is determined in units of scan lines by computing the component of the difference vector in the along-track direction and expressing it in units of scan lines:

$$\Delta l = \frac{\Delta \mathbf{v}(\mathbf{p}_{21} - \mathbf{p}_{11})(n_{s2} - n_{s1})}{|\mathbf{p}_{21} - \mathbf{p}_{11}|^2} \tag{18}$$

where  $n_{s1}$  and  $n_{s2}$  refer to the scan line numbers for the two scan lines.

Along-scan offset  $\Delta p$  is determined similarly in units of frames:

$$\Delta p = \frac{\Delta \mathbf{v}(\mathbf{p}_{12} - \mathbf{p}_{11})}{|\mathbf{p}_{12} - \mathbf{p}_{11}|^2} \tag{19}$$

Note that  $\mathbf{p}_{11}$  and  $\mathbf{p}_{12}$  are assumed to correspond to consecutive frames so the difference in frame is assumed to be 1. The relationship in the equations (18) and (19) is illustrated in Figure D-3.

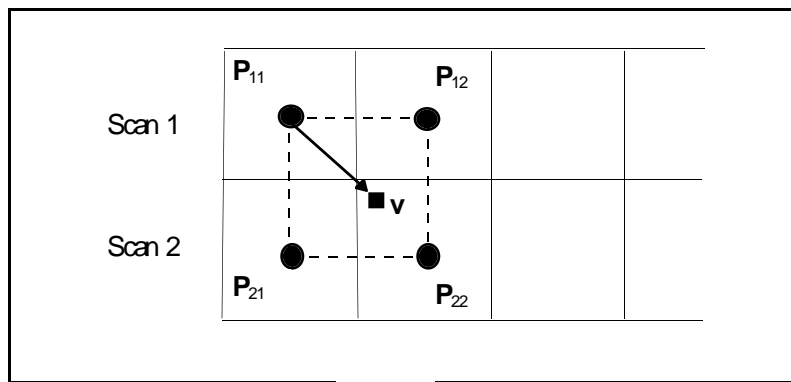


**Figure D-3. Fractional Pixel/Line Number Offsets Using 4 Points**